AD-A258 532

CUMENTATION PAGE

Form Approved
OMB No. 0704-0188

1. AGENCY USE ONLY (Leave blank)	2. REPORT DATE	3. REPORT TYPE AND DATES COVERED
	September 1992	THESIS/DISSERTATION

4. TITLE AND SUBTITLE
The Use of Coarse Resolution Satellite Imagery to Predict Human Puumala Virus Epidemics in Sweden

5. FUNDING NUMBERS

6. AUTHOR(S)
Gary Dean Gackstetter, Major

7. PERFORMING ORGANIZATION NAME(S) AND ADDRESS(ES)
AFIT Student Attending: University of Minnesota

8. PERFORMING ORGANIZATION REPORT NUMBER
AFIT/CI/CIA-92-026D

9. SPONSORING / MONITORING AGENCY NAME(S) AND ADDRESS(ES)
AFIT/CI
Wright-Patterson AFB OH 45433-6583

10. SPONSORING / MONITORING AGENCY REPORT NUMBER

11. SUPPLEMENTARY NOTES

12a. DISTRIBUTION / AVAILABILITY STATEMENT
Approved for Public Release IAW 190-1
Distribution Unlimited
ERNEST A. HAYGOOD, Captain, USAF
Executive Officer

12b. DISTRIBUTION CODE

13. ABSTRACT *(Maximum 200 words)*

14. SUBJECT TERMS	15. NUMBER OF PAGES 145
	16. PRICE CODE

17. SECURITY CLASSIFICATION OF REPORT	18. SECURITY CLASSIFICATION OF THIS PAGE	19. SECURITY CLASSIFICATION OF ABSTRACT	20. LIMITATION OF ABSTRACT

UNIVERSITY OF MINNESOTA

This is to certify that I have examined this bound copy of a doctoral thesis by

GARY DEAN GACKSTETTER, D.V.M., M.P.H.

and have found that it is complete and satisfactory in all respects,
and that any and all revisions required by the final
examining committee have been made.

Sandra L. Melnick, M.P.H., Dr.P.H. Robert W. Jeffery, Ph.D.
Name of Faculty Adviser(s)

Sandra L. Melnick Robert W. Jeffery
Signature of Faculty Adviser(s)

9/11/92 9/11/92
Date

GRADUATE SCHOOL

THE USE OF COARSE RESOLUTION SATELLITE IMAGERY TO PREDICT HUMAN PUUMALA VIRUS EPIDEMICS IN SWEDEN

A THESIS
SUBMITTED TO THE FACULTY OF THE GRADUATE SCHOOL
OF THE UNIVERSITY OF MINNESOTA
BY

GARY DEAN GACKSTETTER, D.V.M., M.P.H.

IN PARTIAL FULFILLMENT OF THE REQUIREMENTS
FOR THE DEGREE OF
DOCTOR OF PHILOSOPHY

SEPTEMBER 1992

...this thesis is dedicated

to

my wife Jeanne

and

our children Katie and John

This project was funded in part by a

Research Development Grant from the
Division of Epidemiology, School of Public Health,
University of Minnesota

and

a grant from
The Army High Performance Computing Research Center

ACKNOWLEDGMENTS

Although it is impossible to name all of the people who have helped me with this project, I'd like to express my sincere appreciation and gratitude as I acknowledge the following for their positive contributions to my work during my time at the University of Minnesota.

I sincerely thank my advisors: Dr. Sandra Melnick, Dr. Paul McGovern, and Dr. Robert Jeffery for their many hours of help, guidance, and support throughout this program. I credit Dr. Melnick, in particular, for having maintained exacting standards and for keeping this project on schedule. I thank Dr. McGovern for his patience, statistical expertise and willingness to spend countless hours helping me to recognize the next statistical procedure. In addition to my co-advisers, I'd like to thank the other members of my committee: Dr. John Potter, Dr. R.Ashley Robinson, and Dr. Marvin Bauer for their time, recommendations, and constructive criticisms. By example, each has taught me scientific investigation at the population level.

I also acknowledge the United States Air Force, specifically Colonel Richard Shafer, for providing me the opportunity to enter the Air Force Institute of Technology, Civilian Institutions' Graduate Degree Program. Furthermore, I acknowledge and thank the University of Minnesota, Division of Epidemiology and The Army High Performance Computing Research Center (AHPCRC) for providing financial support for my project. Within the AHPCRC, I thank Mr. Paul Muzio and his staff, especially Mr. Gary Hansen, for both acquiring and allowing me to use their computer resources and facilities.

I'm especially grateful to Dr. Birger Hörnfeldt from the University of Umeå, Umeå, Sweden. He was gracious enough to provide me with his rodent trapping figures and the daily, study-site weather information, both were essential for the analysis. I'm also grateful to Dr. Ken Linthicum and Dr. James LeDuc from the United States Army Medical Research Institute of Infectious Diseases. Dr. Linthicum coordinated the acquisition and preprocessing of the satellite data. Dr. LeDuc obtained the rodent serologic information from Dr. Bo Niklasson of the Swedish National

Bacteriological Laboratory. I'm also appreciative and indebted to Dave Gilbertson for the technical assistance he provided during the long data analysis phase of this project. Also, a very special thanks goes to Margie Konopliv for her assistance with typing the final document.

I thank Steve Kelder and Beth Virnig, my fellow graduate students, for their friendship and advice as we progressed through the Epidemiology PhD program.

I sincerely thank my parents, Dean and Ardyce Gackstetter, for instilling in me the desire and determination to excel, and for their unconditional kindness and generosity.

And most of all, I deeply and sincerely thank my wife, Jeanne, who beyond loving and tolerating me through numerous years of higher education, has given me more than I will ever be able to repay. She truly has sacrificed much during what must have seemed like endless years of formal education, while continuing to nurture our children and inspire me through all the demands of Graduate Schools. None of this would have been possible without her.

TABLE OF CONTENTS

LIST OF TABLES

LIST OF FIGURES

LIST OF FIGURES (Continued)

LIST OF FIGURES (continued)

ABSTRACT

The Use of Coarse Resolution Satellite Imagery To Predict Human Puumala Virus Epidemics in Sweden

The potential for predicting the occurrence of human Puumala virus epidemics in northern Sweden, using coarse-resolution, digitized satellite data was studied. Puumala virus is effectively maintained in chronically infected, asymptomatic, small-mammal hosts named bank voles *(Clethrionomys glareolus)*. In northern Sweden, bank vole populations are known to fluctuate on a 3-4 year frequency, but with varying amplitudes. A strong association exists between peak bank vole populations and the incidence of human disease. The study area was a 100x100 km site located in northern Sweden (about 64° N, 20° E). Bank vole population numbers were obtained by snap-trapping twice a year at 58 permanent and symmetrically distributed one-hectare plots, and correlated with a Normalized Difference Vegetation Index (NDVI) obtained from NOAA series satellites. Among bank voles trapped in the study area during this investigation, a Puumala virus, antibody-positive prevalence of 24.3% was noted. While older voles tended to be Puumala antibody positive, total bank vole population numbers did not predict antibody-positive population numbers. The NDVI assesses the extent and condition of green vegetation. It was derived using a 30-day maximum-value compositing, thermal cloud-masking technique. The ability of the NDVI to predict bank vole population fluctuations within the study area was evaluated. The findings from this study suggest that relatively coarse-resolution, digitized satellite data, do not predict bank vole population fluctuations. However, given the limited number of data points, this conclusion must be considered tentative. Improving the satellite measure and increasing the frequency of assessment of reservoir host populations may prove useful to further evaluate the

potential for using satellite data to predict human disease. A supplementary finding was that NDVI values were found to be strongly correlated among ever increasing geographic areas. The NDVI values from 5x5 km individual study sites were strongly correlated with its 50x50 km quadrant NDVI value and the quadrant NDVI values were strongly correlated with the entire 100x100 km NDVI value. In contrast, this study was not able to confirm an association between selected meteorological variables (ambient temperatures and precipitation) and monthly NDVI values.

I. INTRODUCTION

1.1. OVERVIEW

In a recent review article, at least twelve different viral Hemorrhagic Fevers (HF) were listed.[1] The HF viruses have been classified into at least four major viral families, are globally distributed, have multiple routes of transmission, and, in humans, can cause clinical disease syndromes ranging from asymptomatic infections to rapidly fatal illnesses. At least five of the HF viruses have the unique ability to cause renal pathology, in addition to the classic hematologic abnormalities. Consequently, these viruses have been grouped under the name Hemorrhagic Fever with Renal Syndrome (HFRS).[2] Within the HFRS group of illnesses, several very mild forms of the disease exist, having a very low case fatality rate, and usually presenting with only minor hemorrhagic symptoms. One of these mild forms of HFRS is recognized in Scandinavia and called Nephropathia Epidemica (NE).[3] NE is strictly a human disease usually characterized by sudden onset, fever, back or abdominal pain, polyuria, rising serum creatinine, proteinuria, and, as a rule, spontaneous recovery, usually within six months.[4] In 1980, the identification of the viral etiologic agent of NE in Scandinavia was documented by Brummer-Korvenkontio et al., and the name "Puumala virus" was suggested.[5] Niklasson and LeDuc listed current prevalence ('82-'85) and incidence (Jun '84-May '85) data in Sweden by county of residence.[6] They noted age-adjusted antibody prevalences of greater than 10% and incidence rates of greater than 20 cases/100,000 population in people living in Västerbotten county.[6] The 100x100 kilometer study area for this project is contained within the same county. The bank vole (*Clethrionomys glareolus*) appears to be the most important chronically infected reservoir host for human Puumala virus in Sweden.[4,6] Bank vole populations fluctuate dramatically over a 2-5 year cycle, varying as much as 200-fold between peak population densities.[7,8] The occurrence of human disease caused by Puumala virus closely parallels bank vole population cycles.[4,8] Bank vole population cycles appear to be significantly influenced by environmental conditions such as weather patterns and vegetation

growth.[8,9] Both weather and vegetation parameters can be monitored and evaluated with satellite imagery.[10]

The purpose of this project was to use existing data from Sweden on bank vole population cycles, the known incidence of NE, and retrospective satellite imagery in an attempt to correlate satellite data with the risk of human Puumala virus outbreaks. Under the research hypothesis that it is possible to predict human Puumala virus epidemics in Sweden using satellite imagery, this study sought to provide information to a growing data base capable of forecasting the potential for a number of vector-borne or zoonotic, reservoir-borne diseases.

1.2. SIGNIFICANCE

Although epidemiologists have attempted to relate remote sensing data to disease incidence or vector populations for more than twenty-three years,[11] it was only recently that satellite-derived data has been successfully employed.[12,13,14] For example, in 1990, Bailey and Linthicum described a method to predict arbovirus outbreaks with data obtained from satellites.[15] In 1991, Rogers and Randolph correlated satellite data with tsetse fly habitat characteristics and animal populations in Africa to show the geographic areas with the greatest risk of trypanosome transmission.[16] Ultimately, their research may lead to pinpoint control of this vector, which in turn may mean the eventual elimination of human and animal trypanosomiasis in some circumscribed areas.

If analyses of satellite imagery of the Swedish countryside can accurately identify the environmental marker(s) that predict rodent reservoir population cycles and the likelihood for human nephropathia epidemica, then it should also be possible to predict the occurrence of many other human diseases that are reservoir- or arthropod-dependent. Even though NE has a relatively low case-fatality rate (<0.5%),[17] other Hantaan hemorrhagic fever viruses like Korean hemorrhagic fever virus, have case-fatality rates approaching 25%.[18] In the United States, several Peromyscus and Microtus species, as well as urban rats, may serve as reservoirs for agents similar or identical to Hantaan viruses.[19] More importantly, if the use of satellite imagery is perfected,

arthropod-borne diseases like malaria, yellow fever, Japanese encephalitis, St. Louis encephalitis, dengue fever, and even Lyme disease endemic areas could possibly be mapped, assuming an environmental marker exists that would identify the vector's habitat. Not only might it be possible to monitor and control some of the major arthropod-borne diseases using satellite data, but also plague, rabies, or other reservoir dependent diseases may be better controlled. Furthermore, schistosomiasis, dracunculiasis, trypanosomiasis, or other parasitic infections might also be better controlled by using satellite imagery to consolidate control measures and concentrate scarce control resources where they would have the greatest impact. As mentioned earlier, satellite imagery has already helped to identify tsetse fly habitats and hence focus surveillance and control efforts in Africa.[16]

Especially in the developing areas of the world, inferior communication networks and inadequate transportation inhibit the use of field studies to inventory vector or reservoir habitats, leaving only subjective disease assessment methods as the best source of information. A possible solution to these problems is to find a remote sensor that could gather accurate and timely environmental data about a given area. Ideally, this would involve a remote sensing instrument with a wide field of view, placed in a sun-synchronous orbit, with no less than a 1-km resolution, capable of regional analyses, and with a low average cost per unit area. The AVHRR/2 sensor, flown on the NOAA-9 satellite platform, is such a system. The AVHRR's synoptic view, daily frequency of coverage and thus a high potential for cloud-free images, all at a reasonable cost, give it great potential for use in public health efforts.

The United States Armed Forces, as well as agencies like The Department of State, the Peace Corps, the U.S. Public Health Service, and World Health Organization have people stationed all over the world. Additionally, the U.S. Government maintains an almost instantaneous global deployment capability. If disease assessment groups possessed the capability to use satellite imagery to predict the potential for arthropod-borne or reservoir-dependent human diseases, then morbidity among those at greatest risk might be better anticipated. Given that

satellite-acquired imagery can predict vector or reservoir population densities, both disease prevention and control measures could be instituted on any number of important illnesses affecting public health. Once perfected, satellite imagery has the potential to become a n economical, quick, and effective "preventive medicine tool" for Public Health practitioners. The goal of this study is to continue to build on the initial steps of applying satellite imagery to the eventual control of the major vector- or reservoir-dependent human diseases.

1.3. REFERENCES

1. LeDuc JW. Epidemiology of hemorrhagic fever viruses. Rev Infect Dis 1989; (Suppl 4):11.

2. Gajdasek CD, Goldfarb LG, Goldgaber D. Bibliography of hemorrhagic fever with renal syndrome. 2nd ed. NIH publication no. 88-2603, August 1987.

3. Myhrman G. Nephropathia epidemica, a new infectious disease in northern Scandinavia. Acta Med Scand 1951; 140:52-6.

4. Settergren B. Nephropathia epidemica (HFRS) in Scandinavia. Rev Infect Dis 1991; 13:736-44.

5. Brummer-Korvenkontio M, *Vaheri* A, Hovi T, Lahdevirta J, et al. Nephropathia epidemica: detection of antibody in bank voles and serologic diagnosis of human infection. J Infect Dis 1980; 141:131-4.

6. Niklasson B, LeDuc J. Epidemiology of nephropathia epidemica in Sweden. J Infect Dis 1987; 155(2):269-76.

7. Hornfeldt B. Regulation of voles cycles by delayed density-dependence [Dissertation]. Umeå, Sweden: University of Umeå, 1991.

8. Nystrom K. The incidence and prevalence of endemic benign (epidemic) nephropathy in AC County, Sweden, in relation to population density and prevalence in small rodents. Acta Med Scand 1977; [Suppl 609]:1.

9. Hansson L. Food as a limiting factor for small rodent numbers: tests of two hypotheses. Oecologia 1979; 37:297-314.

10. Tucker CJ. Red and photographic infrared linear combinations for monitoring vegetation. Rem Sens Env 1979; 8:127-50.

11. Cline BL. New eyes for epidemiologists: aerial photography and other remote sensing techniques. Am J Epidemiol 1979; 92:85-9.

12. Hayes RO, Maxwell EL, et al. Detection, identification, and classification of mosquito larval habitats using remote sensing scanners in earth-orbiting satellites. WHO Bull 1985; 63:361-74.

13. Linthicum KJ, et al. Detection of rift valley fever viral activity in Kenya by remote sensing imagery. Science 1987; 135:1656-9.

14. Linthicum KJ, Bailey CL, et al. Polar-orbiting satellite monitoring of man-made alterations in the ecology of the senegal river basin, as they relate to a rift valley fever epidemic. In: Arbovirus Research In Australia. Proceedings Fifth Symposium, August 28-September 1, 1989. Brisbane, Australia, 1990: 116-9.

15. Bailey EL, Linthicum KL. Satellite remote sensing: a future technology for monitoring vector populations and predicting arbovirus outbreaks. In: Arbovirus Research in Australia. Proceedings Fifth Symposium, August 28-September 1, 1989. Brisbane, Australia, 1990:111-6.

16. Rogers DJ, Randolph SE. Mortality rates and population density of tsetse flies correlated with satellite imagery. Nature 1991; 5:351.

17. Benenson AS, ed. Control of communicable diseases in man. 15th ed. Washington, DC: The American Public Health Association, 1990.

18. Van Ypersele de Strihou C, Mery JP. Hantavirus-related acute interstitial nephritis in western Europe: expression of a world-wide zoonosis. QF Med 1989; 270:941-50.

19. Glass GE, Childs JE, Watson AJ, LeDuc JW. Association of chronic renal disease, hypertension, and infection with a rat-borne hantavirus in the U.S. Arch Virol 1990; [Suppl 1]:69-80.

II. SPECIFIC AIMS

STUDY HYPOTHESIS

The main hypothesis of this study is that it is possible to predict the potential for human Puumala virus epidemics in Sweden using digitized satellite imagery.

Sub-hypotheses are listed with each specific aim and include the following:

2.1. SPECIFIC AIM #1:

To evaluate the potential for using relatively coarse, satellite-derived data, in the form of a normalized difference vegetation index (NDVI), as a predictor of bank vole population fluctuations.

Sub-hypothesis:

NDVI values are strongly correlated with bank vole population fluctuations within the study area.

2.2. SPECIFIC AIM #2:

To assess the association among NDVI values, ambient temperature, and precipitation.

Sub-hypothesis:

A major portion of the variance in bank vole population cycles can be explained by certain environmental indices as measured by a remote sensor.

2.3. SPECIFIC AIM #3:

To estimate the population prevalence of Puumala virus antibody within bank voles trapped in the study area.

Sub-hypothesis:

The bank vole population seroprevalence of Puumala virus varies predictably as their population density changes.

2.4. SPECIFIC AIM #4:

Attempt to develop an infectious disease epidemiologic model that incorporates NDVI values and can be used to accurately predict the potential for human Puumala virus outbreaks in Sweden.

Sub-hypothesis:

A mathematical model exists that can predict the amplitudes of bank vole population cycles.

III. BACKGROUND INFORMATION

3.1. THE EPIDEMIOLOGY OF HEMORRHAGIC FEVER WITH RENAL SYNDROME (HFRS)

3.1.1. Background: Hemorrhagic Fevers in General

LeDuc lists twelve distinct viruses known to cause viral hemorrhagic fever in humans.[1] Table 3-1 summarizes some of the characteristics associated with each of these viral diseases, allowing for direct comparisons. Hemorrhagic fever viruses are a diverse group, classified among several major viral families. The hemorrhagic fever viruses cause serious disease in both temperate and tropical zones throughout the globe and generally have the ability to infect humans of all ages. However, those at greatest risk appear to be people who are occupationally* exposed.[1] Transmission typically occurs when people are either bitten by an infected arthropod vector or are exposed to aerosolized virus particles from infected rodent excreta.[1] Secondary transmission (person-to-person), is the exception rather than the rule. Nevertheless, infection with any of the hemorrhagic fever viruses is an important cause of human morbidity and mortality and as such remains a significant and expanding zoonotic problem of global public health concern.[2,3]

Leaving the large group of all Hemorrhagic Fevers, this section will first, concentrate on the sub-group of diseases termed Hemorrhagic Fevers with Renal Syndrome (HFRS). Again narrowing the focus, but staying within the general group of HFRS diseases, this section will eventually focus on the specific HFRS illness termed Nephropathia Epidemica (NE).

---

*Occupations such as: wild animal handler, farm-related work, forester, etc.

TABLE 3.1.-1. (PAGE 1 OF 3)
HEMORRHAGIC FEVERS (HF)

NAME	VIRUS GROUP	CASE-FATALITY	INCI-DENCE	PREV-ALENCE	SUB-CLINICAL
AFRICAN HF					
MARBURG DISEASE	Filoviridae	25%	low	?	?
EBOLA DISEASE	Filoviridae	50-90%	low	7%	yes
ARENAVIRAL HF	Arenaviridae				
LASSA FEVER	Lassa	36%(hosp)			10-30X hosp
ARGENTINE HF	Junin	5-30%	3C-6C/yr	12%	5%
BOLIVIAN HF	Machapo	up to 24%			low
ARTHROPOD-BORNE HF					
	TOGA.				
CHIKUNGUNYA HF	Alphavirus	<5%			
CRIMEAN-CONGO HF	Bun.Nairovirus	2-50%	50-200K/yr		
DENGUE HF	Flav.Flavivirus	High(kid	400K/yr		
KYASANUR FOREST DZ	Flav.Flavivirus	<10%	up to 1K/yr		
OMSK HF	Flav.Flavivirus	1-10%			
RIFT VALLEY FEVER	Bun.Phlebovirus	High	50-100K/yr		
YELLOW FEVER	Flav.Flavivirus	Common			high
HF WITH RENAL SYNDROME			All Renal Syn		
AT LEAST SIX			100K/yr		
HANTAVIRUSES EXIST	Bunyaviridae-				
	#1.Seoul virus	below 1%			
KOREAN HF	Bunya	7-30%	100-800/yr		high
	#2.Hantaan virus		hosp cases		
NEPHROPATHIA EPIDEMICA	Bunya	0.5%	up to 20	8%	up to
	#3.Puumala virus		100K/yr		90%
Others:	#4.Prospect Hill virus (US)				
	#5.Porogia virus (Balkans)				

TABLE 3.1.-1. (PAGE 2 OF 3)
HEMORRHAGIC FEVERS (HF)

[TIME	AREA GEOG	AGE	SEX	EPIDEMIOLOGY/RISK FACTORS OCCUPA/ REC	DISEASE] PATTERN]	RESERVOI	VECTOR
	Africa			HlthCare& An.Hand	epidem	?	?
	Africa				epidemic	?	?
dry-season	W.Africa	all	M&F	HlthCare	epi/endem	Rodent	-
Jan-Aug	Argen farm	adult	male	farm	epi/endem	Mouse	-
Apr-Jul (also3-5yr cycles)	N.E.Bolivia	all	M&F	household	epi/endem	Mouse	-
Jan-Apr	Af,Asia				epidemic	Primates birds	mosquito
Jun-Sep	Af,S.USSR			farm/hlth	endemic	Mammals+ birds	tick
	S.E.Asia	young			epi/endem	Human	mosquito
Jan-Jun	India			forest	epi/endem	Monkey/ Sm.mamm	tick
	Asia,USSR			farm	epi/endem	Rodent	tick+H2O
	Africa				epidemic	Dom.An.	mosquito
	New World Af.Cities				epidemic	Human & Monkey	mosquito
summer	Europe USSR	adult	male	farm or forest+lab	epi/endem	Rodent	-
May-Jun & Oct-Nov	Asia	adult	male	usu rural	epi/endem	Mouse	-
Oct-Feb	Scandinavia	adult	male 2:1	farm	epi/endem	Bank vol	-

TABLE 3.1.-1. (PAGE 3 OF 3)
HEMORRHAGIC FEVERS (HF)

MODE OF TRANSMISSION	INCU-BATION	CLINICAL SIGNS AND SYMPTOMS	DIAGNOSIS	CONTROL
contact w/ body fluids +aerosol	3-9d	fv, GI, Hem, Lv, Jaundice	IFA,EM	
"	2-21d	"	lab	
p to p & contact w/ rodent excret aerosol,food	6-21d	flu+ fever hem,GI, oral ulcers	lab	rodent(?
	10-16d	hem, fv,rash, flu, GI	lab	vacc/rod
	10-14d	"	lab VI,CF,HI,ELISA	rodent
bite		fv + Joint pain	lab	
bite	3-12d	HF common	lab	vector
bite		HF + "break-bone" fv, rash	lab	vector
bite+aerosol			lab	vect(vac
bite + An contact	3-8d	HF	lab	
bite + An contact	3-8d	HF + enceph	lab	
bite		fv + Jaundice	lab see above	vacc + vector
aerosol from rodent excreta	9-35d	H/B ache GI, Hem fv+renal failure	maybe chronic renal disease sero + RNA probe	rodent
	12-16d	most severe	sero (esp IgM	rodent
"	14-21d	most mild	serology	rodent

3.1.2. Hemorrhagic Fever with Renal Syndrome

The "Bibliography of Hemorrhagic Fever With Renal Syndrome, Second Edition," published by the U.S. Department of Health & Human Services, Public Health Service, National Institutes of Health lists more than 155 clinical synonyms used to describe the disease constellation, characterized by hematologic abnormalities, accompanied by renal dysfunction.[4] At the 1982 Tokyo meeting, The World Health Organization Working Group on HFRS officially recommended that all the 155 clinical synonyms be referred to as HFRS.[5] As a result of that recommendation, HFRS is currently the term most widely used in the scientific literature. In spite of the WHO recommendation, Gajdusek et al. has proposed the name *muroid virus nephropathy*.[4] Gajdusek justifies the new name using three main points: First, Hantaviruses are maintained in nature, within asymptomatic rodent reservoirs which excrete virus from their lungs, in saliva and in urine, and all of the unaffected rodent carriers belong to the suprafamily Muroidea. Second, most illnesses caused by the Hantaviruses result in renal abnormalities. And third, the hemorrhagic manifestations that result from Hantavirus infection are extremely variable. Thus the name "*muroid virus nephropathy*" has been suggested.[6]

For the time being then, HFRS, is considered to be a clinical disease caused by one of several viruses belonging to the genus, *Hantavirus* of the family *Bunyaviridae*.[7] The first etiologic agent of HFRS was isolated in 1976 from the lungs of the small mammal *Apodemus agrarius* (the Korean striped field mouse).[8] In 1978, a virus was isolated from a Korean patient suffering from Korean Hemorrhagic Fever (KHF) [like NE, KHF is also now known as HFRS].[9] The causative agent was named Hantaan virus. Since the isolation of Hantaan serotype several other serotypes have been documented.

At least five different serotypes of the Hantavirus genus have been found thus far, and the evidence is mounting for several more.[9,10]

Table 3-2 summarizes five of the Hantavirus serotypes.

TABLE 3.1.-2.[3,10]

Serotypes of Hantaviruses

Virus Name	Rodent Reservoir	Geographic Distribution	Clinical Syndrome
Hantaan	A. agrarius	Far East, Asia	Severe HFRS
Seoul	Rattus rattus R. norvegicus	Worldwide	Mild HFRS
***Puumala**	**Clethrionomys glareolus**	**Europe, Scandinavia West USSR, Balkans**	**Nephropathia epidemica***
Prospect Hill	Microtus pennsylvanicus	United States	None described
Porogia	A. flavicollis	Balkans	Severe HFRS

*virus and disease of interest

Although there are differences in clinical presentation among the different serotypes, they are similar in their mode/route of transmission and their epidemiological characteristics. Serologic evidence has shown that the most severe form of HFRS, found in the far eastern Soviet Union and in China, is caused by a virus very similar to Hantaan virus (the prototype virus).[11] In fact, from 1983 through 1985, 280,000 people were hospitalized with HFRS in China.[12] Of reported HFRS cases, the mortality rate was about 5%.[12] In China the annual incidence rate of HFRS has

increased from 471 cases in 1955 to over 100,000 in 1985.[12] In contrast to the HFRS found in the far east, a milder form of HFRS, termed Nephropathia epidemica (NE), caused by a virus named Puumala virus, has been noted in the far western Soviet Union, Europe, Finland, Sweden, and Norway.[13] Both the severe and the mild clinical forms of HFRS are caused by antigenically related but still distinctly different viruses belonging to the same Hantavirus genus.[14,15,16] Therefore, clinical reports of HFRS in the far western Soviet Union and northern Europe (including Scandinavia) are more than likely NE and are probably identical virologically, clinically, and epidemiologically.[6] It is worth noting that different Hantavirus serotypes isolated from patients with HFRS in different regions of the world possess antigenic markers similar to the strains isolated from the principal rodent reservoir in the same area.[17] This supports the conclusion that basic antigenic differences between serotypes could account for the differences in the severity of HFRS and differences in the clinical presentation as well as differing mortality rates.[16]

3.1.3. Nephropathia Epidemica (NE)

3.1.3.1. The Agent: Puumala Virus

Although Lee et al. isolated the etiologic viral agent of KHF in 1978, it wasn't until 1980 when Brummer-Korvenkontio et al. documented the viral agent of NE.[18] The name Puumala virus was recommended. Puumala virions have a helical capsid symmetry with a diameter of 80-110 nm.[19] The virions also have an ethanol labile, lipid-containing, enveloped membrane and a tripartite single-stranded RNA genome, with a unique nucleotide sequence at the 3' end of each RNA segment.[19] Each of the antigenic subtypes is associated with a specific rodent species.[20] Although Puumala virus antigen and antibodies have been found in several species of small rodent, the virus is maintained in nature principally by asymptomatic, chronic infections of the bank vole, *Clethrionomys glareolus*.[21] Serologic evidence has been used to map the presence of Puumala virus throughout Europe, west of the Ural mountains, as well as Scandinavia.[22]

3.1.3.2. Clinical Presentation of Nephropathia Epidemica

Clinically, NE is usually a benign, febrile illness, predominated by renal abnormalities rather than hemorrhagic manifestations.[20,23,24] Although poorly defined, the incubation period appears to average about 30 days. Johnson has reported incubation periods ranging from 9 days to 5 weeks.[25]

The onset of clinical illness is usually abrupt with very little or no prodromal period. In more than 94% of the cases, fever is the initial finding. Body temperatures of 38-40°C persist for 2-9 days.[24,26,28,35] Usually within two days of illness, headache and malaise are present and continue while the patient is febrile.[28] Mckee et al. reported that presenting symptoms of NE are very similar to influenza, except that the coryza and other respiratory symptoms are absent.[35] Typically, between the third and fourth days of illness, nausea, vomiting, severe-diffuse abdominal pain and sometimes joint pain (in combination with the presenting fever and malaise) usually mark the beginning of the renal phase of illness.[24] Backache occurs in well over half the patients and is typically located in the costovertebral angles as well as the lumbar area.[24,26]

In nearly 100% of the patients, the above clinical signs are followed by proteinuria.[24] This leads to azotemia in about 70% of the patients, and oliguria in just over 50% of the patients with NE.[24] Proteinuria peaks about one week into the illness, and typically, falls steadily over the next three to six days.[24] Serum creatinine levels rise to 2-10 mg/dl.[24] Similarly, blood urea nitrogen levels rise to 50-200mg/dl.[24] Oliguria, if it occurs, usually lasts only a few days and is followed by polyuria of 3-4 liters/days for 7 to 10 days.[27] Beginning the second week of illness and continuing for up to several months, hyposthenuria universally occurs.[24,27] Gross hematuria is seen in 3-7% of the cases, while microscopic hematuria, pyuria, and cylinduria are noted in the majority of patients.[24,27]

During the renal phase of NE, patients subjectively appear severely ill.[27] Settergren et al. noted somnolence, confusion, and restlessness in up to 20% of cases.[24] Although, cerebral spinal fluid analyses usually are normal, elevated protein levels are sometimes seen.[24] Also,

commonly found during the renal phase of NE, is a mild leukocytosis, thrombocytopenia, and an elevated sedimentation rate.[24]

Blurred vision, usually of short duration and found in 6-12% of the patients, is regarded as almost pathognomonic for NE when found with the previously listed clinical signs.[24] The transient, blurred vision is probably the result of interstitial edema of the lens and ciliary body.[24,28] Histologically, the renal abnormalities include interstitial nephritis and hemorrhage.[26] Unlike Korean hemorrhagic fever, total renal failure is uncommon with NE.[27] Hemorrhagic manifestations like epistaxis, gastrointestinal bleeding, oral mucosal petechiae, occur in 5-10% of NE patients.[24,26,28]

Polyuria usually signals clinical improvement.[27] Most patients are subjectively better two weeks after the onset of fever.[24] Renal function rapidly improves, resulting in normal serum creatinine and BUN levels.[27] Although lassitude, backache, and hyposthenuria may persist for several more weeks, complete clinical recovery is the rule.[26]

Clearly, individual cases of NE vary greatly in severity; as host, agent, and/or environmental factors can play a significant role. For instance, Lahdevirta studied 76 Finnish patients with confirmed NE and found 30% of the cases were regarded as mild, 60% as moderate, and 9% as severe.[26] Settergren et al. reviewed the records of 355 Swedish patients with NE and noted 5% with moderate to severe hemorrhage, while 1% required dialysis.[24] He also noted, NE in children under 15 years of age appears to be a much milder disease.[24] According to Settergren et al., patients with NE usually have four or more of the following clinical criteria: acute onset, headache, increased serum creatinine, proteinuria, hematuria, and polyuria of greater than two liters/24hr.[24]

Although diagnosing NE based on clinical signs is relatively accurate, confirmation is usually done by serologic methods. Current tests listed in order of least to highest specificity include an ELISA test, an immunofluorescent-antibody test, and, as of July 1992, a highly specific monoclonal-antibody test. Once perfected, the monoclonal antibody test should become the

'gold-standard', having the advantages of exquisite sensitivity, specificity, and positive predictive value. Case-fatality rates for NE are consistently below 0.5%.[21] Meanwhile, asymptomatic infection is relatively common. In fact, subclinical/ clinical ratios ranging from 14:1 up to 20:1 have been noted in Puumala virus endemic areas of Scandinavia.[21,29]

3.1.3.3. The Epidemiology of Nephropathia Epidemica

NE is the western Eurasian Hemorrhagic Fever with Renal Syndrome variant caused by Puumala virus, one of several Hantaviruses.[4,18,30] The epidemiology of NE is inseparably linked to the of the rodent reservoir, which serves to maintain the viral etiologic agent in nature as an asymptomatic, chronic carrier.[21] Niklasson and LeDuc noted that Puumala virus was very effectively maintained in the wild by its primary reservoir, *Clethrionomys glareolus*, commonly called the bank vole.[21] The disease, NE, and its etiologic agent, Puumala virus, have typically been thought of as just a Scandinavian disease.[26] However, in the last four years, Puumala, or a very closely related virus, has been found in Belgium, Germany, France, and Scotland.[1]

Bank voles are commonly found in much of Europe, Scandinavia, and the far western Soviet Union, but they reach their highest population densities in the Scandinavian countries[31,32] In addition to having the greatest bank vole concentrations, northern Scandinavia also sees the greatest fluctuations in bank vole populations.[31,32] Specifically, this area is north of the 60th parallel and extends to the Arctic Circle. In Sweden, hyperendemic foci have been consistently reported in Vasterbotton county, the study area for this project.[21,33] A number of authors have noted that NE is closely associated with a rural exposure and is usually an illness of adult males in the 20 to 40 year, age group.[21,26,31,33,34] The overall ratio of men to women infected is about 2:1, but in some age categories exceeds 3:1.[21,33] For reasons not entirely clear, cases in children are not common.[24]

In Scandinavia, most cases of NE occur in the late fall and early winter.[21,33] In addition to these seasonal peaks in incidence, another peak typically emerges during the late summer,

following the traditional summer vacation time.[21,33] Cases of NE occurring in the colder months have been thought to be the result of exposure to aerosolized virus from infected bank voles as the rodents seek shelter from the cold in human dewellings.[26,31] In contrast, the evidence suggests that summertime cases are associated with humans going to where the rodents live. For example, summertime activities like camping or hiking or cleaning out barns have all resulted in cases.[35]

At least three distinct disease patterns emerge for NE and clearly are closely related to the ecology of the rodent reservoir:[36]

1. Sporadic forest-associated cases that typically occur in the summer and very early fall months (usually work or recreation related);
2. Late fall cases associated with crop harvesting times;
3. Winter cases associated with the intrusion of infected rodent reservoirs, and the subsequent virus contamination of human dwellings and/or food storage structures.[37]

Thus, NE is fundamentally a reservoir borne, rural, seasonal, gender-related, and occupationally or recreationally related disease.

3.1.3.4. The Transmission of Puumala Virus

Person-to-person transmission of Puumala virus has not been reported and does not appear to occur.[21,38] Adding clear evidence for airborne transmission of Puumala virus, several laboratory workers and animal handlers in Japan, Belgium, Holland, and England have become infected after exposure to infected laboratory rat colonies.[39,40] Both epidemiologic evidence[41] and experimental evidence[42] strongly suggest viral transmission between rodents and from rodents to humans via aerosolized virions from infectious rodent excreta.[43,44,45] Therefore, Puumala virus is carried to humans by aerosols, more than likely from infected respiratory droplets, from healthy or asymptomatic, species-specific rodent carriers. These specific rodent reservoirs

contaminate the environment by excreting the virus from their lungs, in saliva and in urine. Subsequently, virus aerosolization leads to transmission.

In Sweden, above the Limes Norrlandicus (about 60^{0}N), bank vole population densities vary dramatically on roughly a 3-5 year cycle.[1] New cases of NE are highly correlated with peak bank vole cycles.[21,26,33,46,47,48,49] During one four-year period covering a complete bank vole population cycle, crude annual incidence rates for all of Sweden were about 1.3 cases per 100,000 population. During the same time period, but, within a known highly endemic areas, the number of cases reached as high 9.7 per 100,000 people per year.[33] In contrast, annual incidence rates climbed to more than 20 per 100,000 during the single year when bank vole population densities peaked.[21] Also worth noting, antibody prevalences to Puumala virus increased in people as time of residence within a known endemic area increased.[21] Human seroprevalences exceeding 10% have been found in the endemic regions of Sweden.[21] Niklassen et al. compared seroprevalence with incident cases of NE and concluded that as many as 14 to 20 infections may occur for each case that required hospitalization.[50] In other areas of Europe, Clement noted a 1.35% seroprevalence of hantavirus antibodies in people.[51] Small mammal serosurveys have found the bank vole to be the principal reservoir for Puumala virus and have found this species most commonly positive for both antigen and antibody in Europe.[35] This led McKee et al. to conclude that the majority of cases confirmed as HFRS in Europe, (excluding the Balkan region) are the result of aerosolized exposure to Puumala virus.[35]

3.1.3.5. Pathogenesis

In humans, the underlying pathology as a result of Puumala virus infection is vascular damage at the endothelial cell level. Capillaries and small blood vessels are dilated and leak plasma and other cellular elements into the surrounding tissues.[52] Circumstantial evidence from animals appears to implicate both a direct viral invasion of endothelial cells and an indirect, immunopathologic mechanism.[53,54] In patients with NE, Puumala virus may cause nodular

thickening of the renal arteriolar walls and glomerular basement membrane, interstitial edema, and interstitial renal illness.[26,27,55,56] There is also considerable evidence for the activation of the interrelated complement, coagulation, and kinin cascades during the early stages of illness; this has led some investigators to suspect an immunopathologic mechanism for NE.[57] Consequently, the name hemorrhagic fever with renal syndrome adequately describes the disease processes involved in patients with NE.

3.1.3.6. Treatment of Nephropathia Epidemica

Like all potentially serious illnesses, treatment of patients with NE is highly individualized. Although, supportive care remains the most important facet of clinical management, responding to other medical needs is also essential. Attention to fluid balance and volume, electrolyte and acid-base status is also important. Peritoneal dialysis or hemodialysis may become necessary as the illness progresses. Finally, the use of ribavirin as a specific antiviral therapy has been defended by Huggins et al.[58]

3.1.3.7 Prevention and Control

The high risk of NE associated with exposure to infective rodent aerosols is well documented. Therefore, prevention of NE focuses on effective rodent control measures, as well as the avoidance of infected rodents and their habitats. Using another approach, human vaccine clinical trials with inactivated mouse or rat brain preparations are underway.[59] Although expected in the not to distant future, no hantavirus vaccines are currently available for widespread use.

3.1.4. Summary

In summary, at least five specific viruses of the family Bunyaviridae, genus *Hantavirus*, are known to cause an extremely wide range of clinical maladies. Clinical afflictions can range from an asymptomatic infection to a severe illness requiring renal dialysis. It is not uncommon to have

deaths resulting from sever complications. Clinically, HFRS is characterized by fever, followed by a broad range of hemorrhagic manifestations, and mild to severe renal dysfunction. Within the genus Hantavirus, Hantaan virus (the prototype) is known to cause one of the severe forms of HFRS in Korea and China called, Korean hemorrhagic fever and Epidemic hemorrhagic fever, respectively. Within the last three years, another Hantavirus named Porogia virus, was isolated from the Balkan area of south Europe. Like Hantaan virus, Porogia virus also causes an especially severe illness, with similar case-fatality rates, ranging from 5-20%.[60] Hantaviruses that are antigenically related to Hantaan virus but result in much less severe, even mild illnesses, also exist. For example, Seoul virus was isolated in Korea, while Puumala virus results in nephropathia epidemica in Scandinavia, Europe, and the far western Soviet Union. It is entirely possible that additional Hantaviruses will be isolated in the very near future. All the diseases of this group have been classified as HFRS, even though they have a global distribution. Strong scientific evidence exists to support the argument that viruses of the genus *Hantavirus* are maintained in nature in chronically infected, asymptomatic, species-specific small mammal hosts. Human illness results from environmental contamination and subsequent aerosolization of the virus. The risk of human disease from this distinctive group of pathogens continues to grow. Therefore, further study surrounding innovative methods to predict the risk of human disease is justified.

3.1.5. References

1. LeDuc JW. Epidemiology of HFRS. Rev Infect Dis 1989; 11 (Suppl 4).

2. Lee HW, van der Groen G. HFRS. In: Melnick JL, ed. Prog Med Virol. Vol. 36. Basel: Karger, 1989:62-102.

3. Lee HW. HFRS. Scand J Infect Dis 1982; 36 (Suppl 1]:82-5.

4. Gajdasek CD, Goldfarb LG, Goldgaber D. Bibliography of hemorrhagic fever with renal syndrome. 2nd ed. NIH publication no. 88-2603, August 1987.

5. WHO. HFRS. Memo from a WHO meeting. Bull WHO 1983; 61:269-75.

6. Gajdusek DC. Muroid virus nephropathies and muroid viruses of the Hantaan virus group. Scand J Infect Dis 1982; 36 (Suppl):96.

7. The Executive Committee of the International Committee on Taxonomy of Viruses, Minutes of the 17th Meeting, 1987:1-14.

8. Lee HW, Lee PW. Korean hemorrhagic fever. I. Demonstration of causative antigen and antibodies. Korean J Intern Med 1976; 19:371-84.

9. Lee HW, Lee PW, Johnson KM. Isolation of the etiologic agent of Korean hemorrhagic fever. J Infect Dis 1976; 137:298-308.

10. Lee HW. HFRS in Korea. Rev Infect Dis, 1989. [McKee KT, LeDuc JW, Peters CJ. Hantaviruses. In: Belshi RB, ed. Textbook of human virology. 2nd ed. 1991:617]

11. Lee PW, Gajdusek DC, Gibbs CJ, et al. Aetiologic relationship between Korean hemorrhagic fever and epidemic haemorrhagic fever with renal syndrome in the People's Republic of China. Lancet 1980; i:819-20.

12. Lee HW. Seroepidemiologic studies of acute hemorrhagic diseases in Korea from 1984-1987 (HFRS, Leptospirosis, and Scrub typhus). J Korean Med Assn 1988; 31:581.

13. Lee HW, Lee PW, Laehdvirta J, et al. Aetiologic relationship between Korean hemorrhagic fever and NE. Lancet 1979; i:186-7.

14. Lee HW. Seroepidemiologic studies of acute hemorrhagic diseases in Korea from 1984-1987 (HFRS, Leptospirosis, and Scrub typhus). J Korean Med Assn 1988; 31:583.

15. Lee PW, Svedmyr A, Gajdusek DC, et al. Antigenic differences between European and East Asia viruses causing hemorrhagic fever with renal syndrome. Lancet 1981; ii:256-7.

16. Svedmyr A, Lee PW, Gajdusek DC, et al. Antigenic differentiation of the viruses causing Korean hemorrhagic fever and epidemic nephropathy of Scandinavi. Lancet 1980; ii:315-6.

17. LeDuc JW. Epidemiology of Hantaan and related viruses. Lab Anim Sci 1987; 413-8.

18. Brummer-Korvenkontio M, Vaheri A, Hovi T, et al. Nephropathia epidemica: detection of antigen in bank voles and serologic diagnosis of human infection. J Infect Dis 1980; 141:131-4.

19. Giebel LB, Stohwasser R, Zoller L, Bautz EK, Darai G. Determination of the coding capacity of the M genome segment of NE virus strain Hallnas BL by molecular cloning and nucleotide sequence analysis. Virology 1989; 172(2):498-505.

20. Benenson AS. Control of communicable diseases in man. 14th ed. Washington, DC: The American Public Health Association, 1990.

21. Niklasson B, LeDuc JW. Epidemiology of nephropathia epidemica in Sweden. J Infect Dis 1987; 155:269-76.

22. Garrilorskaga IN, Apekina NS, Myasnikov, YA, et al. Features of circulation of HFRS virus among small mammals in the European USSR. Arch Virol 1983; 75:313-6.

23. Van Ypersele de Strihou C, Mery JP. Virus-induced interstitial nephropathy: the hantavirus as an ubiquitous model. In: Davison AM , ed. Nephrology Proc Congr Nephrology, London, 1988; 2:802-31.

24. Settergren B, Juto P, Trollfors G, et al. Hemorrhagic complication and other clinical findings in NE in Sweden; a study of 355 sero-verified cases. J Infect Dis 1988; 157:380-2.

25. Johnson KM. Principles and practice of infectious disease, Chapt 12. In: Mandell/ Douglas/Benett, eds. Hantaviruses. 3rd ed. 1990.

26. Lahdevirta J. NE in Finland. A clinical, histological and epidemiological study. Ann Clin Rev 1971; 3 (Suppl 8):1-154.

27. Lahdevirta J, Collan Y, Jokinen EJ, et al. Renal sequelae to NE. Acta Pathol Microbiol Scand 1978; 86(A):265-71.

28. Lahdevirta J, Savoa J, Brummer-Korvenkontio M, et al. Clinical and serological diagnosis of NE, the milder type of a HFRS. J Infect Dis 1984; 9:230-8.

29. Lahdevirta J. The minor problem of hemostatic impairment in NE, the mild form of HFRS. Rev Infect Dis 1989; 11: S860-3.

30. Schmaljohn CS, Hasty SE, Dalrymple JM, et al. Antigenic and genetic properties of viruses linked to HFRS. Science 1985; 227:1041-4.

31. Nystrom K. Incidence and prevalance of endemic benign (epidemic) nephropathy in AC County [Vasterbotton], Sweden in relation to population density and prevalence of small rodents [Dissertation]. Umeå, Sweden: Umeå University, 1977.

32. Corbet GB. The mammals of the alaeartic region: a taxonomic review. Ithaca, NY: British Museum, Cornell Univ Press, 1978:1-314.

33. Settergren B, Juto P, Wadell G, et al. Incidence and geographic distribution of serologically verified cases of NE in Sweden. Am J Epidemiol 1988; 127:80.

34. Ornstein K, Soderhjelm L. Nephropathia epidemica. Med Welt 1965;17:898-901.

35. Belshi RB, ed. Textbook of human virology. 2nd ed. McKee KT, Leuc JW, Peters CJ. Hantaviruses. Chapter 22, 1991:616.

36. Johnson KM. Principles and practice of infectious disease. Chapt 12. In: Mandell/ Douglas/Benett, eds. Hantaviruses. 3rd ed. 1990.

37. Casals J, Henderson BE, Hoogstraal HH, et al. A review of Soviet HFRS. J Infect Dis 1970; 122:437-53.

38. Niklasson B, Nyman L, Linde A, Grandiea M, Dalrymple J. An epidemiological survey of NE in Sweden. Scand J Infect Dis 1983; 15(3):239-45.

39. LeDuc JW. Epidemiology of hemorrhagic fever viruses. Rev Infect Dis 1989; 11 (Supp 4).

40. Desmyter J, LeDuc JW, Johnson KM, et al. Laboratory rat associated outbreak of HFRS due to Hantaan-like virus in Belgium. Lancet 1983; 2:1445-8.

41. Xu Z-Y, Guo C-S, Wu Y-L, Zhang XW, Liu K. Epidemiological studies of hemorrhagic fever with renal syndrome: analysis of risk factors and mode of transmission. J Infect Dis 1985; 152:137-44.

42. Nozum EO, Rossi CA, Stephenson EH, LeDuc JW. Aerosol transmission of Hantaan and related viruses to laboratory rats. Am J Trop Med Hyg 1988; 38(3): 636-40.

43. Lee HW, Lee PW, Baek LJ, Song CK, Seong IW. Interspecific transmission of Hantaan virus, etiologic agent of Korean hemorrhagic fever, in the rodent Apodemus agrarius. Am J Trop Med Hyg 1981; 30:1106-12.

44. Lee HW, French GR, Lee PW, Baek LJ, Tsuchiya K, Foulke RS. Observations on natural and laboratory infection of rodents with the etiologic agent of Korean hemorrhagic fever. Am J Trop Med Hyg 1981; 30:477-82.

45. Yanagihara R, Amyx, Gajdusek DC. Experimental infection with Puumala virus, the etiologic agent of Nephropathia epidemica, in bank voles (C. glareolus). J Virol 1985; 55:34-8.

46. Nystrom K. The incidence and prevalence of endemic benign (epidemic) nephropathy in AC County, Sweden, in relation to population density and prevalence in small rodents. Acta Med Scand 1977; 609 (Suppl):1.

47. Korpela H, Lahdevirta J. The role of small rodents and patterns of living in the epidemiology of NE. Scand J Infect Dis 1978; 10:303.

48. Nystrom K. Epidemiology of HFRS (endemic benign nephropathy) in Sweden. Scand J Infect Dis 1982; 36 (Suppl):92.

49. Sommer AI, Traavik T, Mehl R, Berdal BP, Dalrymple J. HFRS (NE) in Norway: seroepidemiology 1981-1985. Scand J Infect Dis 1988; 20(3):267-74.

50. Niklasson B, LeDuc JW, Nystrom K, et al. NE: Incidence of clinical cases and antibody prevalence in an endemic area of Sweden. Epidemiol Infect 1987; 99:559-6.

51. Clement J, Lefevre A, Verhagen R, et al. Hantavirus nephropathy in Belgium [Abstract]. 25th Congress of the European Dialysis and Transplant Assoc-Euro Renal Assoc, Madrid, 1988.

52. Giles RB, Langdon EA. Blood volume in epidemic hemorrhagic fever. Am J Med 1954; 16:654-61.

53. Tsai TF, Bauer S, McCormick JB, et al. Intracerebral inoculation of suckling mice with Hantaan virus. Lancet 1982; 2:503-4.

54. McKee KT Jr, Kim GR, Green DE, et al. Hantaan virus infection in suckling mice. Virologic and pathologic correlates. J Med Virol 1985; 17:107-17.

55. Lahdevirta J, Collan Y, Jokinen EJ, et al. Renal sequelae to NE. Acta Pathol Microbiol Scand 1978; 86(A):265-71.

56. Collan Y, Lahdevita J, Jokinen EJ. Electron microscopy of NE. Am J Pathol 1978; 92:167-72.

57. Penttinen K, Lahdevirta J, Kelomaki R, et al. Circulating immune complexes, immunoconglutinins and rheumatoid factors in NE. J Infect Dis 1981; 143:15-21.

58. Huggins JW, Hsiang CM, Cosgriff TM, et al. Intravenous ribavirin therapy of HFRS [Abstract]. Antiviral Res 1988; 9:123.

59. Lee HW, An CM. Development of vaccine against HFRS. J Korean Soc Virol 1988; 143-8.

60. Gajdasek DC. Muroid virus nephropathies and muroid viruses of the Hantaan virus group. Scand J Infect Dis 1982; 36 (Suppl):108.

3.2. THE ANIMAL RESERVOIR

3.2.1. Bank Vole Ecology

The bank vole, specifically *Clethrionomys glareolus*, is one of the most common and widely distributed mammalian species in Europe and Asia. As a result, a very large set of data has been collected on the ecology of this species.[3] Bank voles, also known as red-backed mice, belong to the order Rodentia, the superfamily Muridae, and the genus *Clethrionomys*. Although within the genus *Clethrionomys* there are seven species of bank voles,[1,2,3] this section will focus on *C. glareolus*. As a matter of reference, other members of the Muridae family include rats, mice, hamsters, lemmings, and gerbils.[3,4]

Generally, the adult bank vole head and body length ranges from 70 to 112 mm, tail length is from 25 to 60 mm, and mean body weight is about 18 gm.[3] Compared to the shorter, more rough summer fur, the winter fur is smooth, soft, dense and relatively long.[4] The common name "red-backed mouse" was, no doubt, derived from the bank vole's pronounced reddish coloration over the dorsum. The red is much less prominent on the sides, which have a grayish color, while the ventral fur appears almost white. As with most Muridae, the bank vole's eyes and ears are prominent.[4]

The bank vole's habitat is extremely variable, matching their extensive geographic distribution. They do however, prefer colder climates, mossy, rocky forests and woodlands in both dry and damp areas.[3] They also inhabit tundra and bogs.[4] Bank voles remain active throughout the summer and winter.[4] They can be seen scurrying about stumps, fallen branches, and even climbing rough-barked trees, both during the day and at night.[4] The importance of vegetational cover for the Bank vole has been discussed by numerous authors.[3,5]

Vegetation is used not only for cover, but also for food. Bank voles have a fairly well-developed cecum and an extensive mechanism for retrograde transport of small food particles and bacteria in the proximal part of the large intestine.[6] Therefore, the bank vole is efficient in utilizing foods rich in cellulose. The diet of *Clethrionomys spp.* consists of tender

vegetation, leaves, nuts, seeds, bark, lichens, fungus, and some insects. They also have been known to store some food items in their nests for consumption at a later time. In a 1985 study conducted by Viro and Sulkava, where stomach contents were inventoried; they commonly found lichens in gastric contents (especially Alectoria spp. and Bryoria spp.) and concluded that epiphytic beard lichens were an important food for bank voles. Bank voles, in turn, serve as a food source for several predators, such as Tengmalm's owls, other raptors (birds of prey), the red fox, and other carnivorous fur-bearing animals. In fact, predator population cycles frequently follow bank vole population cycles.[5]

Bank vole reproductive patterns have been well documented.[7] Their breeding season can begin before the end of winter and continue through fall. The gestation period is about 18 days, with an average litter size of about six.[8] Each mature female bank vole bears three or four litters per breeding season.[3] Newborns weigh about two grams at birth, open their eyes between 9 and 15 days of age, and are usually independent three weeks after birth.[3] The young of the spring litters are able to bear their own young when they are about four months old.[3] Although difficult to document in the wild, several investigators have found the life span of bank voles from Scandinavia and the central Soviet Union to be about 15 months.[9] Nonetheless, the life span of a specimen of *C. Glareolus*, housed in captivity, was almost five years.

3.2.2. Bank Vole Population Dynamics

Banfield noted that bank vole populations fluctuate from year to year, but with no readily apparent periodicity.[10] For example, a study conducted by French, Stoddard, and Bobek found population densities of bank voles in Eurasia, ranged from less than 1 to almost 100 individuals per hectare (ha) depending on the year. They also noted the average home range of *C. glareolus* was calculated to be 0.82 ha for males and 0.71 ha for females.[11] Saitoh studied changes in bank vole population densities and home ranges in the northern hemisphere with similar results.[12] On the other hand, Andrzejewski, estimated home ranges of between 3.5 to 7.0 ha for bank voles.[13]

Bank vole populations also show cyclic fluctuations.[14] Especially in central and northern Fennoscandia (Finland, Sweden, and Norway), voles show significant population swings.[15,16] Lahti et al. and Hornfeldt described vole cycles which were characterized not only by a somewhat regular 3 to 5 year periodicity between peak population cycles, but also by a large variability in the highest of the peaks.[5,16] In other words, the frequency of vole population cycles was relatively predictable on a 3 to 5 year schedule. However, the amplitude or total number of voles per cycle was much less predictable.

Numerous theories have been developed to explain the variability in vole population dynamics.[3] Several authors found that in years of abundant acorn and beech mast, vole populations experienced an especially low winter mortality, thus allowing for particularly high numbers of breeding animals to begin the spring breeding season. Petrusewicz summarized some of the factors which could potentially influence the instability in bank vole populations:[3] genetic and/or physiological and abiotic factors like thermoregulation in neonatal rodents; quality and quantity of food supply or other environmental factors; time to maturation; and spacing and social behavior, just to mention a few.[5,17] Hansson described a "maternal effect" in bank voles, which occurs early in the life of autumn-born baby voles from mothers living under good nutritional conditions. Baby voles from these litters matured earlier and thus were able to conceive earlier in the following spring.[5] Therefore, one can conclude that it is possible that the effect of excellent food conditions will eventually contribute to rapidly increasing vole numbers. On the other hand, as food conditions deteriorate, because of peak population densities, reproduction could slow to well below the morality rate. Support for this explanation of bank vole population cycles comes from Hornfeldt's dissertation, where he describes several laboratory experiments that clearly showed earlier breeding times, larger litter sizes, and decreased neonatal mortality in bank voles that received food supplementation.[5] He also noted that under field conditions, moderate ambient temperatures; increased food supplies, and caused the average vole breeding season to be longer than normal.[5]

3.2.3. The Bank Vole as a Reservoir for Puumala Virus

It should also be noted, although Puumala virus has been demonstrated in a number of other rodent species, such as *C. rafocanus, Apodemus flavicollis, Rattus norvegicas*, unlike the bank vole, their importance in the transmission of virus to humans has not yet been established.[21] There is strong scientific evidence confirming the bank vole as the main source of the agent that causes human hemorrhagic fever with renal syndrome (HFRS), specifically NE.[18,19] Evidence for *C. glareolus* as the major reservoir of the particular Hantavirus named Puumala virus, is abundant.[19,20,21]

It appears that Puumala virus and the bank vole have co-evolved from a parasite-host relationship to almost a commensal relationship. Verhagen trapped and tested bank voles for antibodies to Hantavirus and found absolutely no difference in the survival rates between seropositive and seronegative rodents.[21] He found "that the rodents underwent no measurable effect when infected with Hantavirus." This led him to conclude that Hantavirus infection probably "does not have an injurious effect to the health of the animal."[21] In addition, well-controlled laboratory experiments studying the virus-host relationship and transmission of virus among rodents, confirm a highly evolved and compatible relationship between Puumala virus and the bank vole, *C. glareolus*.[22]

3.2.4. The Potential for Predicting Bank Vole Population Cycles with Remote Sensing Data

Briefly summarizing, scientific evidence has established the bank vole as the main reservoir and source of Puumala virus, the etiologic agent of human hemorrhagic fever with renal syndrome (HFRS). Additionally, definite bank vole population fluctuations occur, usually in a 2-5 year cycle, where peak rodent population densities are highly correlated with HFRS in people. Given these facts about the bank vole and its population dynamics, this sub-section will identify

five characteristics of the bank voles' environment that could potentially lead to predicting population cycles using satellite remote sensing.

1. Verhagen in two studies conducted in Belgium found a very close association between wet or very humid habitat types and the presence of Hantavirus-positive bank voles.[23] Several other authors have noted that the bank vole prefers wet habitats.[24] From these studies, three important points emerge: first, voles associated with wet habitats were consistently at greater risk for Puumala virus sero- conversion; second, wet habitats were usually associated with a much greater green biomass (green biomass is a specific parameter that can be detected from a satellite); and finally, water, generally, has an especially distinct spectral response pattern, thus improving a satellite sensor's ability to detect accurately this environmental factor also.

2. Hörnfeldt et al. suggested a model for explaining vole population fluctuations: "vole - food plant interactions trigger the cycle of voles."[5]

3. Hörnfeldt also described the voles of Fennoscandia as "the dominant herbivore" and how important their population dynamics may be to the food vegetation of the area.[25] He indicated that the existence of plant production rhythms may play a significant role as a possible trigger to vole cycles. Hörnfeldt noted that other investigators also believe that plant production cycles are important in helping to explain vole cycles.[26] As an environmental parameter, 'green biomass' can be monitored relatively accurately using satellite sensors.

4. The 100 km^2 study area lies within the county of Vasterbotten, shown by Niklasson and LeDuc to have the highest incidence and sero-prevalence of Puumala virus antibody in both people and bank voles.[19]

5. Lapin wrote that the distribution of the bank vole depended on the density of vegetation, and that more rodents can be found at forest edges,[27] particularly when a forest edge is adjoined by croplands.[28] This is significant because bank voles are primary consumers or herbivores, and since their diet consists mainly of green plants or seeds, the use of a vegetation

index should correlate with available food, which in turn should correlate with bank vole cycles.

3.2.5. References

1. Corbet GB. The mammals of the palaearctic region: a taxonomic review. London: British Museum of Natural History, 1978:314.

2. Hall ER. The mammals of North America. New York: John Wiley & Sons, 1981.

3. Petrusewicz K, ed. Ecology of the bank vole. Acta Theriol 1983; 28 (Suppl No.1):2.

4. Norwak RM, Paradiso JL. Walker's mammals of the world. 4th ed. Vol II. Baltimore: Johns Hopkins University Press,1983:656-7.

5. Hornfeldt B. Synchronous population fluctuations in voles, small game, owls, and tularemia in northern Sweden. Oecologia (Berlin) 1978; 32:141-52.

6. Sperber I, Bjornhag G, Riddertrale Y. Function of proximal colon in lemming and rat. Swedish J Agric Res 1983; 13:242-56.

7. Krebs CJ, Meyers JH. Population cycles in small mammals. Adv Ecol Res 1974; 8:267-399.

8. Wrangel H, 1940. [In: Petrusewicz K, ed. Ecology of the bank vole.]. Acta Theriol 1983; 28 (Suppl 1).

9. Ilyenko AJ, Zubchaninova EV, 1963; Schwarz SS, et al. 1964; Bergstedt B, 1965; Kaikusalo A, 1972. [In:Petrusewicz K, ed. Ecology of the bank vole.]. Acta Theriol 1983; 28 (Suppl 1).

10. Banfield AWF. The mammals of Canada. Univ of Toronto Press, 1974:XX-438.

11. French CH, Stoddard DM, Bobek B. Patterns of demography in small mammal populations. In: Golley FB, Petrusewicz K, Ryszkowski L, eds. Small mammals: their productivity and population dynamics. London: Cambridge Press, 1975:73-102.

12. Saitoh T. Survival rate and mobility in an enclosed population of red-backed voles. Acta

Theriol 1983; 28(19):301-15.

13. Andrzejewski R, Babinska WT. Bank vole populations, are their densities high and home ranges small? Acta Theriol 1986; 31 (27-41):409-22.

14. Pruitt WO, 1968; Grodzinski W, 1971; Koshkina TV & Korotkov YS, 1975; Fuller WA, 1977; Wiger R, 1979. [In: Petrusewicz K, ed. Ecology of the bank vole.] Acta Theriol 1983; 28 (Suppl 1).

15. Lofgren O, Hornfeldt B, Carlsson B-G. Site tenacity and nomadism in Tengmalm's owl in relation to cyclic food production. Oecologia 1986; 69:321-6. {See other refs: Myllymaki et al.'77; Hornfeldt '78; Hanson '79; Hornfeldt et al. '86; Hornfeldt '91.}

16. Lahti S, Tast J, Uotila H. Fluctuations in small rodent populations in the Kilpisjarvi area 1950-1975. Luonnon Tutk 1976; 80:90-107 (english abstract). [In: Hornfeldt B, Lofgren O, Carlsson B-G. Cycles in voles and small game in relation to variations in plant production indices in northern Sweden. Oecologia (Berlin) 1986; 68:496-502.]

17. Alibhai SK, Gipps JHW. The population dynamics of bank voles. Symp Zool Soc Lond 1986; 55:277-313.

18. Brummer-Korvenkontio M, Vaheri A, Hovi T, et al. NE: Detection of antigen in bank voles and serologic diagnosis of human infection.

19. Niklasson B, LeDuc JW. Epidemiology of NE in Sweden. J Infect Dis 1987; 155:269-76.

20. Sommer AJ, Traavik T, Mehl R, Berdal BP, Dalrymple JM. Reservoir animals for NE in Norway: indications of a major role for the bank vole. J Hyg Camb 1985; 94:123-7.

21. Verhagen R, Leirs H, Tkachenko E, van der Groen G. Ecological and epidemiological data on Hantaviruses in bank vole populations in Belgium. Arch Virol 1986; 91:193-205.

22. Tsai FT. Hemorrhagic fever with renal syndrome: mode of transmission to humans. Lab Anim Sci 1987; 37(4): 428-30.

23. Verhagen R, Leirs H, Tkachenko E, van der Groen G.Ecological and epidemiological data on Hantavirus in bank vole populations in Belgium. Arch Virol 1986; 91:193-205.

24. Turcek FJ, 1960; Bergstedt B, 1965; Chelkowska H, 1969; Lozan MN, 1971; Bock E, 1972; Bolshakov VN and Vasilev AG, 1975. [In: Petrusewicz K, ed. Ecology of the bank vole.] Acta Theriol 1963; 28 (Suppl 1).

25. Hornfeldt B, Lofgren O, Carlsson B-G. Cycles in voles and small game in relation to variations in plant production indices in northern Sweden. Oecologia (Berlin) 1986; 68:496-502.

26. Svardson G, 1957; Lauckhart JB, 1957; Kakela O, 1962; Tast J. & Kalela O, 1971; Hansson L, 1979; Laine K and Henttonen H, 1983. [In: Hornfeldt B, Lofgren O, Carlsson B-G. Cycles in voles and small game in relation to variations in plant production indices in northern Sweden. Oecologia (Berlin) 1986; 68:496-502.

27. Lapin IM, 1963. [In: Petrusewicz K, ed. Ecology of the bank vole.] Acta Theriol 1963; 28 (Suppl 1).

28. Curry-Lindah L, 1959. [In: Petrusewicz K, ed. Ecology of the bank vole.] Acta Theriol 1963; 28 (Suppl 1).

3.3. SOME PRINCIPLES OF SATELLITE REMOTE SENSING

3.3.1. An Introduction

The sun continuously showers packets of electromagnetic energy in the form of photons onto the surface of the earth. This energy is either scattered, transmitted, absorbed, and/or reflected. The exact fate of a photon is dependent upon its wavelength, the molecules and particles suspended within the earth's atmosphere, and characteristics of the landscape or the target. It is the interaction of this electromagnetic energy with a target on the surface of the earth that is available for detection by sensors mounted on earth-orbiting satellites. Section 3.3 on the principles of satellite remote sensing, will be divided into four major parts. The first will explain in a general way how solar energy is influenced even before it is detected by a sensor. The second part will contain information on the current applications of satellite remote sensing to the science of epidemiology. Part three will detail the specific characteristics of the satellite system used for this project, namely the NOAA-9 spacecraft and the AVHRR sensor. Finally, part four will illustrate how the Normalized Difference Vegetation Index (NDVI) has unique potential for use as an environmental marker.

3.3.2. An Overview of Satellite Remote Sensing

Figure 3.3-1 illustrates some of the individual components that are required to obtain a digital image for analysis.[23] While some of the incoming solar energy or electromagnetic radiation is significantly influenced by the earth's atmosphere, what's left reaches the earth's surface. As this energy interacts with the landscape, some of it is reflected, some absorbed, and some transmitted. Each process is wavelength dependent. With satellite remote sensing, it is the reflected energy that is the most important. Ideally, each specific landscape feature will have a unique spectral response pattern or "spectral signature."[1] The reflected energy is again influenced by the earth's atmosphere before it is detected by an orbiting sensor. The sensor then records an image as an array of digital values. The digital values are organized into a scene

and are then communicated to a receiving station on earth for processing.

3.3.3. PART ONE: Factors Influencing Electromagnetic Solar Energy

3.3.3.1. Electromagnetic Energy Defined

Solar energy is composed of a whole spectrum of varying energy levels that reach the earth. The spectrum, usually categorized by wavelength, includes those visible to the human eye such as blue, green, and red light. Not only are visible wavelengths present, but other types of energy outside the range of human vision exist as well. Table 3.3-1 lists the major components of the electromagnetic spectrum by wavelength.

Table 3.3-1

MAJOR DIVISIONS OF THE ELECTROMAGNETIC SPECTRUM

Major Divisions	Range of Wavelengths
Gamma rays	<0.03nm
X-rays	0.03-300nm
Ultraviolet	0.30-0.38μm
Visible	0.38-0.72μm
Infrared	
Near-IR	0.72-1.3μm
Mid-IR	1.30-3.0μm
Far-IR	7.00-15 μm
Microwave	0.30-30 cm
Radio	≥30 cm

3.3.3.2. Satellite Remote Sensing and the Atmosphere

Any energy used for remote sensing must pass through the whole depth of the earth's atmosphere. Atmospheric effects, then, can have a significant impact on the quality of the data arriving at or coming from an orbiting sensor. As solar energy passes through the atmosphere, it can be modified by several processes, the most important of which are scattering, absorption and refraction.

The effect of scattering is to redirect the energy. Scattering results from large suspended particles like dust, pollen, smoke, volcanic ash, and water droplets. Also, small molecules like nitrogen and oxygen can cause scattering. To illustrate, consider the fact that the blue color of the sky is the result of the shorter blue wavelengths scattering more than the longer wavelengths. Thus, we see the color blue. However, in remote sensing, the effect of scattering is to degrade the quality of a digital image.

Absorption occurs when something in the atmosphere prevents or significantly attenuates both incoming or upwelling energy. Oxygen, carbon dioxide, and water vapor are responsible for most of the absorption of solar radiation. Although the amounts of atmospheric oxygen and carbon dioxide remain fairly constant, this is not the case with atmospheric water vapor. Moreover, water vapor can change drastically with both time and location. Furthermore, if the atmosphere is extremely humid, a large percentage of some wavelengths may be absorbed, thus effectively eliminating those specific wavelengths for use.

Refraction is the bending of light as it passes through atmospheric layers of varying clarity and densities. Although not as important as scattering and absorption, refraction also can affect remote sensing data quality.

3.3.3.3. Target Factors Influencing Satellite Data

Once solar energy reaches the landscape, a combination of three things will occur: the energy must be reflected, transmitted, and/or absorbed. The nature of the target, the angle of

the incoming energy, and the wavelength of the energy are the major variables which account for the proportions of energy which are reflected, transmitted, and/or absorbed from the landscape or target.

It is the amount of upwelling energy or reflected energy from a specific area, at a specific time, within a specific wavelength range, that a satellite sensor records as a brightness value. In this study, brightness values were recorded in the range from 0 to 1024, with 0 as absolute black and 1024 as the brightest value. In other words, there were 1025 quantizing levels or possible shades of gray, for each grid cell or picture element (also known as a pixel). Each pixel was assigned a digital brightness value, and all the pixels together made up the digital image or scene. A typical scene will contain 1000 scan lines with 2048 pixels. This translates into an area of about 1100 km long and 2700 km wide. Key variables influencing the brightness values for each individual pixel include atmospheric quality, the specific spectral profile or spectral response pattern (also known as the "spectral signature") of the target, the size of target area, the angle and intensity of the solar energy, and sensor capability.

Transmission of energy occurs when solar energy passes through an object without being attenuated. The ability of an object to transmit energy is both a function of the wavelength and the makeup of the target.

Lastly, the specific target or landscape feature may absorb solar energy and subsequently reradiate or emit that energy. If energy is absorbed and then emitted, the emitted energy is almost always at much longer wavelengths, usually in the thermal ranges.

In summary, there are a number of variables which can influence the quality of a digital image. The most important variables are the amount and type of incoming energy, atmospheric effects, and target or landscape factors.

3.3.4. PART TWO:

The Application of Satellite Remote Sensing Techniques to Epidemiology

In 1970, Cline recommended serious investigation of the relationships between remotely sensed, landscape parameters and wildlife populations of reservoir hosts.[2] Twenty years later, Cibula wrote,

> "If for example, a given disease vector can be identified for range and extent by specific plant associations or communities, then this range can be identified and mapped if these specific vegetation types can be classified separately from other vegetation types to be found in a given area."[3]

A number of examples currently exist in which satellite-acquired data has either helped to explain or shows great potential to account for epidemiologic phenomena. For example, throughout much of Africa, a mosquito-borne virus that is responsible for serious disease outbreaks in both humans and livestock is Rift Valley Fever (RVF). Specifically in Kenya, epizootics of RVF occur every five to fifteen years.[5] Interval length is the direct result of large numbers of mosquito-vector populations brought about by greatly increasing mosquito breeding sites as a result of flooding.[4] Using data collected from satellites, Linthicum found that RVF epizootics could be predicted by monitoring vegetation.[5] In addition to RVF, Nicholls in 1986 suggested a method for predicting Murray Valley Encephalitis (MVE) outbreaks in Australia using climatic fluctuations.[6] Like RVF, MVF is also a mosquito-borne virus, and mosquito population cycles are rainfall dependent. It is known that rainfall amounts are highly correlated with vegetation indices.[30] More importantly, vegetation indices can be calculated from satellite acquired data. It stands to reason that satellite data could potentially predict MVE epidemics. In fact Kay, in 1980, evaluated several methods, which were compatible with satellite remote sensing, for predicting MVE activity.[7] Other arboviruses, such as Ross River virus, which cause epidemic polyarthritis in humans, and Akabane virus, which results in fetal abnormalities in cattle, are also thought to be correlated with rainfall fluctuations.[8] Thus, making them potential candidates for satellite remote

sensing analysis, as well.

In order to make mosquito control efforts cost effective, Hayes and colleagues described a method, using data acquired from earth-orbiting satellites, to identify mosquito larval habitats associated with specific fresh-water plant communities along the waterways of the Missouri River.[9] To illustrate further the potential for using satellite data as a public health tool, Barnes and Cibula described the use of satellite imagery for classifying vegetation types and landscapes that had public health and insect vector control significance.[10] A number of other examples have been published, regarding the use of satellite imagery to help document or predict the risk of human disease. Examples include malaria,[11] trypanosomiasis,[12] Lyme disease,[13] schistosomiasis,[2] yellow fever,[2] dengue fever,[2] and Venezuelan equine encephalomyelitis.[2]

3.3.5. PART THREE: The NOAA-9 Spacecraft and the AVHRR Sensor

3.3.5.1. An Introduction to the NOAA Series Satellites

According to Jack Villmow, "The first weather satellite was hailed as the equivalent to meteorology in the twentieth century that the telescope had been to astronomy in the seventeenth century."[14] Since the launch of the first meteorological satellite, in April 1960, great strides have been made in the field of remote sensing, but especially in weather monitoring. In the last 32 years, spacecraft design, onboard sensing equipment, as well as ground-support systems, have all experienced enormous advances. Technological improvements have also been noted in data acquisition, data processing capability, and information utilization. There has also been an equivalent concurrent increase in the demand for this technology, both from the basic scientific research community and from those interested in the direct applications of satellite-acquired information.[15] All of these advances have occurred because more people are interested in better understanding some of the processes influencing the balance between the earth's resources and its biological systems and subsystems.

An example of evolving, weather satellite technology providing information about earth's

environs, is the NOAA-9 spacecraft. The NOAA-9 satellite system evolved from the proven technology of the TIOS (Television and Infrared Observation System) and ITOS-1 (Improved TIROS Operational System) satellite systems.[16] Subsequent spacecraft in this series were named NOAA-1, NOAA-2, through NOAA-10.[16] The equipment, sensors, and operational techniques employed on the early satellites have been enhanced and improved with each launch. This orderly and logical evolution has resulted in constant improvements, from the early spin-stabilized spacecrafts to the current three-axis-stabilized, earth-oriented, despun space platforms like that of the NOAA-9.[17]

Part three, describing the NOAA-9 satellite, will contain three major divisions. Beginning with an overview of the spacecraft and its instrumentation, highlighting the AVHRR sensor; next will follow a section explaining how the NOAA-9 is controlled and how it communicates data. Finally, the third section will describe some of the strengths and limitations of the NOAA-9, again focusing on the AVHRR sensor.

3.3.5.1.1. The NOAA-9 Spacecraft and Its Components

3.3.5.1.1.1. General Description

Except for the sensors, the NOAA-9 was built by RCA Astro-Space Division, of General Electric, in Hightstown, New Jersey.[21] On December 12, 1984,[20] the NOAA-9 was placed on top of an Atlas E rocket and launched from Vandenberg Air Force Base (located along the California coast, near Lompoc, CA) by the United States Air Force under contract to The National Oceanic and Atmospheric Administration (NOAA-7's launch date was June 1981).[16] Designed specifically to provide information for both weather prediction and weather monitoring, the NOAA-9 is

currently just partially operational,* while continuing to orbit in a sun-synchronous, near-polar orbit. The National Oceanic and Atmospheric Administration (NOAA) funds and manages the entire NOAA satellite series from its Satellite Operational Control Center in Suitland, MD.[21] At least twelve (including ITOS-1 and TIROS-N) satellites have flown in the NOAA series. The even-numbered missions have a north-to-south equatorial crossing time at 7:30AM, while the odd-numbered missions have a nighttime (2:30AM), north-to-south equatorial crossing time.[22] As mentioned above, the NOAA-9 travels in a sun-synchronous, near-polar orbit. Satellites in sun-synchronous orbits are oriented so the plane of the satellite orbit maintains a constant angular relationship with the sun.[24] The satellite maintains its sun-synchronous orbit and precesses (rotates) eastward about the earth's polar axis 0.986^0each day, which is the same rate and direction as the earth's average daily rotation about the sun.[18] This precession keeps the satellite in a static position with reference to the sun, thus achieving consistent, perceived illumination throughout the year. The passage of the sun-synchronous NOAA-9 satellite over each line of latitude at a constant local solar time, produces similar seasonal illumination and shadowing for images of a specific region. Both the earth's mass and spin carry the satellite track westward at about 15^0 of longitude each hour.[22] Because the earth rotates beneath the satellite 25.59^0 during each orbit,[19] the satellite observes a different portion of the earth's surface with each pass, making complete global coverage possible.

A near-polar orbit, refers to the satellite's orbital inclination. The orbital inclination of NOAA-9 is 98.9^0, this is the angle that the orbital plane forms as it crosses the equatorial plane.[24] An exact polar orbit would have an orbital inclination of 90^0; since the NOAA-9's orbital inclination is 98.9^0, it is said to be in a near-polar orbit. Figure 3.3-3, adapted from reference 24, helps to

---

*The information available regarding the current operational status of NOAA-9: In Feb. 85, two of the five onboard digital tape records had vailed. The ERBE-Scanner failed Jan. 87. The AVHRR has exhibited anomalous behavior in its synchronization with the Manipulated Information Processor (MIRP), MSU bands 2 and 3 have failed, and the power system continues to degrade. NOAA-11 is scheduled for launch in the early 1990's.

explain both sun-synchronous and near-polar orbits.

From an altitude of about 470-nmi, the NOAA-9's typical ground swath width is 2400 to 2700 kilometers. Figure 3.3-4 shows the swath width matched to a satellite ground track.[22] At nadir or right along the dotted-line, a ground resolution for the advanced very high resolution radiometer (AVHRR) sensor, for example, is 1.1 square kilometers, which is usually generalized up to 4 km^2.[20] However, one must keep in mind that resolution becomes coarser as the viewing angle off-nadir increases. The NOAA-9 completes 14.1 orbits per 24 hour period, taking only 102 minutes per orbit. The distance between orbits is 25.5^0, allowing complete global coverage every 12 hours.[18,20,22] As such, the NOAA-9 provides daily (visible) and twice-daily (thermal infrared) coverage of the earth. The physical characteristics of NOAA-9 include:[20] a total weight of 2,220 lbs and a payload capacity of 850 lbs. Non-deployed, the NOAA-9 is 13.8 feet long and has a diameter of 6.2 feet. The solar array panel of 125 square feet, constructed with violet, high efficiency solar cells, is expected to provide 515 watts of power, even at the worst solar angle. At full operation, the NOAA-9's power requirements are 475 watts. A consistent electrical supply is required to power the NOAA-9's instrumentation.

3.3.5.1.1.2. The NOAA-9's Onboard Instrumentation

The instrument systems on board the NOAA-9 provide both direct readout (real time) and onboard recording (for later playback) of environmental and other data during both day and night operation. In addition to the communication equipment and the instruments that maintain and monitor the satellite itself, the NOAA-9 carries the following instrument complement:[14]

1. Advanced Very High Resolution Radiometer (AVHRR)
2. High Resolution Infrared Radiation Sounder (HIRS/2)
3. Stratospheric Sounder Unit (SSU)
4. Microwave Sounder Unit (MSU)
5. Space Environment Monitor (SEM)
6. Search and Rescue (SAR)

7. Satellite Aided Tracking (SAT)
8. Solar Backscatter UV Radiometer (SBUV/2)
9. Earth Radiation Budget Experiment (ERBE)
10. Data Collection System (DCS)

The primary imaging system, and the most important sensor for this dissertation project, is the AVHRR. The AVHRR made by ITT Aerospace/Optical Division and flown on the NOAA-9, was designed to permit multispectral analyses which would improve the acquisition of data on meteorologic, oceanographic, and hydrological variables.[20] The optics of the NOAA-9 AVHRR include an eight-inch diameter, afocal, Cassegrainian, aperture telescope combined with secondary optics which separate the radiant energy into discrete spectral bands which are then focused onto their respective field stops.[14] The AVHRR on the NOAA-9 has five specific spectral bands.[19,20,22,23] Band ONE with a wavelength range of .58 to .68μm is in the red region of the visible spectrum, and is used to collect data about daytime clouds and vegetation. Band TWO with a wavelength of .725 to 1.0μm lies in the near infrared portion of the spectrum and is used to discern land-water boundaries (shorelines), snow and ice extent, and vegetation.[21] Coincidentally, the spectral ranges of bands ONE and TWO are positioned to record significant biologic properties associated with vegetation. Band ONE records the chlorophyll absorption of red wavelengths and Band TWO records the strong reflectance of IR wavelengths by the cell structures of leaves.[22] Figure 3.3-5 illustrates how a leaf behaves as a remote sensing target. [SECTION 3.3.7. contains a much more detailed discussion on the calculation and use of the normalized difference vegetation index (NDVI).] Band THREE, with a wavelength of 3.55 to 3.93μm, lies in the thermal infrared area and is used to detect hot targets, such as forest fires or volcanoes. Bands FOUR and FIVE, with a wavelength of 10.3 to 12.4μm, again in the thermal region, are used for detecting sea temperatures and for both daytime and nighttime cloud data. When interpreting Band FOUR or FIVE, bright signatures represent relatively cool areas, and dark

signatures relatively warm, radiant temperatures. Table 3.3-2, summarizes the characteristics and bands (channels) of the AVHRR sensor. For a detailed description of the other sensors onboard the NOAA-9 see listed references.[14,18,19,20] Figure 3.3-2 is an NOAA-9 line drawing, showing the conformation of the satellite platform, plus instrument and antenna location.[14,20]

Once the sensors have gathered data, this information must be transmitted back to earth. In addition, as the satellite orbits the earth, it must receive almost constant command and control instructions from the ground. Both data transmission and flight commands require an effective communications system.

3.3.5.1.2. NOAA-9's Communications System

The National Oceanic and Atmospheric Administration operates two Command and Data Acquisition (CDA) stations, one located at Fairbanks, Alaska and the other in Wallops Island, Virginia.[14] Both CDA stations transmit command programs to the NOAA-9, and also acquire, and record meteorological and engineering data from the NOAA-9.[20] However, during three sequential orbits of the earth (four, on some days), the NOAA-9 remains out of contact with the U.S. sites.[14] To eliminate the delay in receipt of high priority temperature profile data during this period, a data receipt-only station is being built in Lannion, France.[14] This station will acquire stored data and transmit them to the CDA centers. Once the French station is in operation, the NOAA-9 will be out of contact with the ground for no more than one orbit period per day.[14] The communication system uses ten separate transmission links to handle communications between the NOAA-9 and the ground stations.[19,20] Table 3.3-2 summarizes the NOAA-9's communication links.[19,20]

The NOAA-9 is considered a third generation meteorological spacecraft and it has served the research and applications user-communities well.[21] The NOAA-9 has some obvious advantages over its predecessors; it also has some definite advantages and disadvantages when compared to its land-oriented relative, LANDSAT-TM.

3.3.5.1.3. NOAA-9 Strengths And Limitations

Because the NOAA-9 was specifically designed to provide data for both weather prediction and weather monitoring, its sensors generally depict very coarse spatial resolution[18] (this does not diminish its potential application to epidemiologic problems). The lack of resolution is readily apparent when NOAA-9 images are compared to the land-oriented systems.[22] On the other hand, the very course spatial resolution has the advantage of greatly reducing the volume of data that must be processed for certain applications. In addition to smaller data sets, the NOAA-9 also has the advantages of global coverage at high temporal resolution.[23] As a result, NOAA-9 data has been used in numerous natural resource applications where frequent, large area coverage is needed but fine detail is not.[17] When compared directly with LANDSAT-Thematic Mapper (TM), the NOAA-9 has two distinct advantages and several disadvantages pertaining to vegetation monitoring. As mentioned above, the advantages of NOAA-9 are its more frequent repeat time and its wider-area coverage.[16] If the target area of interest is cloudy, large data gaps occur in LANDSAT-TM coverage. The two disadvantages occur when specific information is necessary on the scale of individual fields, in which case LANDSAT-TM has higher spatial resolution; and secondly, when specific details about the types of vegetation are required, LANDSAT-TM will deliver better spectral resolution.[14,22,24]

Section 3.3.5 began with some information about the history of NOAA-9. Subsection One, within Part Three, contained basic information about the NOAA-9 spacecraft and its onboard instrumentation, highlighting the AVHRR. Subsection Two contained a discussion on how the NOAA-9 receives commands and transmits data back to earth. Finally, Subsection Three, mentioned a few of the NOAA-9's strengths and weaknesses. Part FOUR will discuss the applications of the NDVI.

3.3.6. PART FOUR: The Normalized Difference Vegetation Index (NDVI)

As briefly mentioned earlier, a mathematical combination of the brightness values from the near-infrared band (channel two) and the visible band (channel one) of the AVHRR sensor allow for an estimate of the extent and condition of green vegetation, called a "vegetation index" or an NDVI. Although the NDVI is purely a mathematical combination of the radiometric values from bands 1 and 2, it has been strongly correlated with the density and photosynthetic ability of vegetation.[24] The NDVI is computed from the following equation:

NDVI = Band 2 - Band 1 / Band 2 + Band 1

The NDVI is a bounded ratio with values ranging from -1 to +1. It makes an excellent index because it compensates for changing illumination conditions, different surface slopes, and varying viewing aspects.[25] Major atmospheric effects, like clouds, are also mostly eliminated by compositing daily maps for a 30-day period, retaining the value at each pixel with the brightest or "greenest" value. Therefore, the values for the clearest or cloud-free days are retained for use in a digital image. This technique, according to Holben, minimizes cloud contamination, reduces bidirectional reflectance and off-nadir viewing effects.[26] He also states that sun angle and shadow effects, aerosol and water vapor effects are minimized.[27] The NDVI correlates positively with greenness, because as vegetation biomass increases, it absorbs more energy in the visible red region and reflects more energy in the near-infrared region of the spectrum. The result is an increasing difference between the two as biomass increases. Figure 3.3-5 illustrates a spectral response pattern of a healthy leaf. Note how the red and blue wavelengths are mostly absorbed by the chlorophyll and are used for photosynthesis.[23] Contrary to the red and blue wavelengths, there is a large amount of reflectance in the near-infrared wavelengths by the internal tissues of the leaf. These features insure a high digital value for the NDVI ratio whenever healthy vegetation is found. Conversely, the NDVI will be small (<0.06) for landscapes which do not contain

vegetation. Some examples of targets that have small NDVI values include urban areas, bare soil, open water, and senescent or stress vegetation. The use of the NDVI as a measure of plant biomass has been widely published.[27,28,29,30,31,32,33,34,35] Also, mapping and monitoring changes in the condition of vegetation at regional or even continental scales is possible using an AVHRR sensor to obtain NDVI values.[35,36,37,38,39] The advantages of using the AVHRR sensor to monitor vegetation include its comparatively coarse resolution, which allows for a relatively large area of coverage, as well as its daily global coverage. An early application and experimental verification of these principles is presented by Tucker et al.[39,40]

Figure 3.3-1

The Components of a Simplified Satellite Remote Sensing System[23]

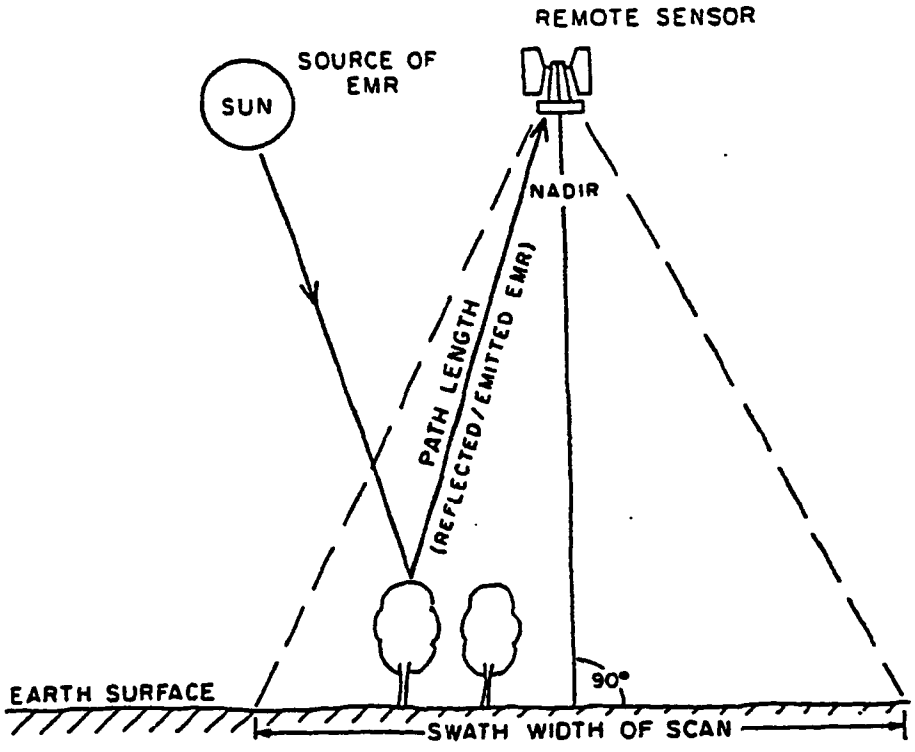

Figure 3.3-2. Major Features of the NOAA-9[19,20,40]

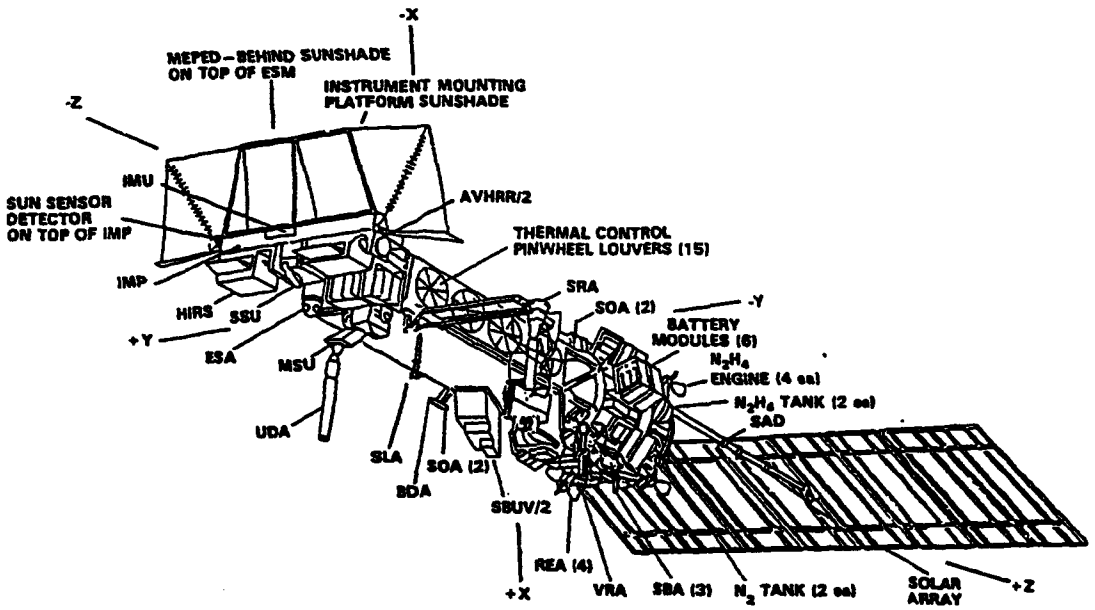

LEGEND	
AVHRR/2	ADVANCED VERY HIGH RESOLUTION RADIOMETER
BDA	BEACON/COMMAND ANTENNA
ESA	EARTH SENSOR ASSEMBLY
HIRS/2I	HIGH-RESOLUTION INFRARED SOUNDER
IMP	INSTRUMENT MOUNTING PLATFORM
IMU	INERTIAL MEASUREMENT UNIT
MSU	MICROWAVE SOUNDING UNIT
REA	REACTION ENGINE ASSEMBLY
SAD	SOLAR-ARRAY DRIVE
SBA	S-BAND ANTENNA
SBUV/2	SOLAR BACKSCATTER ULTRAVIOLET SPECTRAL RADIOMETER
SLA	SEARCH-AND-RESCUE TRANSMITTING ANTENNA (L-BAND)
SOA	S-BAND OMNI ANTENNA
SRA	SEARCH-AND-RESCUE RECEIVING ANTENNA
SSD	SUN SENSOR DETECTOR
SSU	STRATOSPHERIC SOUNDING UNIT
UDA	ULTRA-HIGH-FREQUENCY DATA COLLECTION SYSTEM ANTENNA
VRA	VERY-HIGH-FREQUENCY REAL-TIME ANTENNA
SEM	SPACE ENVIRONMENT MONITOR (DUMMY)

Figure 3.3-3

Illustration of a Sun-Synchronous, Near-Polar Orbit[24]

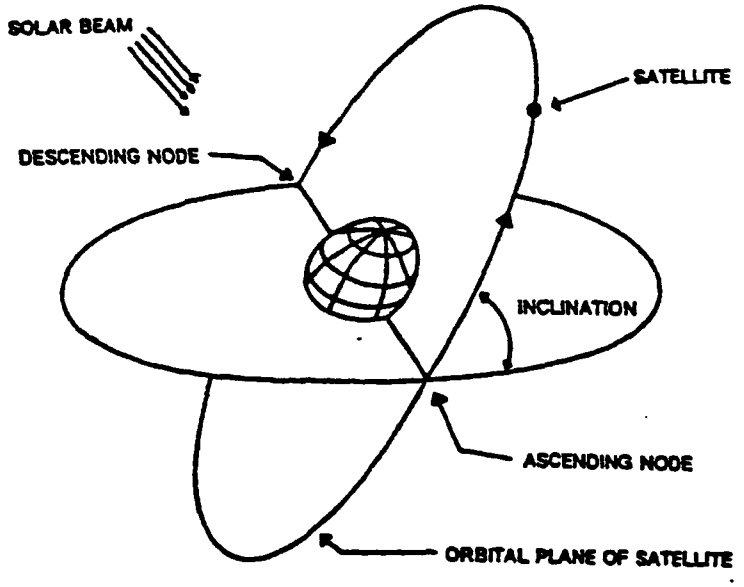

Figure 3.3-4

Typical Swath Width Matched to a Satellite Ground Track[22]

Figure 3.3-5

Healthy Leaf Spectral Signature[23]

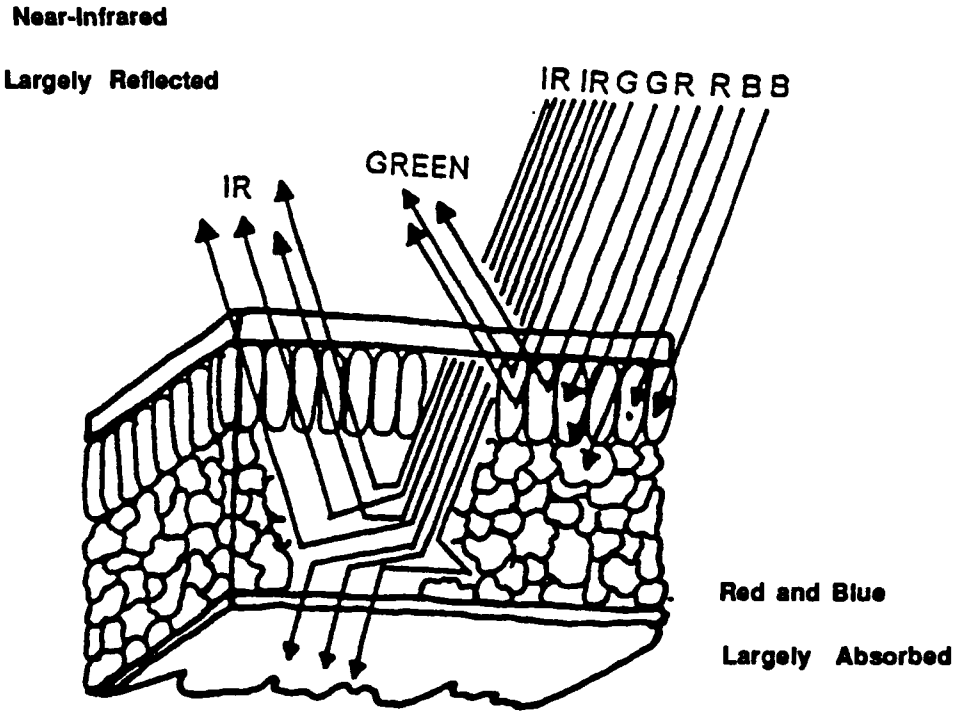

Table 3.3-2

Advanced Very High Resolution Radiometer (AVHRR)[19,20]

Characteristics	Channels				
	1	2	3	4	5
Spectral range (micrometers)	0.58 to 0.68	0.725 to 1.0	3.55 to 3.93	10.3 to 11.3	11.4 to 12.4
Detector	Silicon	Silicon	InSb	(HgCd)Te	(HgCd)Te
Resolution (km at nadir)	1.1	1.1	1.1	1.1	1.1
Instantaneous field of view (IFOV) (milliradians)	1.3 sq.	1.3 sq.	1.3 sq.	1.3 sq.	1.3 sq.
Signal-to-noise ratio at 0.5 albedo	>3:1	>3:1	—	—	—
Noise-equivalent temperature difference at (NEΔT) 300 K	—	—	<0.12 K	<0.12 K	<0.12 K
Scan angle (degrees)	±55	±55	±55	±55	±55
Optics—8-inch diameter afocal Cassegrainian telescope Scanner—360-rpm hysteresis synchronous motor with beryllium scan mirror Cooler—Two-stage radiant cooler, infrared detectors controlled at 105 or 107 K Data output—10-bit binary, simultaneous sampling at 40-kHz rate					

Table 3.3-3. NOAA-9 Communications Links[19,20]

Link	Carrier Frequency	Information Signal	Baseband Bit Rate	Modulation	Subcarrier Frequency
Command*	148.56 MHz	Digital commands	1 kbps	Ternary frequency-shift keyed (FSK/AM)	8, 10, and 12 kHz
Beacon	137.77 and 136.77 MHz	HIRS, SSU, MSU, SBUV/2 SEM, DCS data, spacecraft attitude data, time code, housekeeping telemetry, memory verification; all from TIP	8,320 bps	Split-phase phase-shift keyed PSK	
VHF real time	137.50 and 137.62 MHz	Medium-resolution video data from AVHRR	2 kHz	AM/FM	2.4 kHz
S-band real time	1,698 or 1,707 MHz	High-resolution AVHRR and TIP data	665.4 kbps	Split-phase PSK	
S-band playback	1,698, 1,702.5, or 1,707 MHz	High-resolution AVHRR data from MIRP, medium-resolution AVHRR data from MIRP; all TIP outputs	2.6616 Mbps	Randomized nonreturn-to-zero/PSK	
Data collection (uplink)	401.65 MHz	Earth-based platforms and balloons	400 bps	Split-phase PSK	
S-band playback to European ground station	1,698, 1,702.5, or 1,707 MHz	TIP data recovered from tape recorders	332.7 kbps	Split-phase PSK	
S-band contingency and launch	2,247.5 MHz	Boost during ascent and real-time TIP in orbit	Boost 16.64 kbps TIP in orbit 8.32 kbps	Split phase PCM/BPSK	1.024 MHz
SAR L-band downlink	1,544.5 MHz	Data transmission from SARR and SARP to ground LUT's	300 kHz (video)	PM 2 rad peak	
SAR uplinks	SARR 121.5 MHz 243 MHz 406.05 MHz SARP 406.025 MHz	From ground ELT/EPIRB's to spacecraft	(video) 25 kHz for 121.5 MHz 45 kHz for 243 MHz 400 bps for 406 MHz	AM for 121.5/243 MHz PM for 406 MHz	

*Uplink to the satellite

3.3.7. References

1. Parker DC, and Wolff MF. Rem Sens Int Sci Tech1965; 43:20-31.

2. Cline BL. New eyes for epidemiologists: aerial photography and other remote sensing techniques. Am J Epi 1970; 92:85-9.

3. Cibula WG. International Conference on Applications of Remote Sensing to Epidemiology and Parasitology, Louisiana State University, Baton Rouge, LA, June 1990.

4. Davies FG, Linthicum KJ, James AB. Rainfall and epizootic Rift Valley Fever. Bull WHO 1987; 63:941-3.

5. Linthicum KJ, Baily CL, Davies FG, Tucker CJ. Detection of Rift Valley Fever activity in Kenya by satellite remote sensing imagery. Science 1987; 235:1656-9.

6. Nicholls N. A method for predicting Murray Valley encephalitis in southwest Australia using the southern oscillation. Aust J Exp Biol Med Sci 1986; 64 (6):587-94.

7. Kay BH. Toward prediction and surveillance of Murray Valley encephalitis activity in Australia. Aust J Exp Biol Med Sci 1980; 58:67-76.

8. Everett RE. Arboviruses and foetal defects -- epidemiology, New England area. [In:St George TD, French EL, eds. Arbovirus research in Australia] Proc Symp CSIRO-QIMR 1986; 2:125-30.

9. Hayes RO, Maxwell EL, Mitchell CJ, Woodzick TL. Detection, identification, and classification of mosquito larval habitats using remote sensing scanners in earth-orbiting satellites. Bull WHO 1985; 63(2):361-74.

10. Barnes CM, Cibula WG. Some implications of remote sensing technology in insect control programs including mosquitoes. Mosquito News1979; 39:271-82.

11. Roberts D, Wood BL, Rodriguez M, Washino R, Paris J, Sebesta P, Lawless J, Legters L.

Sci News 1989; 138:70.

12. Rogers DJ, Randolph SE. Mortality rates and population density of tsetse flies correlated with satellite imagery. Nature1991; 351.

13. Kitron U. International Conference on Applications of Remote Sensing to Epidemiology and Parasitology, Louisiana State University, Baton Rouge, LA, June 1990.

14. Richason B. Introduction to remote sensing of the environment. 2nd ed. Chapter 22. Dubuque, IA: Kendall/Hunt Publishing Co.,1983.

15. A Report To The Congress, September: space-based remote sensing of the earth, prepared by NOAA, USDC, and NASA, 1987.

16. Schnopf A. Twenty years of weather satellites: where we have been and where we are going. 17th Annual Space Congress, Cocoa Beach, Fl. 1980.

17. Colwell R. Manual of remote sensing, 2nd ed. Chapter 14. Falls Church, VT: American Society of Photogrammetry, 1983.

18. Schwalb A. The TIROS-N/NOAA A-G satellite series, NOAA Technical Memo NESS 95, Washington DC, 1978.

19. NASA, Tiros program. Greenbelt, MD, Goddard Space Flight Center, 1989.

20. NOAA Polar-Orbiting Satellites TIROS-N Series, NOAA/PA78016, National Earth Satellite Service and NOAA, Washington DC, 1980.

21. Lillesand T, Kiefer R. Remote sensing and image interpretation 2nd ed. Chapter 9. New York: John Wiley & Sons, 1987.

22. Sabins F. Remote sensing principles and interpretation. 2nd ed. Chapter 9. New York: WH Freeman & Co., 1986.

23. Campbell J. Introduction to remote sensing. Chapter 5. New York: The Guilford Press, 1987.

24. Yates H, Strong A, McGinnis D, Tarpley D. Terrestrial observations from NOAA operational satellites. Science 1986; 231:463-70.

25. Smith WL, Bishop WP, Dvorak VF, et al. The meteorological satellite: overview of 25 years of operation. Science

26. Holben BN. Characteristic of max-value composite images from temporal AVHRR data. Int J Rem Sens 1986; 7(11):1417-34.

27. Goward SN, Tucker CJ, Dye DG. North American vegetation patterns observed with the NOAA-7 AVHRR. Vegetation 1985; 64:3-14.

28. Justice CO, Townshend JRG, Holben BN, Tucker CJ. Analysis of the phenology of global vegetation using meteorological satellite data. Int J Rem Sens 1985; 6:1271-1318.

29. Monteith JL. Climate and efficiency of crop production in Britain. Philos Trans R Soc Lond B 1977; 281:277-94.

30. Goetz AFH, Rock BN, Rowan LC. Remote sensing for exploration: an overview. Econ Geol 1983; 78:573-90.

31. Horler DNH, Dockray M, Barber J. The red edge of plant leaf reflectance. Int J Rem Sens 1983; 4:327-88.

32. Tucker CJ. A critical review of remote sensing and other methods for nondestructive estimation of standing crop biomass. Grass Forage Sci 1980; 35:177-82.

33. McFarlane JC, Watson RD, Theisen AF, et al. Plant stress detection by remote measurement of fluorescence. Appl Optics 1980; 19:3287-9.

34. Hardisky MA, Gross MF, Klemas V. Remote sensing of coastal wetlands. Bioscience

1986; 36(7):453-88.

35. Tucker CJ, Vanpruet MJ, Sharman, et al. Satellite remote sensing of total herbaceous biomass production in the Senegalese Saheli: 1980-1984. Remote Sens Environ 1985; 17:233-49.

36. Tucker CJ, Hielkema JU, Roffey J. The potential of satellite remote sensing of ecological conditions for survey and forecasting desert-locus activity. Int J Rem Sens 1985; 6:127-38.

37. Tucker CJ, Newcomb WW, Los SO, Prince SD. Mean and inter-year variation of growing-season NDVI for the Sahel 1981-1989. Int J Rem Sens 1991;12(6):1133-5.

38. Tucker CJ, Sellers PJ. Satellite remote sensing of primary production. Int J Rem Sens 1986; 7:1395.

39. Tucker CJ, Holben BN, Elgin JH, McMurtrey JE. Remote sensing of total dry matter in winter wheat. Rem Sens Environ 1981; 13:461.

40. Schwalb, A. Modified version of the TIROS N/NOAA A-G satellite series (NOAA E-J) advanced TIROS N (ATN), NOAA Technical MEMO NESS 116, Washington DC, 1982.

IV. EXPERIMENTAL METHODS

4.1. RESEARCH OBJECTIVE

The goal of this project is to study the potential for predicting the occurrence of human Puumala virus epidemics in Sweden using digitized satellite data.

4.2 STUDY DESIGN

Classical ecologic studies are empirical investigations, usually involving a population rather than an individual, as the unit of analysis. This study is an ecologic study in which the NDVI values from large geographic areas (5x5 km, 50x50 km, and 100x100 km) are compared with rodent population cycles for the same areas. The units of analysis are specific geographic locations from which NDVI values and rodent population fluctuations were measured.

A classic observational ecologic study involves a study design that attempts to document an association between the average exposure level of a large group (independent or predictor variable) and the disease rate of the same population (dependent or outcome variable). This study does the same, but with some minor differences. The exposure level, or predictor variable, is the satellite-derived NDVI values. The outcome variable is bank vole population density. The goal of this study is to test for a relationship between the two, allowing for a possible lag period between a given change in NDVI and a subsequent change in bank vole population cycles.

The advantages associated with this type of study design include the use of existing data sources, usually lowering overall cost, and, hopefully, reducing analysis time, when compared with conducting studies involving individual micro-environments and individual bank voles as the units of analyses. On the other hand, data on important variables may not be available at the ecologic level. Consequently, the results of this type of study may generate hypotheses and at best, any findings must be interpreted cautiously. Even if solid and complete information exists for all of the significant predictor and outcome variables, studies done at the ecological level run

the risk of inappropriately characterizing the epidemiologic associations. The specific strengths and limitation of this study are examined more closely in the Discussion section.

4.3. STUDY AREA

Figure 4.4.-1 shows the location of the overall 100x100 km study area in Vasterbotten County, just north of Umeå, Sweden (for reference purposes about 64^{0}N, 20^{0}E).[4] Within this large area, sixteen 5x5 km regularly distributed sub-area squares were delineated. Furthermore, within each of the sixteen sub-area squares, four one-hectare plots (100x100 m) were identified from the Swedish National Grid (see Fig. 4.4.-1).[4] Within the 10,000 km^2 study area, 74 percent of the land area was classified as forest, 15 percent as peat land, 6 percent as agricultural, 2 percent rocky surface, and 2 percent miscellaneous.[1] The predominant tree species were spruce (*Picea abies*) and pine (*Pinus silvestris*).[1] According to Ahti et al., the study area lies within the middle boreal vegetation zone.[2] The growing season typically begins on about 7 May and continues through late September, averaging about 144 days each year.[4] On average, persistent snow cover begins around 8 November and continues through 6 May, usually lasting about 177 days per year.[4]

4.4. DATA COLLECTION

4.4.1. Satellite Data Sets

Satellite data (raw AVHRR data) were acquired from the same study area described earlier, from 1982 to 1987 for each of the sixteen, 5x5 km sites; for each of four quadrants (50x50 km); and for the entire 100x100 km study area. Converting raw AVHRR data into usable digital images required a number of processing steps. The first step involved an orientation procedure, called rectifying the image. Second, it was necessary to register each of the images and geometrically correct the images to a standard map projection.

The EROS Data Center in Sioux Falls, South Dakota was responsible for receiving raw AVHRR data and applying an automated processing procedure which resulted in geometrically corrected, registered images. If color coding was undertaken at this point, the result would be a map-like, false-color, digital image of the area of interest. Rectified and registered digital images were sent to the Goddard Space Flight Center in Green Belt, MD, where normalized difference vegetation indices (NDVI's) were computed and NDVI-specific color codes applied. Figure 4.4.-2 shows the relationship and arrangement of the sixteen 5x5 km sites, the four 50x50 km quadrants, and the entire 100x100 km scene. Although each site was five-square kilometers, the actual satellite sensor's resolution was set at "global area coverage" or about four-square kilometers. Therefore each of the sixteen sites represents about one pixel. The NDVI value for each quadrant was generalized from individual pixel data and represents 96 pixels for the Kalvtrask, Skelleftea, and Vindeln quadrants. The NDVI value for Robertsfors quadrant represents 85 pixels because its eastern boundary is coast line. Individual pixel values were further generalized in order to obtain monthly NDVI values for the entire one hundred-square kilometer study area, representing 373 pixels. The satellite data-set was constructed from monthly, maximum-value, NDVI composites derived from daily AVHRR digital images. Compositing and cloud screening techniques were applied to the data as described by Holben.[3] Pre-flight sensor calibrations were available from NOAA, and applied to the individual bands during data processing. Figures in Section V. graphically illustrate the satellite data. Mathematically, NDVI values can range from 1 to -1. However, typical NDVI values of 0.5 are common for a cover type of dense green-leaf vegetation. Cover types consisting of sparse green-leaf vegetation would have NDVI values of 0.09. Because negative NDVI values are typical for snow, ice, or open water, in all the analyses, NDVI values that were less than 0.0001 were made to equal 0.0001. Therefore, negative NDVI values were eliminated and could not complicate any summary measures.

NDVI values were used as the exposure variable to investigate their potential as a predictor of bank vole population cycles. Both temporal and spatial relationships were examined.

4.4.2. Weather Data Set

Daily meteorological data were obtained from 1971-1988 by the Swedish Meteorological and Hydrological Institute field station, through Dr. Birger Hornfeldt.* The data came from the Hallnas-Lund station, which is located near the center of the 100x100 km study area.[4] The daily weather variables included minimum, maximum, and daily average temperatures (°C); precipitation (mm); and snow depth (cm). From these variables, a "warm index" was calculated by adding the daily high temperature to the daily average temperature and then averaging these values over each month. In addition, a "precipitation index" was obtained by summing all precipitation values for each month.

Because NDVI values were available only from 1982 through 1987 and rodent population data extended from 1971 through 1988, the weather data set was examined to discover if it could be used as a possible surrogate measure for NDVI values.

4.4.3. Rodent Data Set

The bank vole data were collected from 1971-1988 by Dr. Birger Hornfeldt and colleagues from the University of Umeå, Umeå,Sweden.[4] Using a symmetrical sampling grid design, sixty-four, 100 meter by 100 meter (one hectare), trapping sites were potentially available (see Fig. 4.4.-1). Voles were actually trapped in 58 of the 64 possible one-ha-plots (six one-hectare plots were unsuitable as trapping sites because of open water or some other geographic factor that made trapping impossible).[4] Rodent population dynamics were monitored by a snap-trapping method twice each year. Beginning in the fall of 1971, every spring (20-26

*Hornfeldt, B. Personal communication. Department of Animal Ecology, University of Umeå, Umeå, Sweden, 1992.

May) and again in the fall (23-30 September), and continuing through fall 1988, small mammals were trapped and identified using about 2,800 baited snaptraps.[4] Hornfeldt et al. used the following published, trapping procedures: Within a one meter radius, five traps were set in each of ten permanent stations, centered and spaced ten meters apart along the diagonal of each one hectare plot, for three consecutive nights (as shown in the one hectare square of Fig. 4.4.-1).[4] The traps were baited with unfried Polish wicks and dried apples.[4] For every hectare plot, trapping effort was normally 150 trap-nights for each spring and fall sampling period. The total trapping effort per spring and fall ranged from 7,950 to 8,550 trap-nights, in which 7,891 bank voles (*C. glareolus*) were trapped.[3] All the bank vole population data were standardized to number of voles trapped per 100 trap-nights. The following information was recorded for each snap-trapped bank vole: trapping date, identification number, the exact trapping coordinates and body weight.

The rodent data base also contained Puumala virus antibody titers for all bank voles trapped between Fall, 1979 and Fall, 1987. An optical density value was obtained using an enzyme-linked immunosorbent assay (ELISA) laboratory test.*[5] A sample with an optical density greater than 0.1 was considered positive. A total of 2,542 bank voles were trapped during this period. The prevalence information allowed for the opportunity to explore the relationship between the Puumala antibody positive bank vole population over time, relative to the whole bank vole population. In addition, antibody positive populations were evaluated for any unique spatial associations.

4.4.4. Time Coverage

Figure 4.4.-3 summarizes the time relationships of the various data sets.

---

*Serology was conducted by the Department of Virology, National Bacteriological Laboratory, Stockholm, Sweden, and is described by Niklasson and LeDuc.

4.5. DATA ANALYSES

Data analyses were divided into three major sections. Section 4.5.1. contains mostly descriptive statistics for the satellite and weather data sets. In addition, NDVI values at the individual site, quadrant, and entire scene level were correlated across years. The value of using meteorologic data as a surrogate measure for NDVI was evaluated as well. Section 4.5.2. includes an analysis of the relationship of bank vole population cycles and Puumala antibody prevalence in trapped bank voles. Also, the relationship of bank vole age and Puumala antibody status was examined. Finally, Section 4.5.3. investigates the ability of the NDVI to predict bank vole cycles.

4.5.1. Descriptive Statistics and Correlations

4.5.1.1. Correlations of Sites, Quadrants to Entire Scene

Regression analysis was conducted to determine how closely the individual site NDVI values could predict their quadrant NDVI value and to assess intra-quad homogeneity.[6] The analysis was continued to determine if the quadrant NDVI values could predict the NDVI for the entire scene.

4.5.1.2. Weather Variables as Surrogates for NDVI Values

The satellite data set (1982-87) had NDVI values for only a portion of the bank vole trapping time-span (1971-88). Analyses to find an appropriate NDVI surrogate measure(s) using selected meteorological variables were attempted.

Within the framework of General Linear Models, multiple regression analyses were conducted.[6] Numerous independent weather variables such as temperature, precipitation, and various mathematical indices were used in an attempt to predict NDVI values. In other words, using the method of least squares to fit general linear models (where deviations from averages are used to predict deviations from averages), NDVI values were predicted in terms of several weather variables.

4.5.2. Puumala Antibody Status of Bank Voles

4.5.2.1. Puumala Antibody Prevalence in Bank Voles

As described above, for all analyses, vole population numbers were standardized to the number of bank voles trapped per one hundred trap nights. A statistical weighting procedure (inverse to variance) was also applied in order to account for changes in vole population sample sizes.[6]

The proportion of trapped bank voles which were positive for Puumala virus antibody was calculated. Prevalence was defined as the proportion of trapped bank voles that tested positive for a specific level of Puumala virus antibody at a certain point in time. The numerator was the number of positive bank voles, while the denominator was based on all the bank voles that were trapped in the study area between 1979 and 1987.

4.5.2.2.

The Relationship Between Bank Vole Age and Puumala Antibody Status

The relationship of bank vole weight (age) to antibody status was analyzed. Vole weight (grams), as a continuous variable, was used as a predictor of Puumala antibody status. Antibody status was considered positive if optical density (OD) was greater than 0.1.

4.5.3. The Relationship Between NDVI Values and Bank Vole Population Cycles

The usefulness of coarse resolution satellite data as a predictor of vole cycles was evaluated. The statistical relationship between NDVI values and the temporal trends in population cycle frequencies was assessed in a series of operations. First, an NDVI summary measure was constructed by making all values less than 0.0001 equal to 0.0001. Once negative values were eliminated, the monthly NDVI values for April-July and for August-November were summed to create a Spring and Fall NDVI value, respectively. Annual Spring and Fall NDVI values were then

used as predictors of bank vole population cycles, through time. Also, the spatial relationship between NDVI and bank voles found at each of the geographic locations was studied. Analyses were conducted at the individual site, the quadrant, and the entire scene levels. After adjusting for season, regression analytic procedures involving standardized bank vole numbers as the dependent variable and NDVI values as the independent variable were studied. [6] The residuals of each variable were also used in regression models, as well as time lags of up to five seasons.[6]

Figure 4.4.-1. Study Area[4]

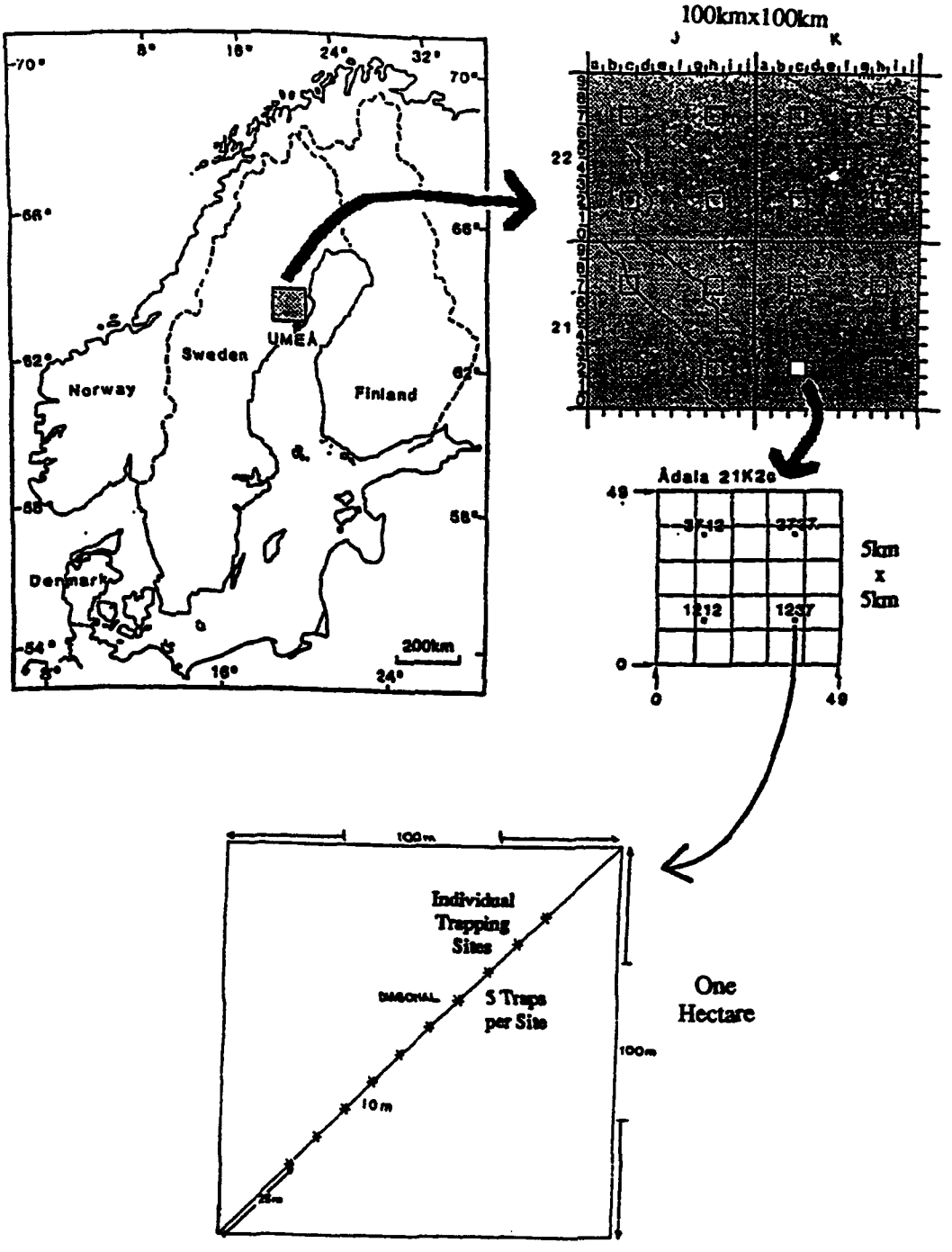

Fig. 4.4.-1. Geographic location of the 100x100km study area in northern Sweden. In each of the sixteen, 5x5km study sites; four, 1-hectare-plots were selected by the Swedish National Grid. Five snap-traps were placed at each of the ten individual trapping sites.

Figure 4.4.-2
Study-Site Arrangement

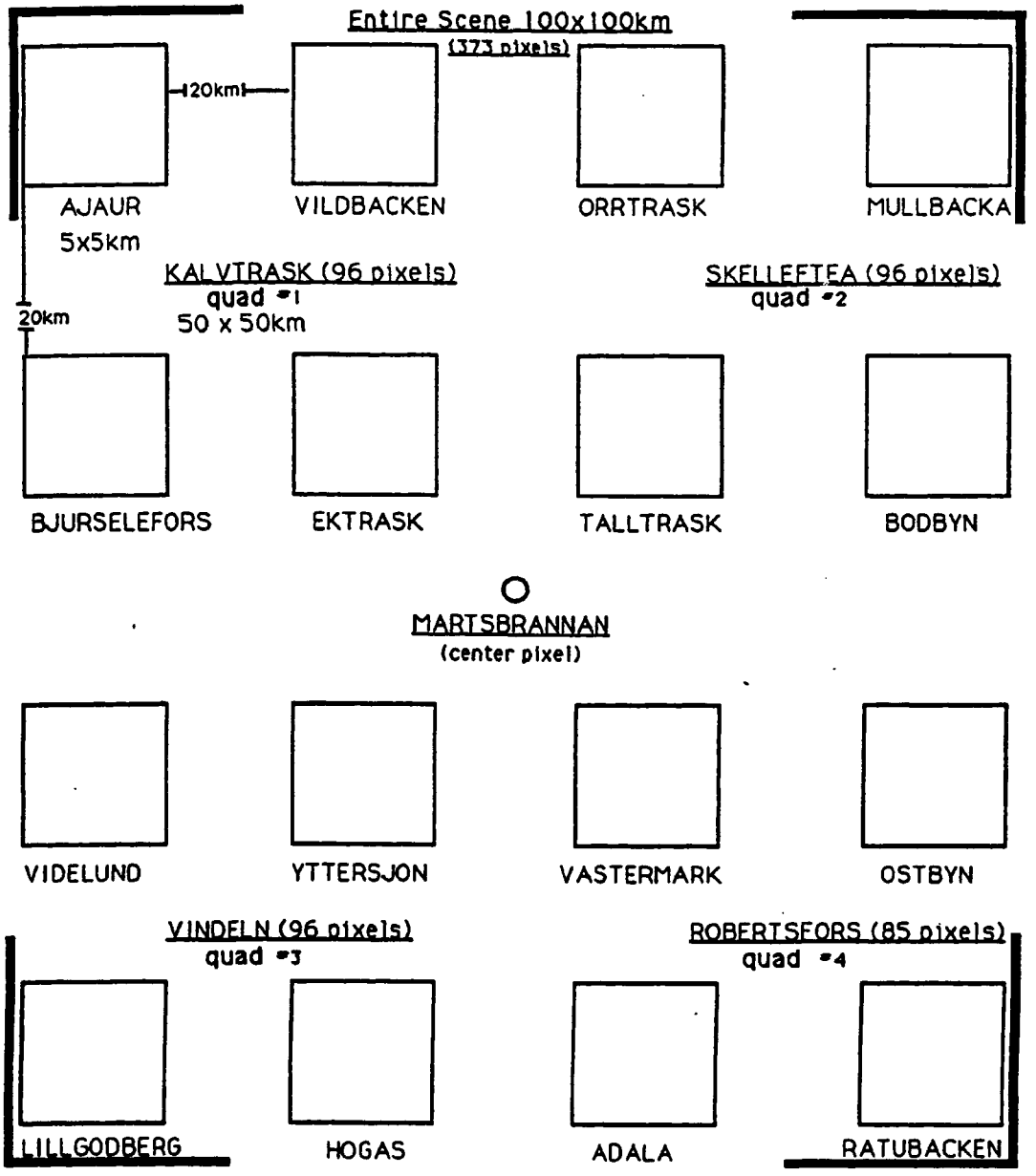

Fig. 4.4.-2. Arrangement of the sixteen 5x5km study sites and the four 50x50km quadrants, relative to the entire 100x100km scene.

Figure 4.4.-3.
Data Time-Lines

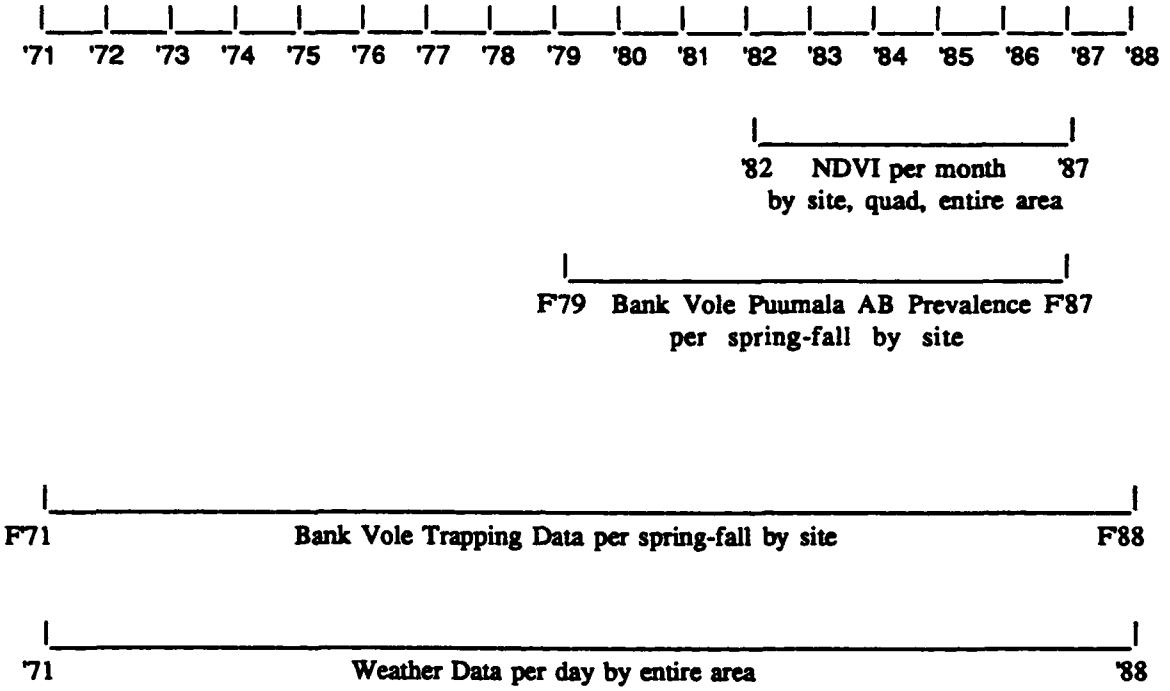

Fig. 4.4.-3. Data time-lines for each of the major data sets.

4.7. REFERENCES

1. Svensson SA. The Swedish National Forest Survey 1973-77. State of forests, growth and annual cut. Report 30, Department of Forest Survey, Swedish University of Agricultural Sciences, Umeå. 1980. (In: Hornfeldt B. Cycles of voles, predators, and alternative prey in boreal Sweden [Dissertation]. Umeå, Sweden: University of Umeå, 1991.)

2. Ahti T, Hamet-Ahti L, Jalas J. Vegetation zones and their sections in northwestern Europe. Annales Botanici Fennici 1968; 5:169-211. (In: Hornfeldt B. Cycles of voles, predators, and alternative prey in boreal Sweden [Dissertation]. Umeå, Sweden: University of Umeå, 1991.)

3. Holben BN. Characteristics of maximum-value composite images from temporal AVHRR data. Int J Rem Sens 1986; 7:1417-34.

4. Hornfeldt B. Cycles of voles, predators, and alternative prey in boreal Sweden [Dissertation]. Umeå, Sweden: University of Umeå, 1991.

5. Niklasson B, LeDuc JW. Epidemiology of NE in Sweden. J Infect Dis 1987; 155:269-76.

6. SAS/STAT User's Guide, Version 6.03. Cary NC: SAS Institute, Inc., 1991.

V. RESULTS

5.1. DESCRIPTIVE STATISTICS FOR THE DATA SETS

5.1.1. NDVI Data Set

5.1.1.1. Sites, Quadrants and the Entire Scene

The monthly NDVI data from 1982-1987 are shown in Figures 5.1.-1 through 5.1.-21 for the entire study area, the four quadrants, and for each of the sixteen study sites. Figures 5.1.-2 through 5.1.-21 can be found in Appendix One. (Refer to Figure 4.4.-3 for the spatial arrangement of each area.)

5.1.1.2. NDVI versus NDVI Correlations

Figure 5.1.-22A and 5.1.-22B portray how each quadrant's NDVI values change through time and how strongly correlated the NDVI values remain. Figure 5.1.-22A illustrates actual NDVI values, while 5.1.-22B shows how the residuals continue to be strongly correlated. After de-seasonalizing, the Pearson correlation coefficients from regression analyses are listed in Figure 5.1.-23. P-values were all highly significant at $p < 0.001$.

Direct correlations of the NDVI values, over time, between sites within quadrants, among quadrants, and between quadrants and the entire scene, remained statistically significantly before and after adjusting for individual months. Likewise, repeating the correlations as above, regression analyses using residuals yielded Pearson correlation coefficients all above 0.92 ($p < 0.001$). Figure 5.1. - 23 shows that the individual site's NDVI value predicts its quadrant value. Moreover, quadrant NDVI values predict the entire scene's NDVI value. The strong correlations remained even after adjusting for individual months and when substituting residuals, in effect de-seasonalizing the monthly NDVI values. Thus, this evidence suggests that collapsing individual 5x5 km site or 50x50 km quadrant NDVI data into a 100x100 km entire-scene value may be an

efficient way of incorporating NDVI data into a problem involving large homogeneous geographic areas.

5.1.2. NDVI Data Set and Weather Data Set Descriptive Statistics

Descriptive statistics for both the NDVI and weather data sets are shown in Table 5.1.-1 and 5.1.-2. Tables 5.1.-1 and 5.1.-2 list the averages and standard errors for monthly NDVI values, mean daily temperatures, summed precipitation values, and warm indices. Descriptive statistics were computed on an annual, a Spring-Fall, and monthly basis. The annual statistics are based on the months April-November for each of the years 1982-1987. Spring was April-July and Fall was August-November for the years 1982-1987. Lastly, the monthly measures were each May, each July, and each September for the years mentioned previously. Several trends emerge from these data. Considering the annual values first, NDVI values remain fairly constant over years, with a range of 0.24 to 0.32. Also, the highest NDVI value (1986) does not correspond to any other variables highest value and the lowest NDVI value (1983) does not correspond to any of the other variables' lowest values, except precipitation. Note that the year with the highest warm index (1984) had the second lowest average NDVI. Ranking each variable from its highest to lowest value yielded very little correlation among the four variables. Monthly values generally peaked in July for each variable (except precipitation) indicating the usefulness of de-seasonalization or adjusting for month in the statistical analysis.

5.1.3. Weather Variables as Predictors of the NDVI

Before de-seasonalizing, two specific meteorological variables emerged as statistically significant predictors of NDVI: monthly average precipitation and a monthly warm index. Monthly average precipitation was the mean monthly precipitation, while the monthly warm index was calculated by first adding the daily average temperature to the daily maximum temperature and then calculating a monthly mean. Initially, the NDVI values for the entire scene were used in a General Linear Models regression analysis, where NDVI was the dependent variable and

precipitation and warm index were predictor variables. The initial finding for this two-variable model was an R-squared of 0.831; precipitation average and warm index had F-values of 7.16 ($p < 0.01$) and 166.87 ($p < 0.001$), respectively. When these two variables were included in the above model as an interaction term, the interaction term was not significant ($p=0.25$) and the fit was not meaningfully improved.

However, since both weather and NDVI are highly seasonal, one would expect to find the two highly correlated. In an attempt to account for the seasonal effects of each data set, residual analyses procedures were used. Regression analyses were conducted using the residuals of the monthly precipitation average and the residuals of the monthly warm index as predictors of the residuals of the monthly NDVI. The R-square value was 0.09, precipitation average lost statistical significance ($p = 0.72$), while the warm index p-value rose to 0.05.

Identical regression analyses, adjusting for month, using residuals of the log transformed variables were conducted. In this regression model the residuals of the log transformed weather variables were slightly better able to predict the residuals of the log transformed NDVI values, as the R-square increased to 0.22, P-values for the residuals of the precipitation and warm index were $p=0.31$ and $p=0.005$, respectively. All of the above regression analyses were repeated, but with time lags of 1 month, 2 months, 3 months, and 4 months. The best R-square was again 0.22 for a two-month lag, P-values for the residuals of the precipitation and warm index were $p=0.0008$ and 0.686, respectively. Months were also grouped into two-month categories (i.e., Jan.-Feb. became Group 1, etc.) and four-month groups and analyzed as above (i.e. residuals, logs, and time lags). The best R-square was 0.23 for a four-month grouping at one time-lag, $p=0.056$ and 0.381, respectively. Even though statistical significance was achieved at R-squared values of 0.22 or 0.23, this level of association was not considered strong enough to use meteorological variables as surrogates for NDVI values. Figure 5.1.-24A. and B. illustrates the relationship, through time, between the NDVI residuals and both meteorological variables.

5.1.4. Bank Vole Data Set

Figure 5.1.-25 illustrates bank vole population cycles for the entire study area, from 1971 to 1988. Four bank vole population cycles emerged over the seventeen years of rodent trapping data. Fluctuations of three to four years between population peaks of varying amplitudes are evident.

Summed over years, figure 5.1.-26 shows the number of bank voles trapped for each season within each of the four quadrants. Figures 5.1.-27 through 30 show annual bank vole trapping values for each quadrant. Note how relatively consistent trapping data is for each quadrant. Finally, Figure 5.1.-31 illustrates bank vole population cycles for the entire area by year.

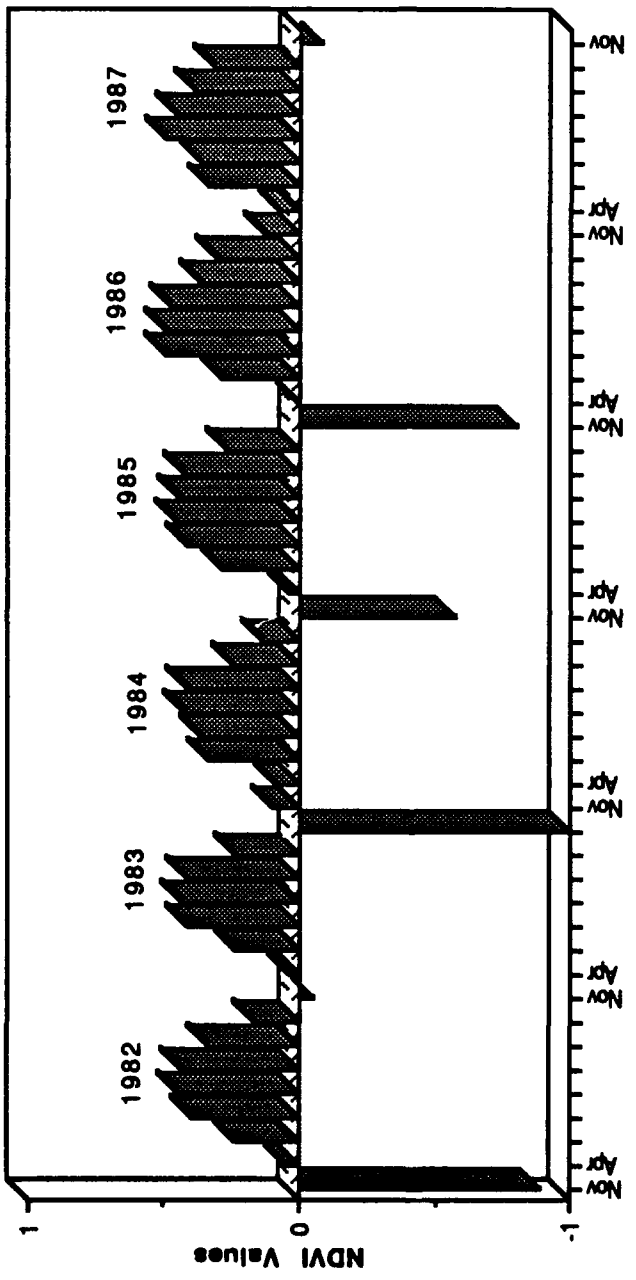

Fig 5.1.-1. Satellite Data - Martsbrannan 100x100 km

Fig. 5.1.-22.A. Summed NDVI Values For Each Quadrant

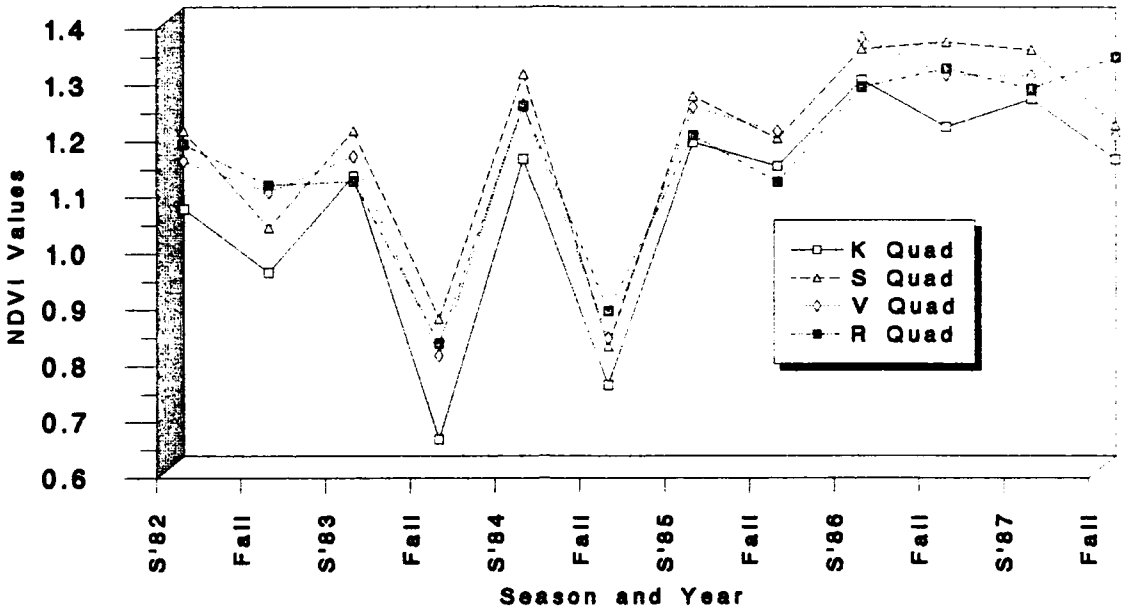

Fig.5.1.-22B. Residuals Of The Summed NDVI Values For Each Quadrant

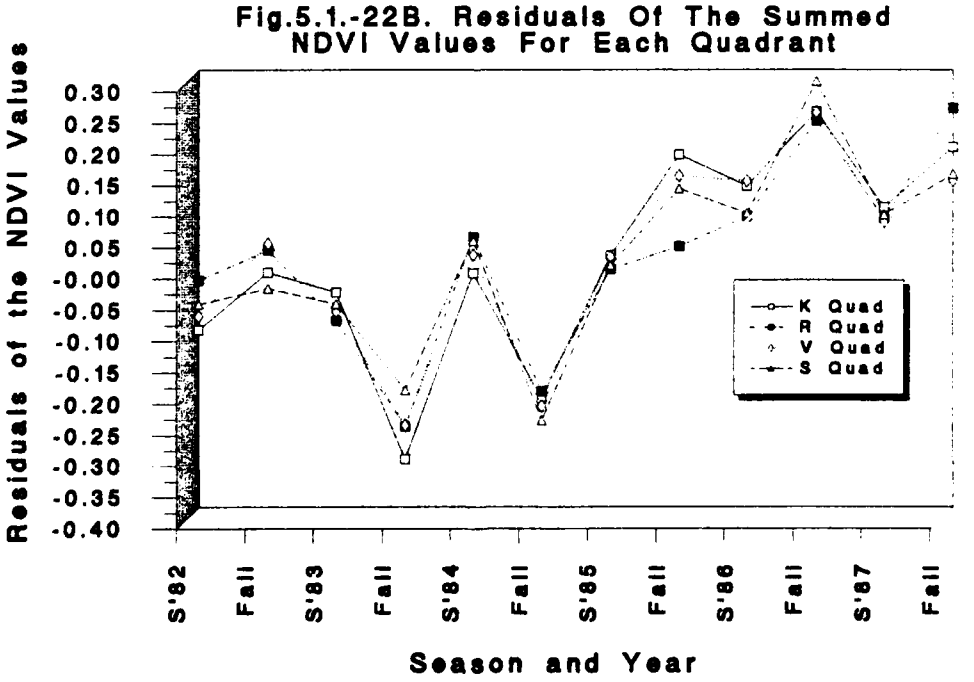

Fig. 5.1.-23. Pearson Correlation Coefficients of individual site NDVI values with its Quadrant NDVI value and the Correlation Coefficients of the four Quadrant NDVI values with the Entire scene NDVI value. Based on monthly data from 1982-1987 [8months x 6 years = 48 points*].

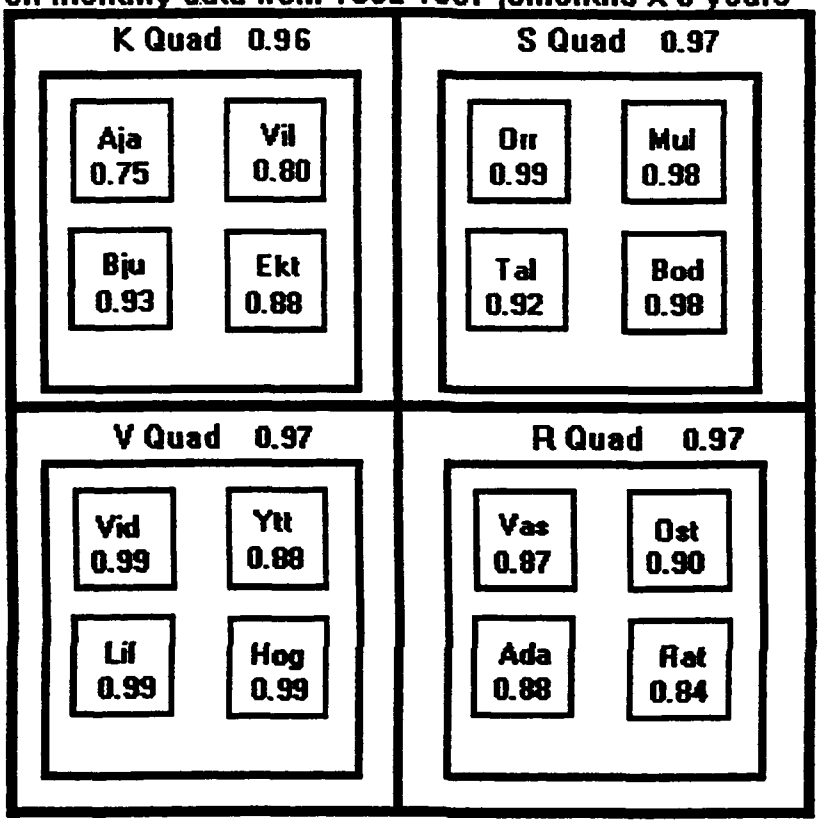

*All points were corrected for seasonality (de-seasonalized)

Fig.5.1.-24.A. NDVI and Precipitation Residuals From 1982-1987

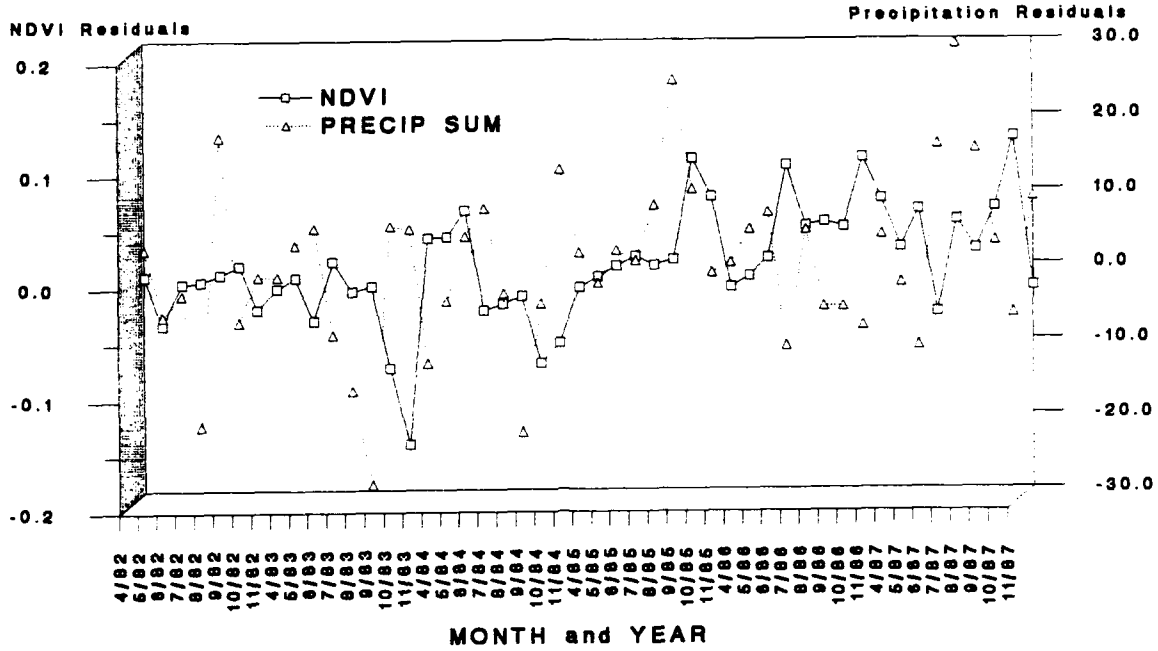

Fig.5.1.-24.B. NDVI and Warm Index Residuals From 1982-1987

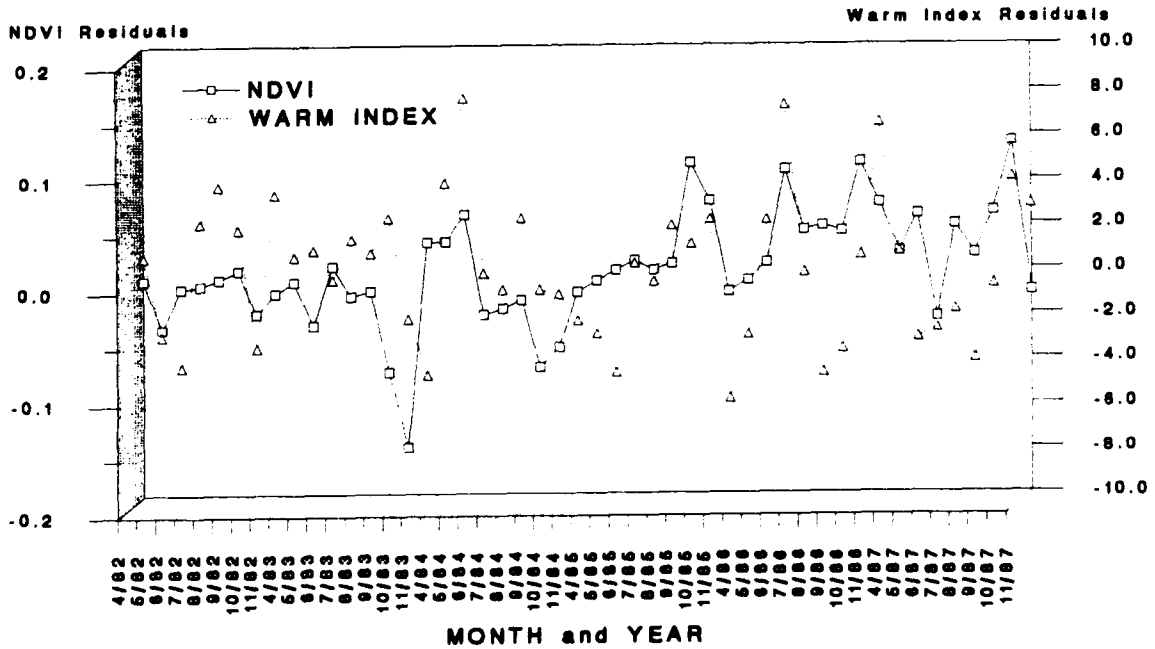

Fig. 5.1.-25. Total Number of Bank Voles Trapped Each Spring and Fall for Each Quadrant, Beginning Fall 1971 - Fall 1988. (Standardized per 100 Trapnights)

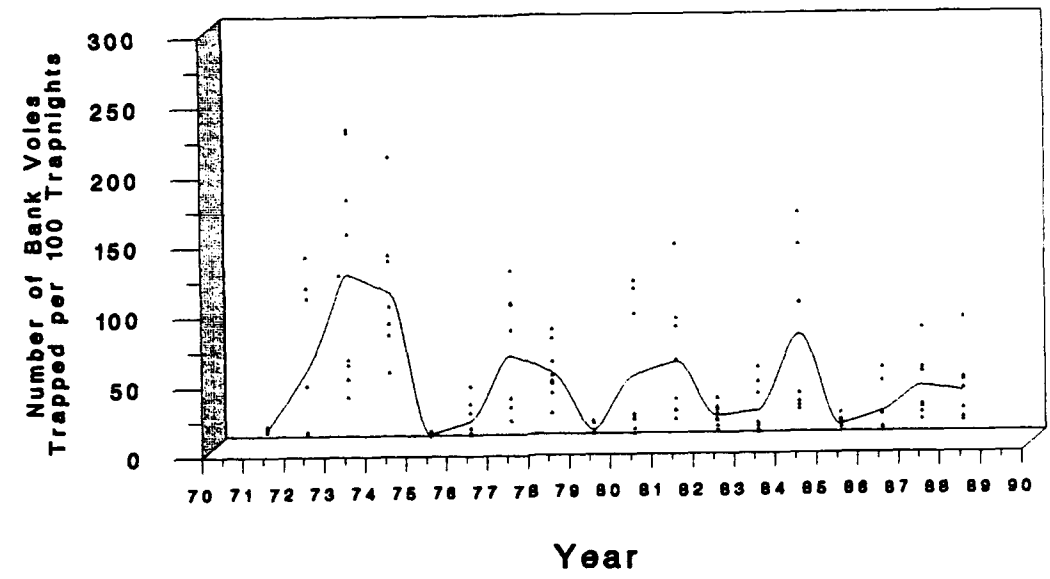

Fig. 5.1.-26. Bank Voles Trapped by Quadrant, 1979-87

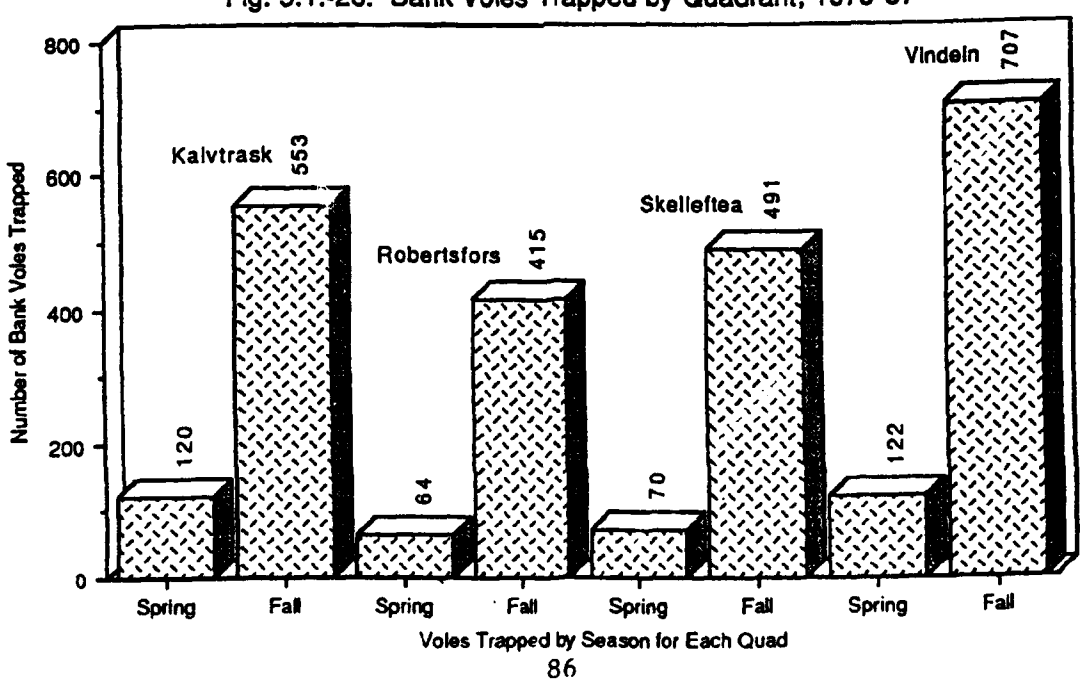

Fig.5.1.-27. Kalvtrask Quadrant Standardized Bank Vole Population Cycles, 1971-1988

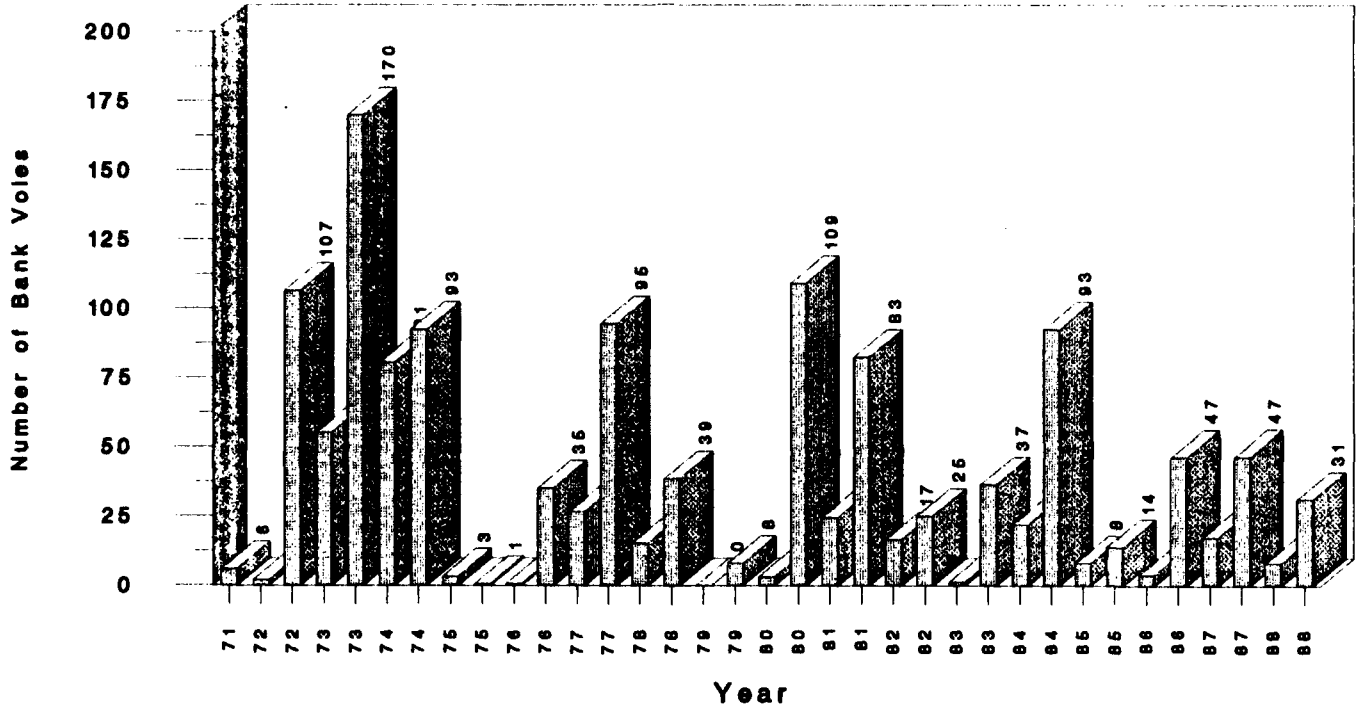

Fig.5.1.-28. Skellefteå Quadrant Standardized Bank Vole Population Cycles, 1971-1988

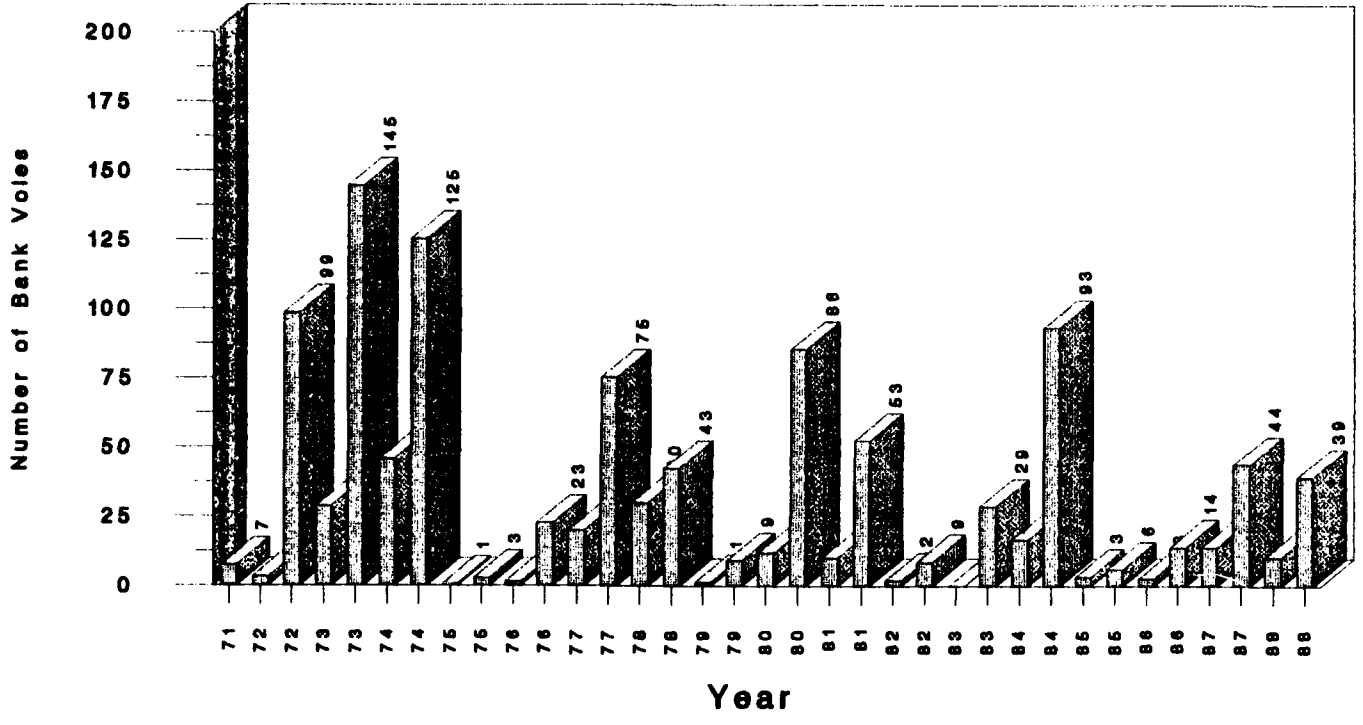

Fig.5.1.-29. Vindeln Quadrant Standardized Bank Vole Population Cycles, 1971-1988

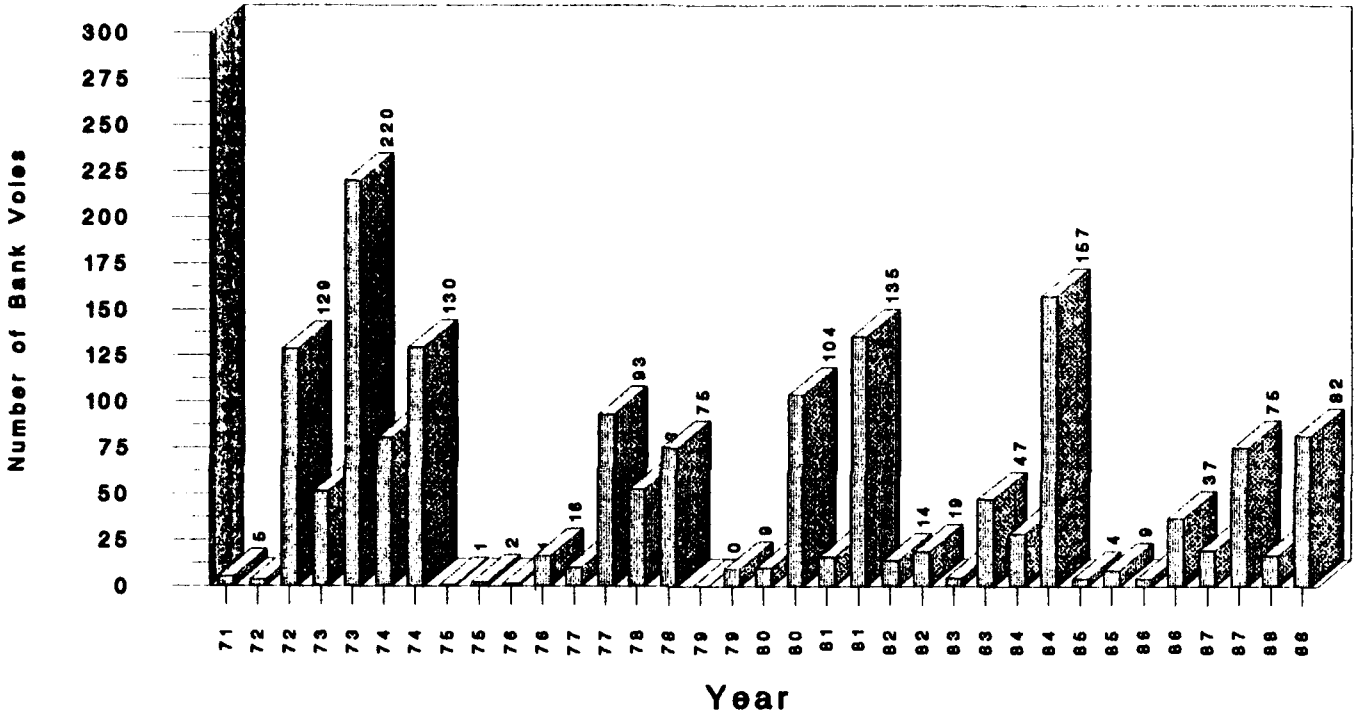

Fig. 5.1.-30. Robertsfors Quadrant Standardized Bank Vole Population Cycles, 1971-1988

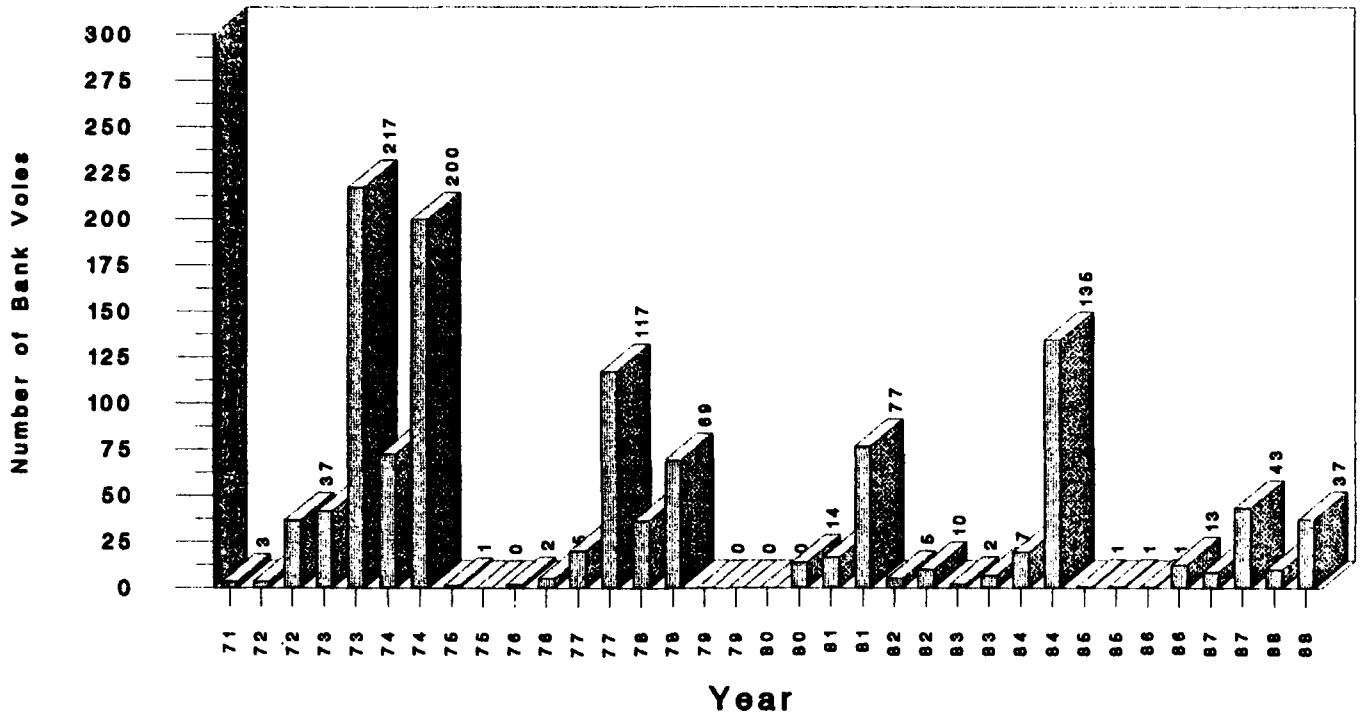

Fig. 5.1.-31. Entire Study Area Standardized Bank Vole Population Cycles 1971-1988

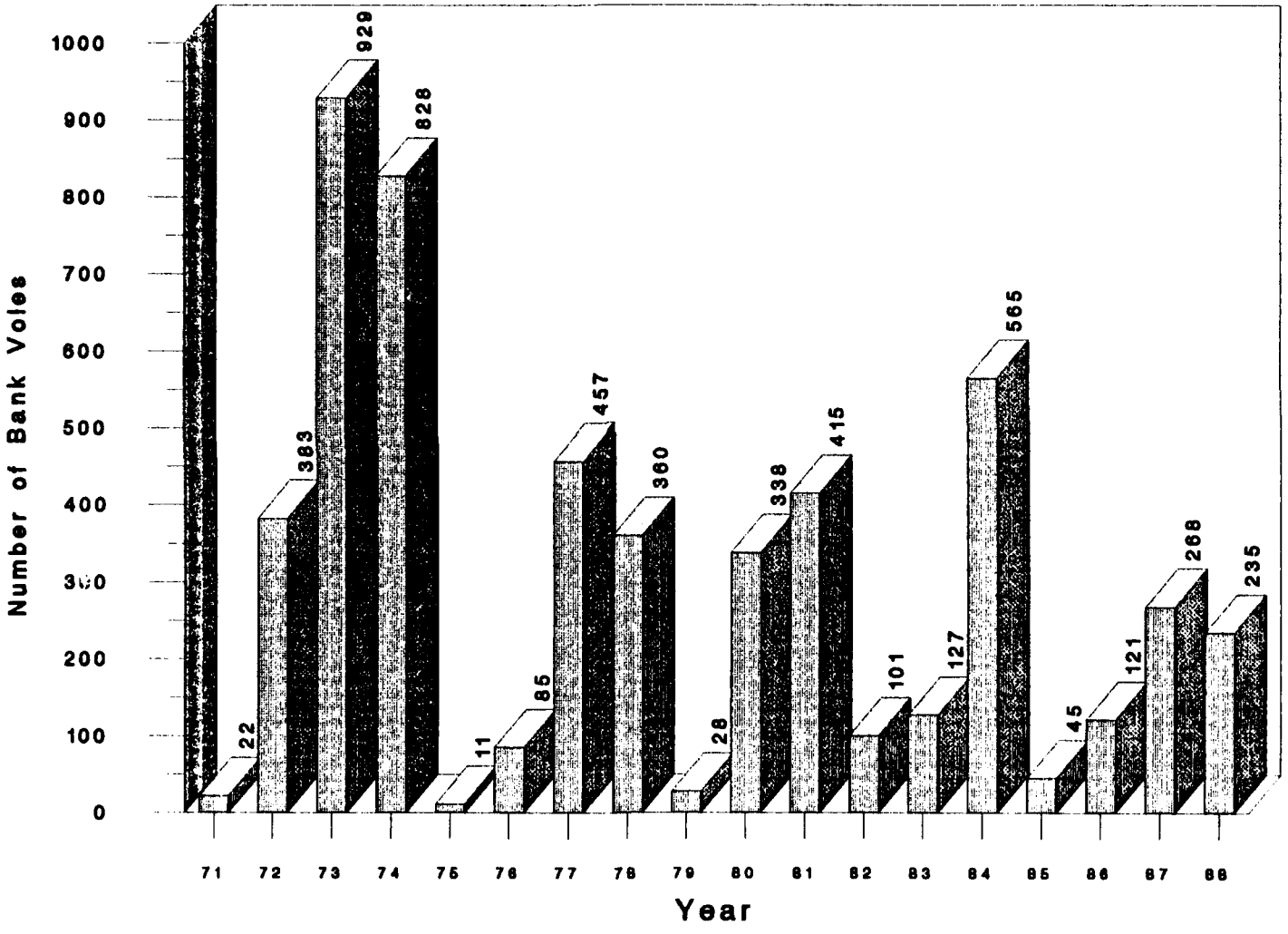

Tables 5.1.-1. and -2. Descriptive statistics from the Satellite and Weather data sets.

Table 5.1.-1.

	1982	1983	1984	1985	1986	1987
Average ± SE						
NDVI	0.26 ± 0.061	0.24 ± 0.063	0.25 ± 0.057	0.29 ± 0.065	0.32 ± 0.063	0.31 ± 0.062
Temp (ºC)	6.39 ± 0.431	6.40 ± 0.506	7.09 ± 0.477	5.84 ± 0.514	6.74 ± 0.424	6.34 ± 0.37
Precip (mm)	32.24 ± 3.645	30.31 ± 3.504	34.99 ± 3.483	41.52 ± 4.962	34.21 ± 3.83	42.18 ± 6.087
Warm Index	17.57 ± 0.922	17.29 ± 1.048	18.53 ± 1.006	16.42 ± 1.05	18.09 ± 0.89	16.86 ± 0.776

Table 5.1.-2.

	Spring	Fall	May	July	Sept
Average ± SE					
NDVI	0.3 ± 0.034	0.24 ± 0.035	0.29 ± 0.018	0.46 ± 0.012	0.33 ± 0.031
Temp (ºC)	8.69 ± 0.23	4.24 ± 0.269	7.52 ± 0.283	14.29 ± 0.171	6.79 ± 0.23
Precip (mm)	30.21 ± 2.523	40.53 ± 2.46	35.03 ± 4.907	43.19 ± 7.374	48.06 ± 5.257
Warm Index	22.57 ± 0.482	12.35 ± 0.551	20.44 ± 0.652	33.82 ± 0.42	17.58 ± 0.429

Blank Page

5.2. PUUMALA ANTIBODY PREVALENCE

5.2.1. The Relationship Between Bank Vole Population Cycles and Puumala Virus Antibody Prevalence in Bank Voles

Figure 5.2.-1 and Figure 5.2.-2 demonstrate how the antibody positive bank vole population and the total number of trapped bank voles cycle by season and by year, respectively. The relationship between bank vole population cycles and the prevalence of Puumala antibody in trapped bank voles was analyzed by location and through time. Prevalence of Puumala antibody in bank voles was regressed on total bank vole population numbers, using an inverse to variance statistical weighting procedure, for each of the sixteen individual sites, and for each of the four quadrants collapsing over time (Fall 1979 - Fall 1987). Additionally, the same procedures were conducted for the same time period, but collapsing over all the geographic areas. Figure 5.2.-3 depicts how Puumala antibody prevalences change through time. An overall Puumala antibody prevalence of 24.3% [with a 95% confidence interval of 26.0%-22.6%] was calculated for all trapped bank voles. No relevant statistical relationships emerged either spatially or through time using regression analytic procedures when Puumala antibody prevalence was regressed on total bank vole population numbers. The analyses were repeated using log and exponential transformations of weighted vole populations, and an arc sign transformation of antibody prevalence. Similarly, time lags of one, two, and three seasons were also included at the site, quadrant, and entire study area levels.

A single significant relationship emerged when the log-transformed standardized bank vole population was used to predict the arc sign transformed prevalence; $p=0.004$ with a correlation coefficient of 0.173. Statistical significance was not achieved in any of the other spatial or time dimension analyses. Even though the variation in total bank vole numbers dramatically changed through time, the antibody positive population did not vary as a set proportion for any specific season or year. Figure 5.2.-3 illustrates the lack of a relationship between the total

number of bank voles trapped and the prevalence of Puumala antibody in those voles. Note how highly variable prevalence is when population numbers are low. In other words, the highest prevalence of 0.5 was noted when one of two animals tested positive. Figure 5.2.-5 and Figure 5.2.-6 illustrate the prevalence of Puumala antibody by site and quadrant, respectively. Figure 5.2.-6 also shows the overall prevalence of Puumala antibody in trapped bank voles. Figure5.2.-7, like Figure 5.2.-4, exemplifies the lack of a clear relationship between location and the prevalence of Puumala antibody.

Fig.5.2.-1. Number of Puumala antibody positive bank voles trapped compared to the total number of bank voles trapped.

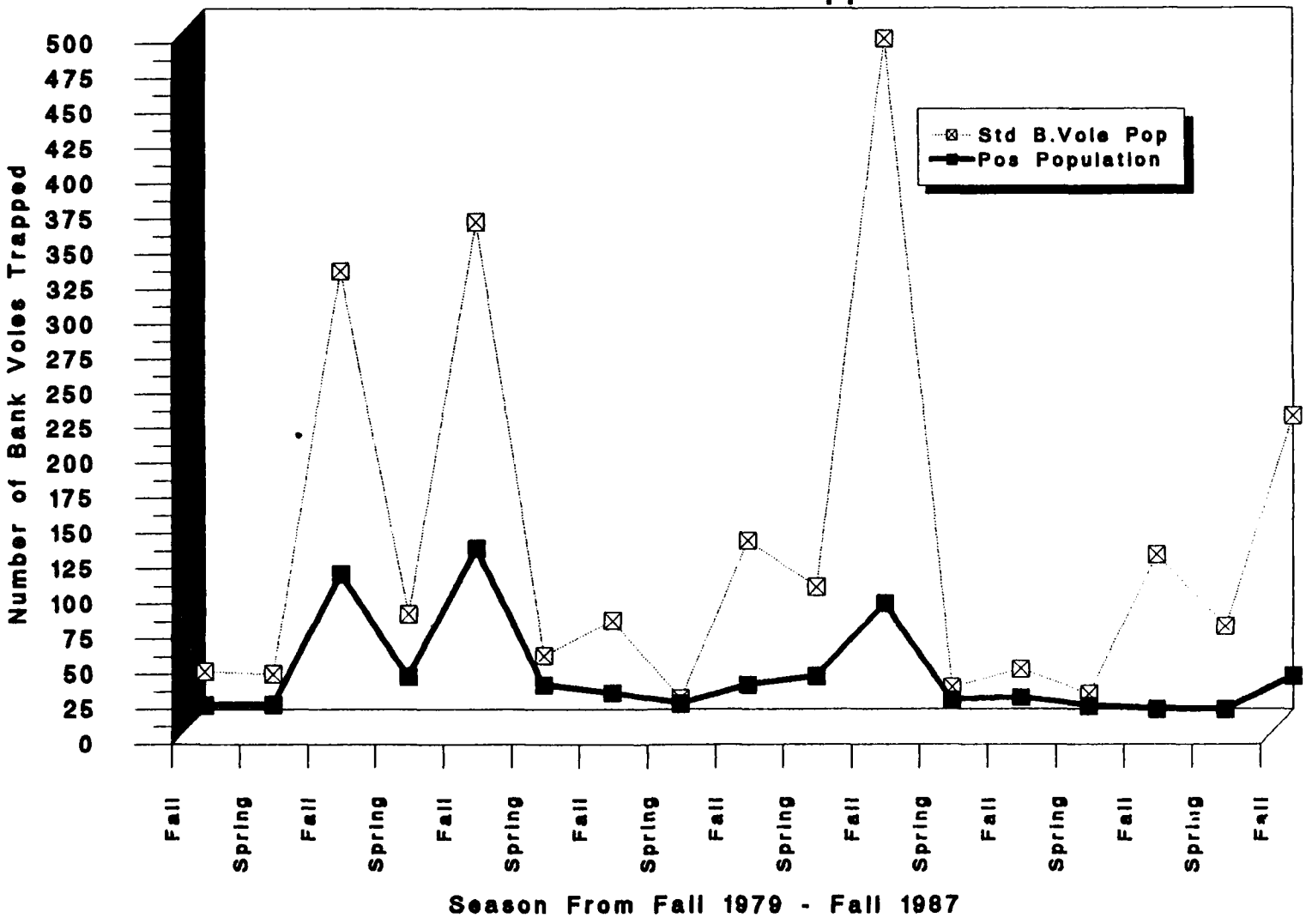

Fig. 5.2.-2. Total number of bank voles trapped by year versus the number of Puumala antibody positive animals.

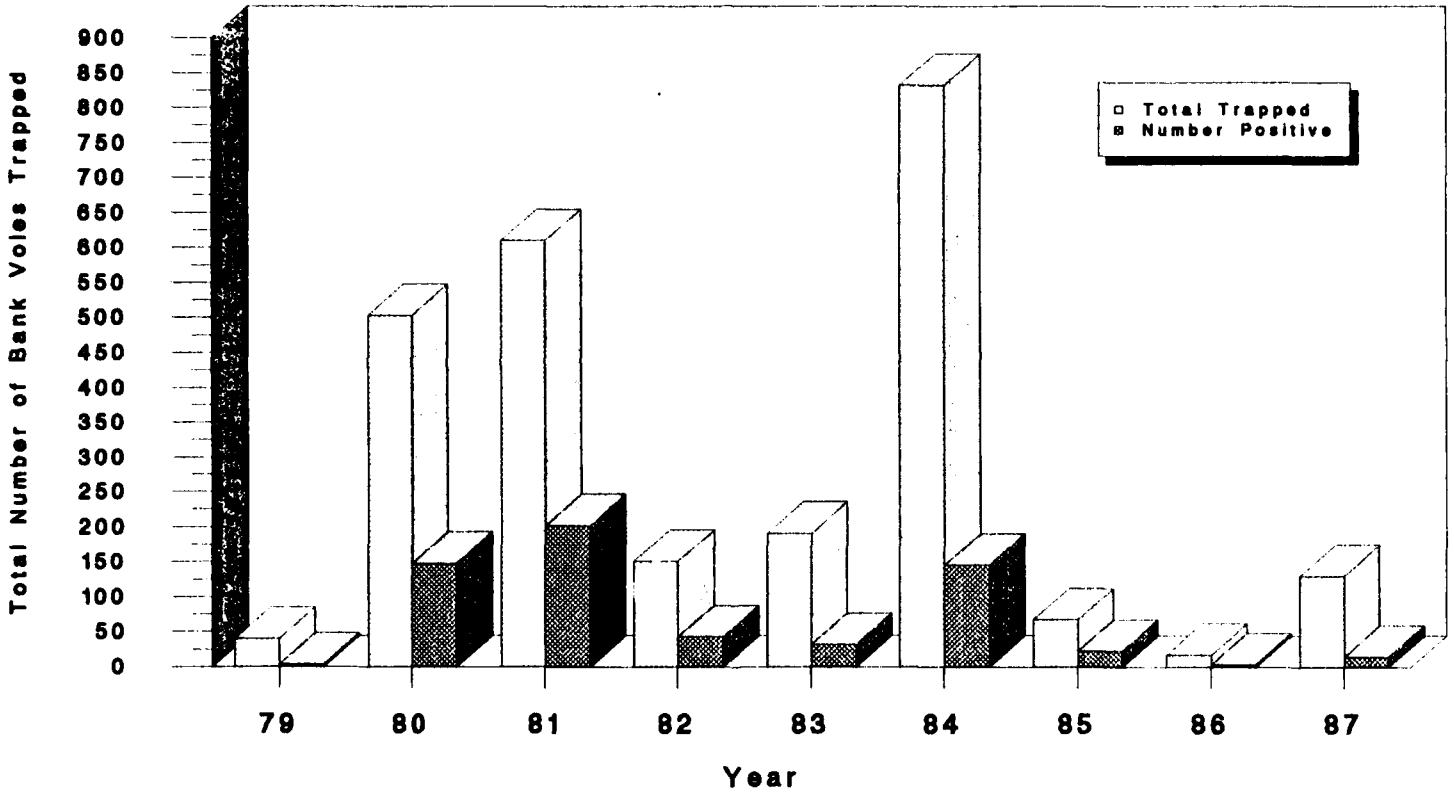

Fig.5.2.-3. Puumala Antibody Prevalence in Trapped Bank Voles, Collapsing Over Geographic Location, 1979-87

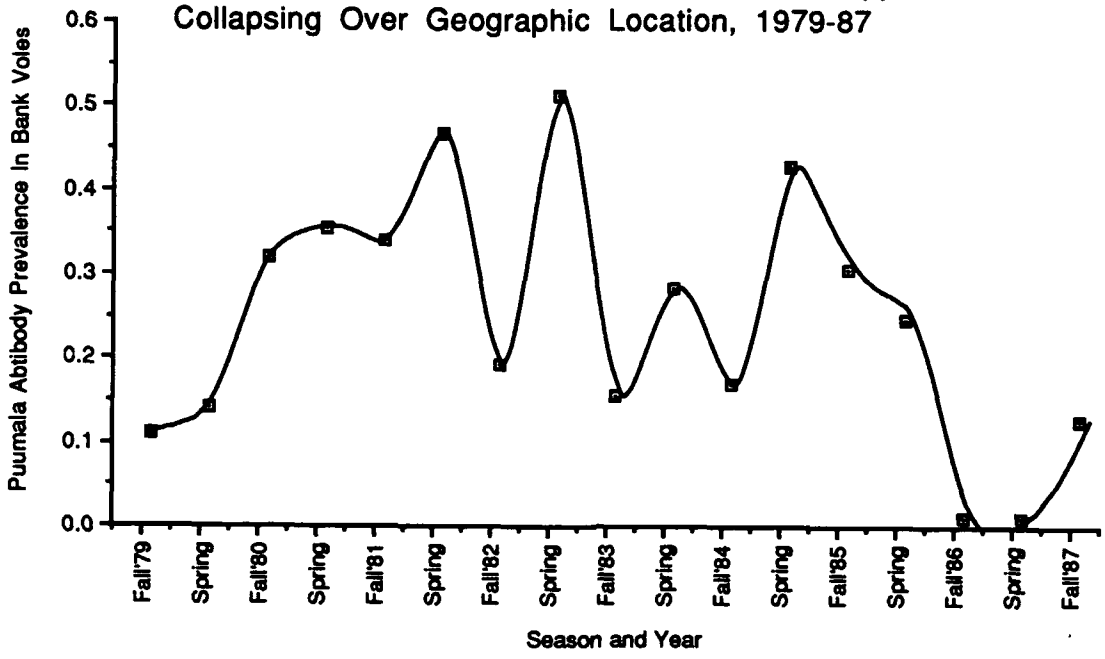

Fig 5.2.-4. The Relationship Between Bank Vole Population Numbers and Puumala Antibody Prevalence.

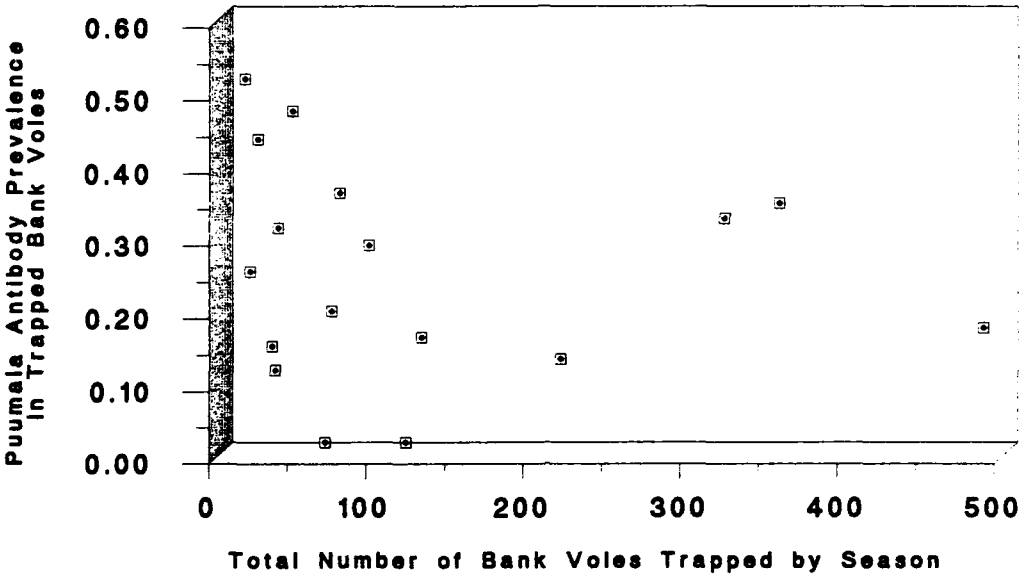

Fig.5.2.-5. Puumala Antibody Prevalence In Bank Voles by Site, Collapsing Over Time, 1979-87

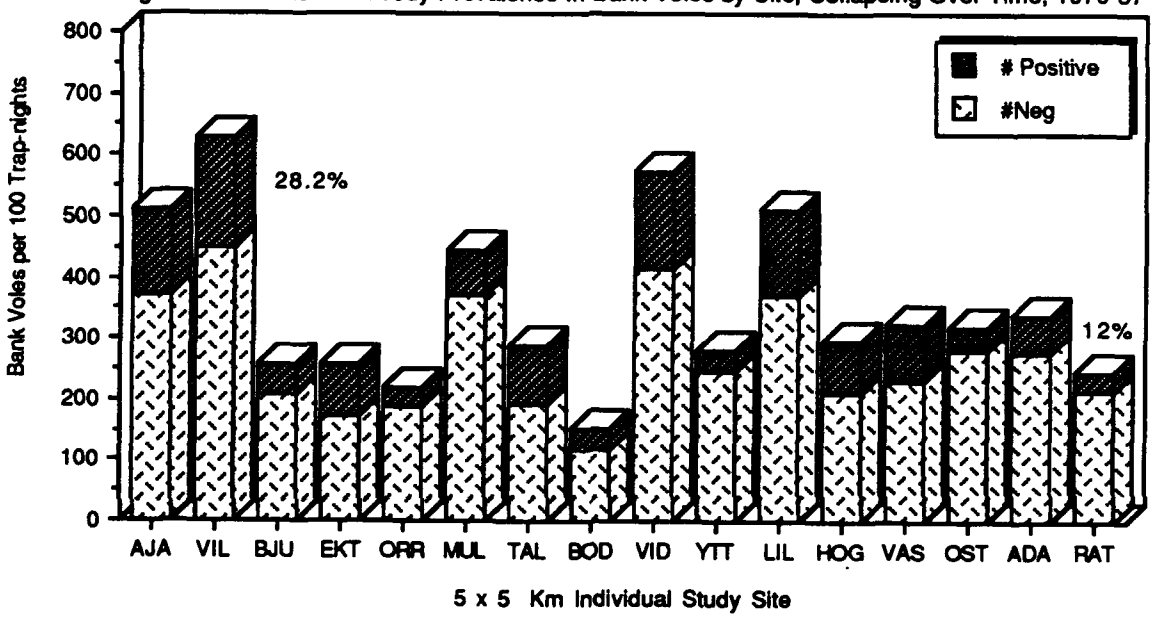

Fig.5.2.-6. Prevalence of Puumala Antibody In Trapped Bank Voles For The Entire Area and For Each Quadrant, Collapsing Over Time, 1979-1987

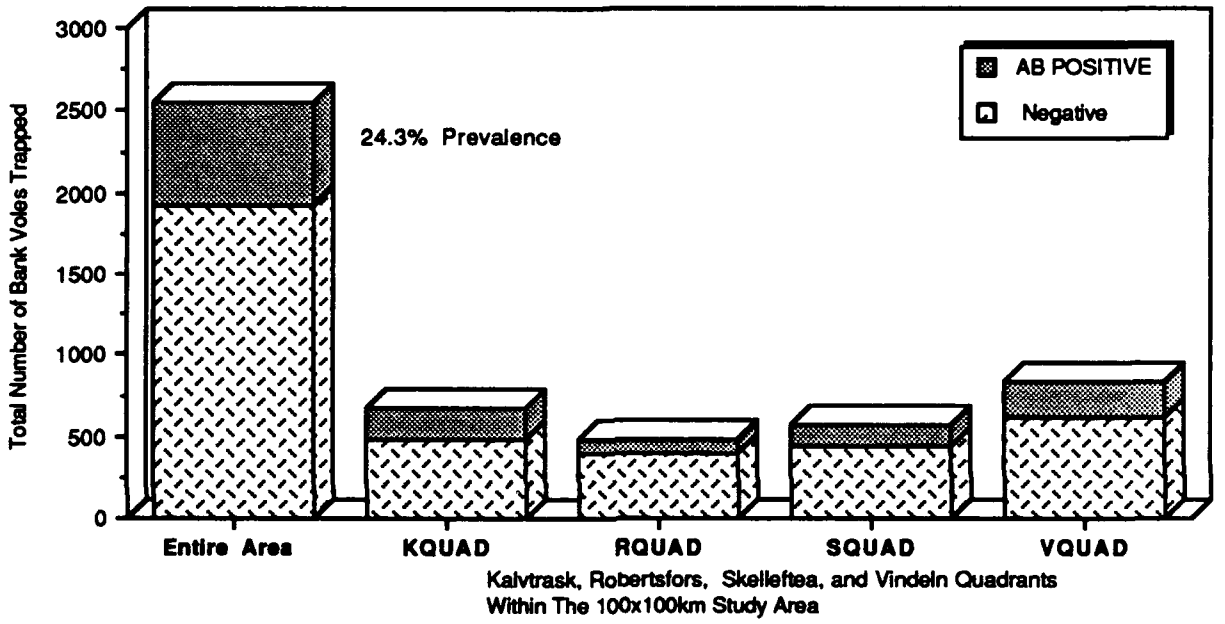

Fig.5.2.-7. Puumala Antibody Prevalence by Location

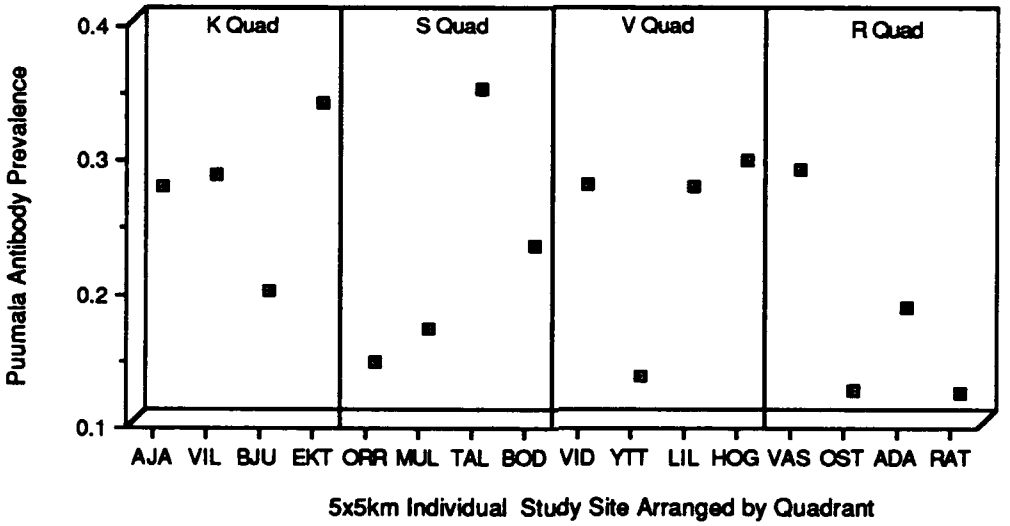

5.2.2. The Relationship Between Bank Vole Weight (Age) and Puumala Antibody Status

The average weight among the 2542 bank voles tested for antibody in this study was 18.25 grams. An average weight of 19.47±4.73 gms was noted in the 617 voles testing positive. The 1,925 voles considered to be antibody negative had a mean weight of 17.86±3.93 gms. The difference in means was statistically significant ($p<0.001$). Considering those voles captured in the Fall separately from those captured in the Spring, ANOVA procedures were used to compare the average weight of voles categorized as either antibody positive or antibody negative. Statistical significance ($p<0.001$) was present only for voles trapped in the Fall. For voles trapped in the Spring, average weight of antibody positive voles was not statistically different from the antibody negative bank voles ($p=0.42$). Table 5.2.-1 summarizes these findings.

Continuing the regression analyses, bank vole weight in grams was used to predict increasing optical density (antibody level as a continuous measure). Regression analysis revealed a statistically significant association, even though the correlation coefficients were small. Table 5.2.-2 summarizes these findings. Finally, fifteen weight classes were constructed in order to examine cross-comparisons of the frequency distributions for the following categories: Total Number of Bank Voles Trapped, Spring Captures, Fall Captures, and Antibody Status for each category. Table 5.2.-3 shows the frequency distributions. The number of bank voles trapped in the Fall always exceeded Spring captures. Also, Spring bank voles tended to weigh more than voles captured in the Fall. Finally, Puumala antibody positive bank voles tended to weigh more than negative bank voles. Therefore, those voles that survived the winter, to be trapped in the Spring, were slightly older than Fall captures, and older voles were at slightly greater risk for exposure to Puumala virus.

Table 5.2.-1. The relationship among bank vole weight, season, and antibody status.

		Sample Size	Mean Weight	F-value	P-value
Antibody Status					
	No. Pos	617	19.47		
	No. Neg	1925	17.86	71.421	<0.001
Season					
	Fall	2166	17.42		
	Spring	376	22.99	726.382	<0.001
Fall Only					
	No. Pos	497	18.57		
	No. Neg	1669	17.08	63.866	<0.001
Spring Only					
	No. Pos	120	23.23		
	No. Neg	256	22.89	0.652	0.42

Table 5.2.-2 Regression analysis of vole weight as a predictor of antibody status. (n = 2,542)

Dependent Variable	Independent Variable	F-Value	P-Value	R-squared
OD*	Weight	148.00	<0.001	0.06
(Sqrt) OD	Weight	121.13	<0.001	0.05
OD	Log (Weight)	111.46	<0.001	0.04
Log (OD)	Weight	25.09	<0.001	0.01
1/OD	Weight	8.88	0.003	0.004

*OD = optical density

Table 5.2.-3. Frequency distributions for fifteen weight classes

Weight Class (gms)*	Total Number Trapped	Season Total	Number Antibody Positive	Number Antibody Negative
(Spring)				
1.0-2.5	3	1	1	0
2.6-5.0	4	0	0	0
5.1-7.5	13	0	0	0
7.6-10.0	21	3	0	3
10.1-12.5	78	2	0	2
12.6-15.0	354	6	0	6
15.1-17.5	752	5	0	5
17.6-20.0	653	41	17	24
20.1-22.5	272	106	31	75
22.6-25.0	208	125	41	84
25.1-27.5	122	54	19	35
27.6-30.0	40	17	9	8
30.1-32.5	18	13	2	11
32.6-35.0	2	2	0	2
35.1 +	2	1	0	1
(Fall)				
1.0-2.5		2	1	1
2.6-5.0		4	1	3
5.1-7.5		13	1	12
7.6-10.0		18	4	14
10.1-12.5		76	13	63
12.6-15.0		348	66	282
15.1-17.5		747	144	606
17.6-20.0		612	127	485
20.1-22.5		166	58	108
22.6-25.0		83	39	44
25.1-27.5		68	28	40
27.6-30.0		23	14	9
30.1-32.5		5	3	2
32.6-35.0		0	0	0
35.1 +		1	1	0

*Rounded to one digit by scale

5.3. NDVI AS A PREDICTOR OF STANDARDIZED BANK VOLE POPULATION CYCLES

When NDVI was used as a predictor of standardized bank vole population cycles, statistical significance, with positive correlation coefficients, was not achieved at either the site, quadrant, or entire scene levels. Regression analyses with standardized bank vole population numbers as the dependent variable and NDVI values as the independent variable were conducted. At the individual site level the best positive correlation had an R-square of 0.007, ($p=0.794$). Likewise, no positive correlations emerged at either the quadrant or the entire scene levels. Residuals of both the bank vole and NDVI variables were calculated and used as above in regression models, yielding the same non-relationship at the site, quadrant, and entire scene levels. In fact at the quadrant and entire scene levels, all correlations were negative and were not significant. Thus de-seasonalizing or adjusting for season did not change any of the above (non-) relationships.

In addition to conducting the regression analyses with de-seasonalized variables, each of the above analyses was repeated with log transformed variables (including log transformed residuals), as well as time-lags of from 1 to 3 seasons. Together, neither positive correlations, nor statistical significance was achieved, except once. Ratubacken site, at a one-season time lag had an R-square of 0.38 ($p=.034$). Otherwise the best p-value was $p<0.08$ at an R-squared of 0.30.

Figure 5.3.-1 illustrates the statistical non-relationship between bank vole cycles and NDVI Values at the entire scene level. Although not a consistent relationship, note how bank vole population numbers peaked in the Fall 1985 while NDVI values were at a low. Figures 5.3.-2 through 5.3.-6 also illustrate how quadrant bank vole cycles and NDVI values are not well correlated.

Fig.5.3.-1. NDVI Values For the Entire Study Area versus Standardized Bank Vole Population Cycles, 1982-1987.

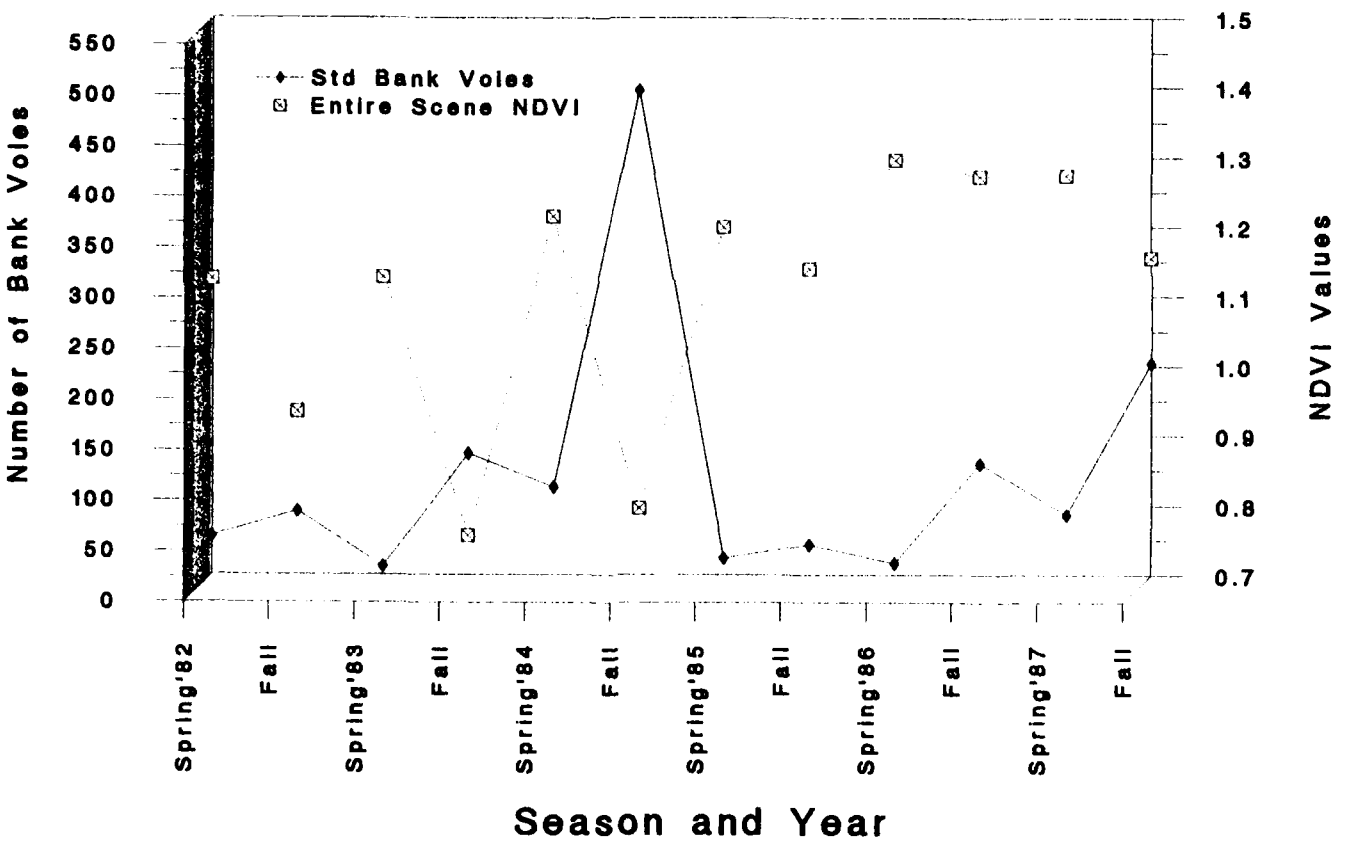

Fig.5.3.-2. Kalvtrask Quadrant NDVI Values versus Bank Vole Population Cycles

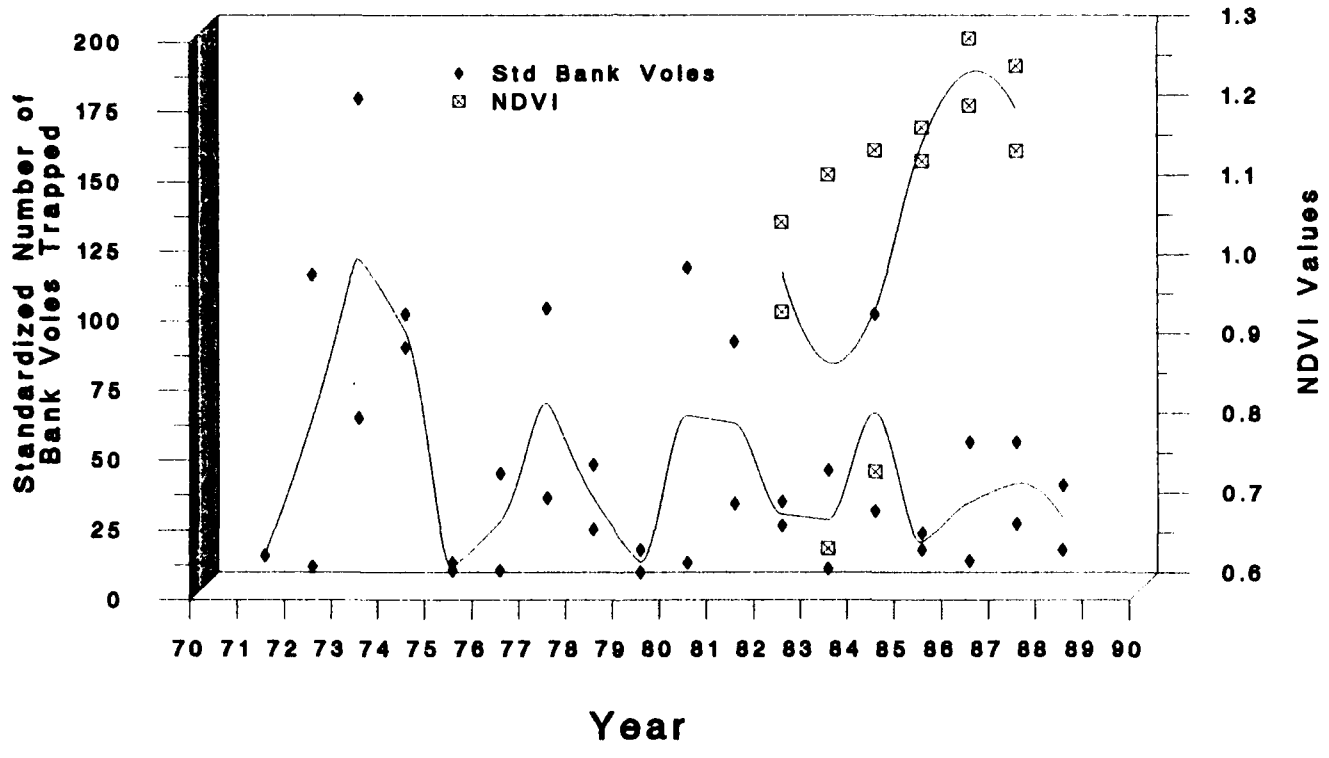

Fig.5.3.-3. Skelleftea Quadrant NDVI Values versus Bank Vole Population Cycles

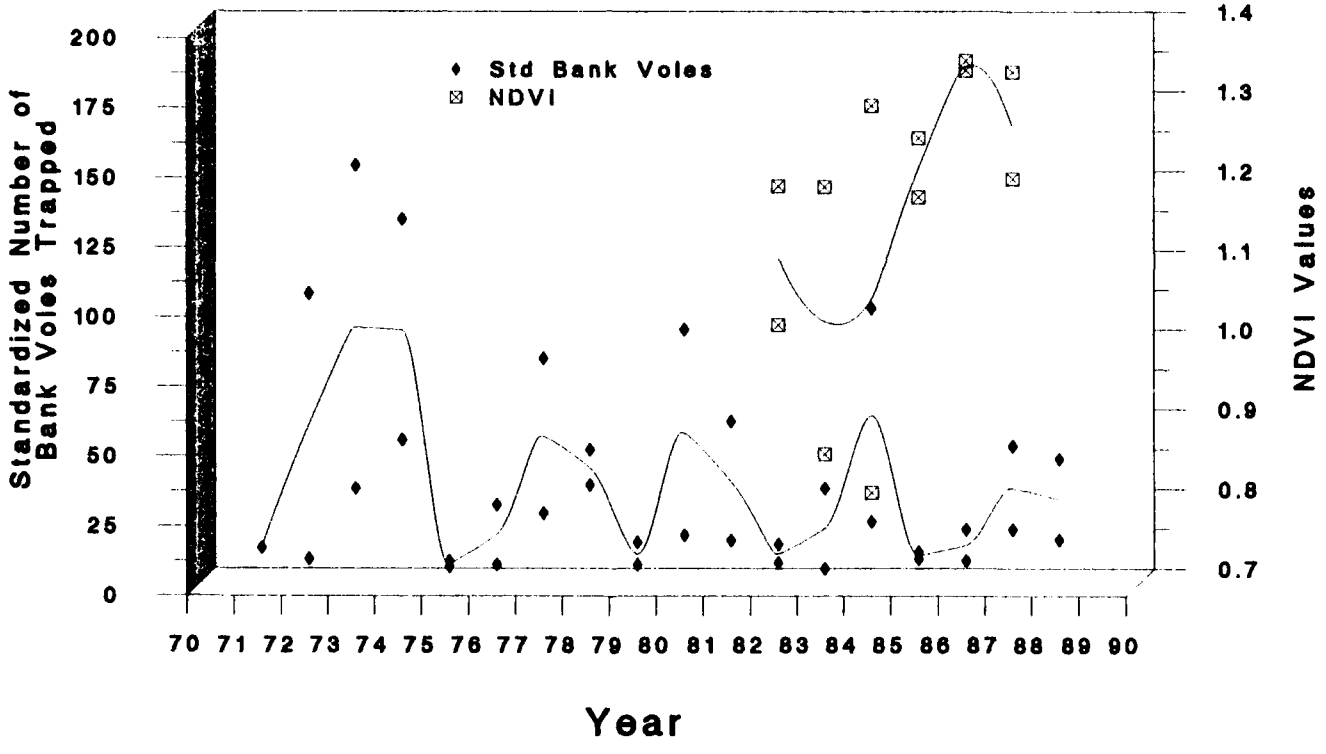

Fig.5.3.-4. Vindeln Quadrant NDVI Values versus Its Bank Vole Population Cycles

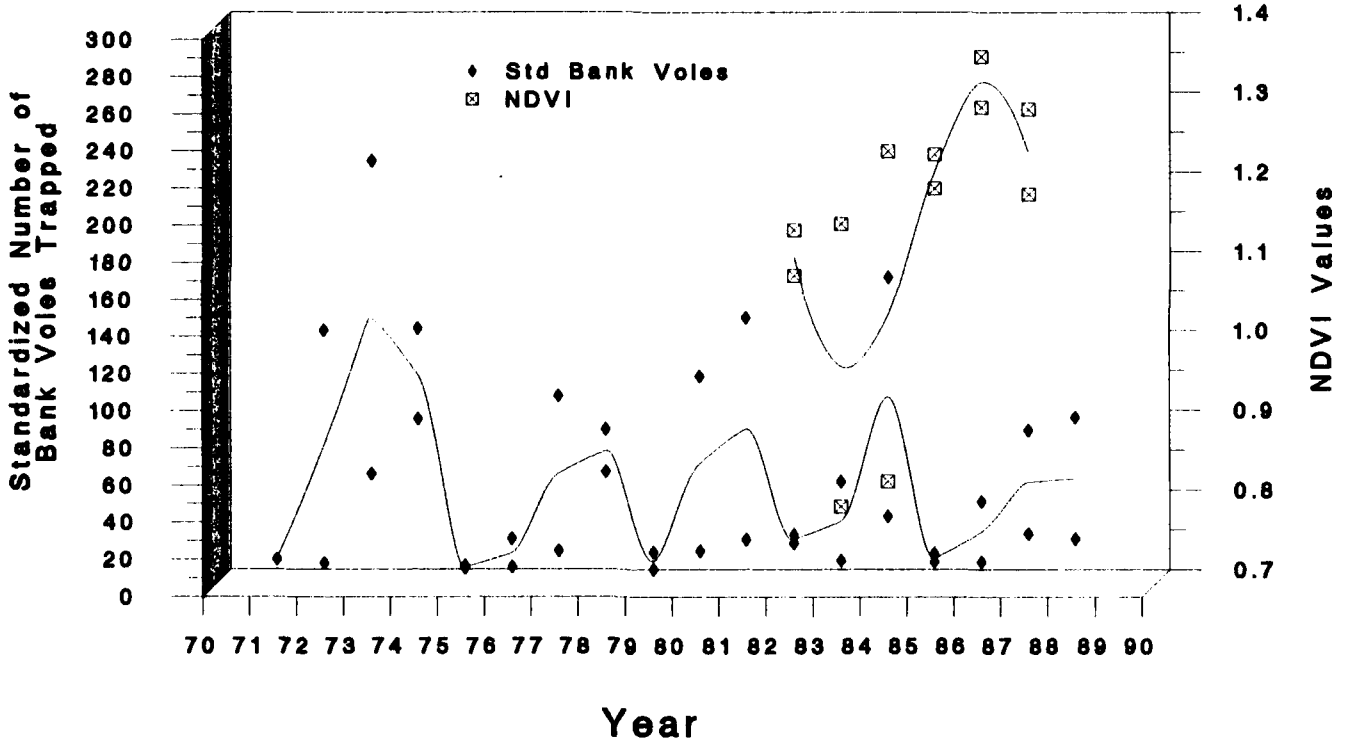

Fig.5.3.-5. Robertsfors Quadrant NDVI Values versus Its Bank Vole Population Cycles

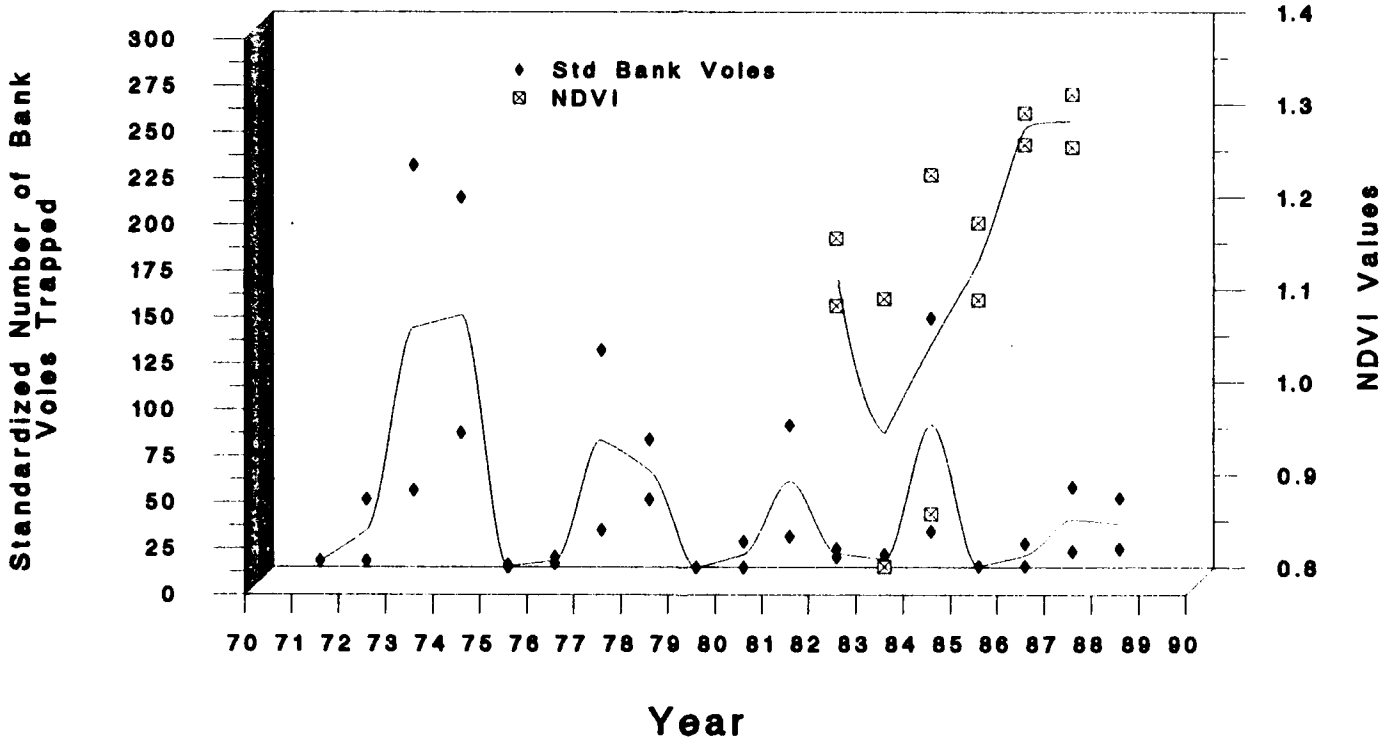

VI. DISCUSSION

6.1. INTRODUCTION

Central to understanding the epidemiology of the group of human diseases known as hemorrhagic fever with renal syndrome (HFRS) is understanding the ecology of the rodent-reservoir hosts. In Sweden, Nephropathia Epidemica (NE), resulting from Puumala virus infection, is the Scandinavian variant of HFRS. The bank vole (*Clethrionomys glareolus*) is the most important reservoir of Puumala virus. Because the bank vole is the most-numerous small mammal in Sweden and it is fundamental to the epidemiology of human Puumala virus infection, Niklasson and LeDuc stated that the basic biology of the bank vole is directly related to the probability of human disease.[1]

6.1.1. Key Findings

The experimental results from this study provide some insight into the ability to predict disease-reservoir population fluctuations, using coarse resolution remote sensing data. The key findings from this study are:

1. Relatively coarse resolution, digitized satellite data (in the form of NDVI values), do not predict bank vole population fluctuations.

2. Although NDVI values are strongly correlated among quadrants, ambient temperatures and precipitation values for the study area do not correlate well with monthly NDVI values.

3. The bank vole population prevalence of Puumala virus antibody within the study area is 24.3 percent.

4. Based on the non-existent correlation between bank vole population cycles and NDVI values, it is not possible from these data to develop an infectious disease model using satellite data to predict human Puumala virus outbreaks in Sweden.

6.1.2. Quality of the Satellite Data

The satellite data set contained monthly (Apr.-Nov.) NDVI values for the entire study area and all the sub-areas from 1982-1987. In addition to covering only one complete bank vole population cycle (1983-1986, see Fig. 5.1.-25.), in northern Sweden, snow cover during the months of November through March of each year makes it impossible to obtain meaningful NDVI values for those months. Thus, based on the limited time period for which satellite data and vole data were available, no association was found in this study. Several explanations exist for this lack of association. It may be true that no relationship exists between rodent cycles and NDVI values. Alternatively, the true relationship between rodent cycles and NDVI values may not have been observable in the time period, or the true relationship may have been obscured by the insensitivity of the NDVI measure and/or bank vole population measure.

Considering the insensitivity of the NDVI measure first: as mentioned earlier, the spectral sensitivity of the AVHRR sensors were arranged specifically for cloud mapping, as well as sea and atmospheric temperature mapping. Coincidentally, a mathematical combination of radiometric values from channel 1 and channel 2 (called the NDVI) were uniquely suited to measure the dynamic changes of green vegetation. To improve the sensor's ability to detect vegetation dynamics while at the same time decreasing the adverse effects of cloud contamination, Tucker, et al.[2] and Justice, et al.[3] developed an NDVI maximum-value compositing procedure. This procedure uses up to 30 consecutive scenes, retaining the highest NDVI value for each pixel from a 30-day, multitemporal data set. Because of the multitemporal nature of the data set, maximum-value compositing requires accurate geo-referenced or registered scenes on an individual pixel basis. The accuracy of the AVHRR sensor, set at 1.1 km resolution, is given as ±5 one-km^2 pixels per scene. If the pixel in the satellite image does not directly correspond to the same geographic area on the ground the NDVI value becomes less meaningful. However, in this study, the homogeneous nature of the landscape should have negated any location accuracy problems. Nevertheless, whenever multitemporal data sets are used, if daily images are

misregistered with each other or not correctly registered with the ground, then the quality of the NDVI values readily decreases. In the end, the highest NDVI value per pixel per month is still the yield.

Considering the time interval when constructing a maximum-value composite image, in a Spring or early Summer month with few clouds, each pixel is likely to have an end-of-month value. In the autumn months, because of normal plant senescence, each pixel is likely to have its highest NDVI value in the beginning of each month. However, depending on what day is cloudless, in a generally overcast month, the maximum NDVI value could have come from the beginning, the middle, or the end of any 30-day period. The actual date each pixel had its NDVI value assigned is not recorded by the satellite. Therefore, comparing what one thinks are monthly values may in reality be nothing more than comparing NDVI values only one day apart. The implications of not knowing the exact date at which a monthly NDVI value was recorded are greater when trying to identify a relationship between a specific habitat's effect on animal population dynamics (as opposed to just using the NDVI to monitor changing vegetation patterns). In that, by assuming each NDVI value represents a whole month, when in reality it represents a random day from within a month, may result in loss of precision. A potentially better way to obtain habitat related NDVI values would involve shortening the maximum-value compositing time frame and/or using a seven or fourteen day mean NDVI value calculated from the daily satellite fly-overs. At the very least knowing the exact day that each NDVI value was recorded would allow for a statistical assessment of its validity.

For the NDVI data set used in this study, in addition to the maximum-value composite procedure, a thermal cloud-masking technique was added.[4] Clouds typically have extremely high radiometric (digital) values and thus, by retaining maximum values, as in a 30-day maximum-value composite procedure, the potential exists for clouds to confound the NDVI measure. The thermal cloud masking technique identifies pixels that have temperatures below a pre-determined threshold and resets those pixels' digital values to zero; therefore, this procedure eliminates

potentially misleading NDVI values that have cloud-like temperatures. This assumes that the surface temperatures are higher than the defined threshold for cloud temperatures. In this way, whole pixels that are contaminated by clouds are identified and not given the opportunity to enter the NDVI data set.

The combination of a thermal cloud-mask and a 30-day maximum-value composite procedure applied to each pixel, maximizes the potential of the AVHRR's ability to detect green vegetation. In fact, when using maximum-value composite--cloud masked data, the effects of a number of undesirable variables are significantly decreased. In addition to minimizing cloud contamination, atmospheric effects, less than perfect viewing or sun angles, and surface bi-directional reflectance effects are also diminished.[5]

The ideal NDVI image is obtained from a cloudless scene, at high sun angles, under very low atmospheric humidity, and at a nadir viewing angle for each pixel. Rarely are all these ideal conditions met. However, by applying cloud-masking and compositing procedures to multitemporal data, the odds of acquiring meaningful NDVI values are improved. In spite of the tremendous advantages of cloud-masking and maximum-value compositing for improving the quality of NDVI data, several limitations can still contribute to poor NDVI data quality and hence poor sensitivity. In fact, even under the best of circumstances the current accuracy at a monthly time resolution is said to be ± 0.1 NDVI values. A measurement precision of ± 10 percent may not meet the sensitivity requirements that habitat studies generally require. [6] In fact in 1991, Goward et al. stated that further refinement and thus improved precision of satellite remotely sensed NDVI-like values, appears possible and should be a primary research focus.[6]

In addition to the potential problems of precision, misregistration, and not knowing the exact NDVI acquisition date, several other problems associated with the AVHRR sensor may contribute to poor data quality. For instance, the AVHRR's channels 1 and 2 were calibrated before launch, and do not have in-flight calibration capability. As with any scientific instrument, parameters change, moving parts wear and deteriorate, introducing uncertainty. With time,

gravitational forces may slightly change the AVHRR's viewing angle, also contributing to less than ideal NDVI data quality. Therefore the adverse effects on NDVI data quality can occur in both the spatial and temporal dimension. In other words, a specific pixel value recorded in 1986, for example, may not be the same pixel in 1989. However, given the homogeneity of the northern Swedish landscape, this error as well as any minor spatial errors had minimal affects on this study.

In addition to satellite position changes and sensor calibration drift, channels 1 and 2 of the AVHRR have very broad band widths. Narrowing these bands along with the technology to detect narrower band widths would improve sensitivity and precision thus improving data quality.

Lastly, the size and thickness of clouds over the targeted landscape could impact NDVI value accuracy. Sub-pixel size clouds or thin clouds would result in less accurate NDVI values. Inaccurate NDVI values would also result if the remote sensor attempts to detect green vegetation which is over water. Because water is known to absorb wavelengths very effectively in the Channel 1 and especially Channel 2 band region, the yield is much lower than expected NDVI values. Since the study area is not known for its cumulus cloud formations nor for having large areas of vegetation growing over water, these potential threats to NDVI quality were minimal.

As with any scientific instrument, anything that lowers sensitivity, specificity, predictive values, or simply lacks the necessary precision, also tends to decrease the quality of the data and, more importantly, the ability to predict an association. It may not be possible for a relatively crude NDVI value to predict an amplitude or frequency of a rodent cycle based on a less than ideal vegetation measure. Continued refinement to reduce the sources of NDVI error, may hold the answer for future applications.

Even though some validity issues remain unresolved, reliability of the NDVI values, between quadrants, was evaluated using correlation analyses. Between quadrants, each month's NDVI value was correlated across all six years. Cronbach Coefficient Alpha (for raw variables) values were all greater than 0.94 (with the exception of the April values, which was 0.87). Therefore, the monthly NDVI values were considered highly reliable.

In summary, although maximum-value compositing and cloud-masking techniques tend to improve NDVI data quality; inability to determine the NDVI acquisition date, ±10% NDVI error, misregistration, no in-flight calibration capability, broad band widths, and sub-pixel size or thin clouds, as well as a wet landscape would all tend to compromise the quality of the NDVI measure. These effects may explain the poor NDVI : bank vole cycle correlations found in this study.

Using a higher resolution remote sensor, with narrow band widths may be one potential solution to improving the quality of the satellite data. Even though the entire study area landscape was found to be relatively homogeneous, by concentrating on the actual one-hectare trapping sites, a more accurate picture of vegetation changes within the bank voles' habitat would result. The increased precision of a higher resolution remote sensor probably would more accurately reflect the dynamics of the vole habitat. In addition to higher resolution, at least weekly maximum value-cloud masked NDVI data, rather than monthly values, would improve satellite data quality.

6.1.3. Precision of the Bank Vole Population Measure

The frequency of the bank vole population measure could also explain the lack of an NDVI : bank vole relationship. Even though rodent cycles were carefully observed for more than seventeen years, counts were done only twice each year. Therefore, bank vole population figures may not have represented true population fluctuations. Since bank voles were trapped on a semi-annual schedule, the true peaks and valleys of the population cycles may have been obscured. Hörnfeldt confirmed an approximate four-year periodicity using time series, autocorrelation methods applied to the bank vole population cycles presented in Figure 5.1.-1 ($r=0.653$, $p < 0.001$).[7] Likewise, his spectral analyses revealed an approximate 3-4 year periodicity, although distinct spectral peaks were difficult to achieve. Hörnfeldt also noted that for Fall bank vole numbers, fitting a second order autoregressive process in a pseudoperiodic time series model, a pseudoperiod of 4.44 years emerged.[7] In other words, bank vole populations cycled somewhat regularly but with inconsistent amplitudes. Conversely, bank vole population

cycles did not fit a periodic time series model where both periodicity and amplitudes are consistent through time.[7] Hörnfeldt also confirmed a dramatic seasonal component where, in addition to the 4.44 year population cycles of bank voles, a clear pattern of regularly decreasing bank vole numbers in Winter, followed by increasing numbers in Summer, was evident.[7]

Hörnfeldt's work documents the importance of long-term, high-quality field studies. Only because of efforts like his, can studies involving the evaluation of remote sensing instruments take place. A semi-annual measure of rodent populations was all that Hörnfeldt needed to illustrate the cyclic nature of bank vole populations in boreal Sweden. However, if changes in habitat (i.e. amount and quality of rodent food supply, shelter, etc.) play a role in population cycles and may even be indicators of vole cycles, then more frequent population counts may be necessary. Ideally, a twice-monthly (or more frequent) rodent-count using a capture-mark-release system would improve the precision of the bank vole population numbers. However, because of adverse weather conditions, as well as higher costs, twice-monthly rodent population counts may not be practical.

Nevertheless, the combination of more frequent high quality NDVI values as well as more frequent bank vole population samples could yield the precision necessary to begin to identify or rule-out some of the environmental issues surrounding the triggers of rodent cycles.

6.2. NDVI CORRELATIONS BETWEEN EVER INCREASING GEOGRAPHIC AREAS AND METEOROLOGICAL VARIABLES

6.2.1. NDVI versus NDVI Correlations

Monthly NDVI values from each of the individual 5x5 km sites (approximately 1 pixel each) are strongly correlated with its quadrant NDVI value. Likewise, the NDVI values from each of the four 50x50 km quadrants (usually 96 pixels) are strongly correlated with the entire 100x100 km study area (373 pixels). Given the relative homogeneity of the northern Swedish landscape (74 percent forest, 15 percent peat land, and 6 percent agricultural land), one would expect to see

strong correlations between NDVI's obtained from individual pixels and NDVI's from larger groups of pixels in about the same geographic and topographic area. This is a convenient finding since the weather data were collected at the entire scene level. The strong correlations among NDVI values found in this study, from ever-increasing geographic areas (5x5 km to 50x50 km to 100x100 km), suggests that, as long as the landscape of a study area is relatively homogeneous, using the NDVI values of the largest unit may be an efficient way to perform large-scale habitat evaluations.

6.2.2. NDVI versus Meteorological Variables

The original goal was to use meteorological data as a surrogate for NDVI values. This would allow for the extension of the NDVI data set to coincide with the whole time period in which bank voles were trapped. It is generally accepted that highly significant correlations exist between NDVI values and specific weather variables. In particular, strong positive correlations between precipitation and NDVI have been noted. In this analysis, an R-Square of 0.83 ($p=0.01$) was obtained using General Linear Models Procedure with monthly NDVI values as the dependent variable, and both monthly precipitation and a monthly warm index as predictor variables. However, both NDVI and weather variables tend to have highly seasonal rates of variation. For example, warmth and NDVI typically peak in July. Conversely, weather parameters and NDVI values are low in early Spring and late Fall. Also worth noting, because of snow cover, NDVI values are not available for the winter months. Additionally, because the large study area is located in northern boreal Sweden, close to the Arctic Circle, the growing season is compressed-when compared with more southern latitudes. Thus, both the long winter and short growing season contribute to highly regular, seasonal changes in weather parameters and NDVI values. This regularity, which guarantees high correlations between monthly NDVI values and weather parameters, is uninformative in the possible prediction of bank vole population fluctuations. because the NDVI and meteorological data are very consistent and predictable through time, while bank vole population cycles are not, particularly the population amplitudes. It is therefore

important to de-seasonalize each of the variables in order to make valid comparisons. In this study, deseasonalization through residual analysis was used as one approach to highlight the exceptional values in both the satellite and meteorological data sets. The NDVI and meteorological data sets are very similar to stationary time series models. A stationary time series is defined to be a random process whose mean, variance, and covariation between separate terms do not vary in time. As a result both the NDVI and meteorological data sets are very consistent and predictable through time, while bank vole population cycles are not as predictable. Therefore the regular, almost metronomic NDVI and meteorological data should not be expected to have any predicting value as a forecasting tool for bank voles. Rather, any exceptional or extraordinary months may impact or indirectly influence, and thus predict bank vole numbers. Residual analysis or deseasonalization, both a form of differencing, served to remove the expected background noise, while emphasizing the uncommon data points. Residual analysis therefore, allowed for the statistical evaluation of each June with all the other Junes in the time series, where deviations from average monthly values were compared. The values for each month were compared to what is normal for that particular month. The effect is to control for the known yearly cycles, where July is always the peak and November is always the valley. Residual analysis assesses the appropriateness of a model according to the behavior of the set of observed residuals. The residuals of the variables reflect the amount of difference or discrepancy between the observed and the predicted values that is still present after having fit the least-squares model. In this way the "normal" or "usual" amount of variance is removed, leaving only the exceptional variance for analyses. Once the variables are de-seasonalized, the weather variables lose almost all of their ability to predict NDVI values. As a result, extension of the NDVI data set by using weather variables as surrogate NDVI measures was not practical. Therefore, it was not possible to confirm an initial assumption that NDVI values are strongly associated with several meteorological variables. It appears that, contrary to the initial assumption, monthly NDVI values are not strongly associated with monthly precipitation and a monthly warm index in these data.

6.3. BANK VOLE PUUMALA ANTIBODY STATUS

6.3.1. Antibody Prevalence as Predicted by Population Fluctuations

Bank vole population prevalence of Puumala antibody was 24.3 percent, using an ELISA test, where an optical density (OD) of 0.1 was considered positive. As mentioned earlier, under carefully controlled laboratory conditions, the antibody status of bank voles does not appear to affect any physiological variables including eating behaviors, activity levels, or life-span when antibody-positive voles were compared with antibody-negative voles. It is also worth noting that Puumala antibody positive bank voles continue to effectively shed Puumala virus in all body secretions. Also, as mentioned earlier, the incidence of HFRS, specifically NE, rises with each bank vole population peak.

Using several different types of laboratory tests, Puumala antibody prevalences of 10-15 percent in bank voles is considered usual. The results of this study indicate a prevalence of 24.3 percent. Several possible explanations exist for the higher prevalence found in these data. All bank voles trapped in this study came from Vasterbotten County in northern Sweden, a known, highly endemic Puumala virus regions, with one of the highest incidence rates of NE in Sweden. It is not surprising therefore, to find a higher than usual Puumala antibody prevalence rate in the sub-population of bank voles living in this region. On the other hand, the ELISA test used to identify antibody positive bank voles is thought to lack some specificity, while remaining an extremely sensitive test. As a result, false-positives may have been a problem. Currently, a highly sensitive and highly specific monoclonal-antibody test is under development. Once perfected, the monoclonal-antibody test will have the ability to detect the actual Puumala virus strains and their associated antibodies in both bank voles and humans which are directly responsible for the human illness.

Once specific pathogenic strains of Hantavirus (including Puumala virus) are identified by a series of monoclonal-antibody tests, it will be possible to trace the most virulent strains back to specific geographic locations. Knowing high-risk locations would help to concentrate preventive

measures and thus decrease the risk of disease in those areas. Likewise, public health education efforts could also be undertaken, offering effective intervention strategies to people who are at the highest risk of infection. Preventive measures could include targeting specific rodent species for control. In addition to improving diagnostic tests, identifying high-risk locations, and implementing public health education programs, monoclonal-antibody technology should lead to the development and production of safe and efficacious human Puumala virus and/or other HFRS vaccine(s).

Although one would have expected to find an increase in the proportion of antibody-positive bank voles as total bank vole populations peak, this was not found in this study. In fact, the total and positive populations were almost independent of one another. The answer for this independence, more than likely will be found in Puumala virus--environmental survivability studies. Although data on Puumala virus survivability do not currently exist, it would seem logical that the virus would have a short environmental life-span. If it cannot survive long outside of its host, a constant supply of newly susceptible rodents, in addition to an efficient transmission mechanism would be needed for virus perpetuation. Alternatively, a threshold transmission mechanism could conceivably explain why total bank vole population numbers did not predict antibody-positive population numbers. In short, a certain proportion of individual bank voles must be capable of shedding Puumala virus before transmission (at a predictable rate) to the rest of the susceptible bank vole population can occur. Another possibility could involve the level of Puumala virus contaminating the environment, where once a critical threshold level of environmental contamination is reached, only then can transmission of virus proceed at a predictable rate through the susceptible bank vole population. In this study, quite possibly, because theoretical thresholds of either virus positive bank voles, or the required level of virus in the environment was not achieved, total bank vole population cycles were not able to predict Puumala antibody positive population cycles. Recall that Puumala viral transmission among voles, and between voles and humans, is probably the result of exposure to virally-contaminated

aerosols. No relevant statistical association existed between the total bank vole population and the antibody-positive population. Indeed no relevant associations were found, either in time or in space. The implication of such a finding may prove useful when considering rodent-control methods; controlling the total bank vole population may have an impact on absolute numbers only, but may not affect the Puumala virus-positive population. In other words, controlling total bank vole numbers may not be the most effective or efficient way of decreasing the risk of human disease.

6.3.2. Bank Vole Age and Antibody Status

As bank voles mature from neonate to adult, their body weight increases at a relatively constant rate. Bank voles weigh about 2 grams at birth; a typical adult averages around 18-19 grams. Because weight and age are almost linearly related in the first few months of life, weight can be used as a surrogate measure of age. Although there are a number of other factors that cause significant weight variation, the age:weight relationship generally applies as long as gravid or lactating females are excluded. Pregnant females, especially those near term, are considerably heavier than either males or non-gravid females of the same age. Figure 6.3.-1. (adapted from Raczynski[8]) shows graphically how age and weight are related.

Recall that the bank vole breeding season begins in early Spring and can continue through Fall of each year. A mature female can potentially produce 3-4 litters per year, with litter sizes of 3-7 newborns. More importantly, females born in the first litter of each Spring may themselves produce their first litter by Fall of that same year. Assuming bank vole weight is a reasonably good estimate of age, older voles were more likely to be trapped in the Spring sample. Also, older voles were more likely to be Puumala antibody positive. However, because gender, pregnancy, or lactation status was not available on trapped bank voles, the weight of pregnant or lactating females would tend to over-estimate their age. Therefore, any age : antibody status conclusions must be interpreted cautiously.

Fig.6.3.-1.
The Relationship Between Bank Vole Weight and Age

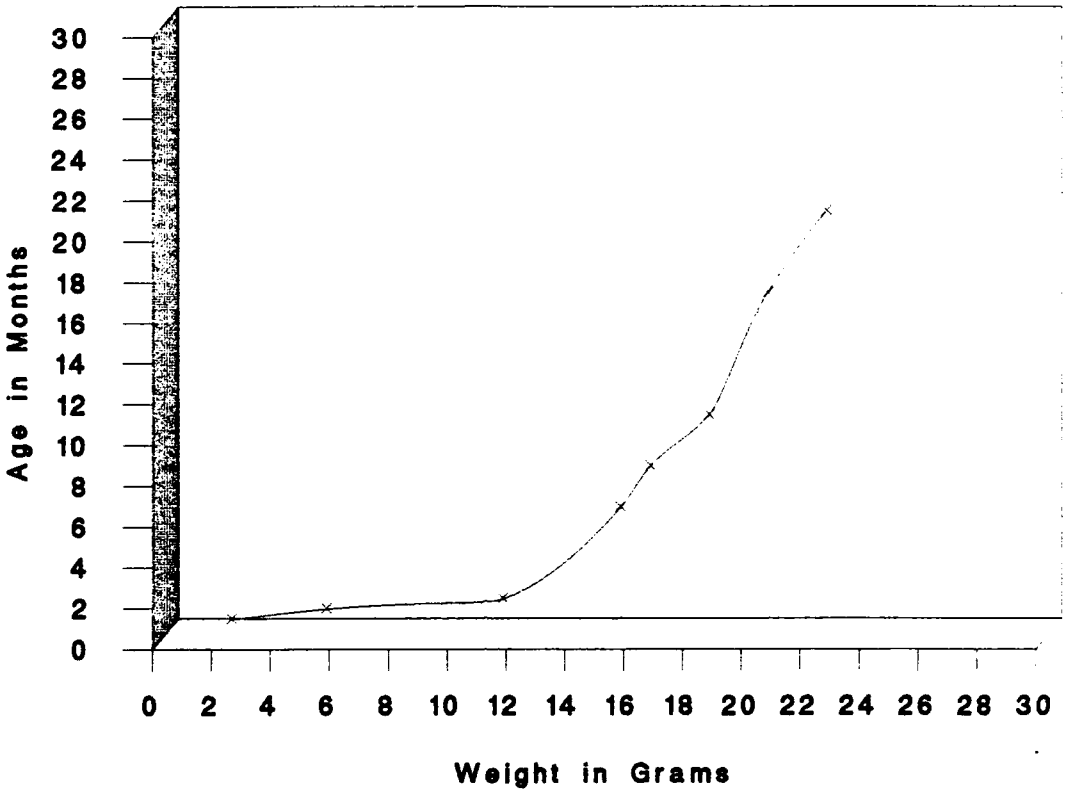

6.4. References

1. Niklasson B, LeDuc JW. Epidemiology of Nephropathia epidemica in Sweden. J Infect Dis 1987; 155(2).

2. Tucker CJ, Townshend JRG, Goff TE. African land cover classifications using satellite data. Science 1985; 227:369.

3. Justice CO, Townshend JRG, Holben BN, Tucker CJ. Phenology of global vegetation using meteorological satellite data. Int J Rem Sens 1985; 6:1271.

4. Tucker CJ, Gatlin J, Schneider SR, Kuchinos MA. Monitoring large scale vegetation dynamics in the Nile Delta and River Valley from NOAA AVHRR data. Proceedings of Conference on Remote Sensing of Arid and Semi-Arid Lands, Cairo, Egypt, January, 1982: 973.

5. Holben BN. Characteristics of maximum-value composite images from temporal AVHRR data. Int J Rem Sens 1986; 7(11):1417-34.

6. Goward, SN, Markham B, Dye DG, Dulaney W, Yang J. Normalized difference vegetation index measurements from the AVHRR. Rem Sens Environ 1991;35:257-77.

7. Hörnfeldt B. Cycles of voles, predators, and alternative prey in boreal Sweden [Dissertation]. Umeå, Sweden: University of Umeå, 1991.

8. Raczynski J. Characteristics of the species. [In: Petrusewicz K, ed. Ecology of the bank vole.] Acta Theriol 1963; 28 (Suppl 1):11,19,21,24.

VII. SUMMARY AND CONCLUSIONS

There is convincing evidence that the bank vole (*Clethrionomys glareolus*) is the most important reservoir host for human Puumala virus in Sweden. Bank vole populations fluctuate dramatically over a 3-4 year cycle, and in this study varied as much as 150-fold between peak population densities. The occurrence of human disease caused by Puumala virus has been shown to parallel closely bank vole population cycles. Hornfeldt's findings suggested bank vole population cycles are influenced by environmental conditions such as weather patterns, vegetation growth, food supply, and predators, as well as other factors. Of these factors which are thought to modify bank vole cycles, some vegetation parameters can be efficiently monitored and evaluated over large geographic areas with satellite imagery. This was the basic rational for this study.

The purpose of this project was to use existing data from Sweden on bank vole population cycles and retrospective satellite imagery in an attempt to correlate satellite-derived, Normalized Difference Vegetation Indices (NDVI) with bank vole population cycles and to identify, more accurately, the risk of human Puumala virus outbreaks. Under the research hypothesis that it would be possible to predict human Puumala virus epidemics in Sweden using satellite imagery, this study sought to provide information relevant to a growing capability of forecasting a number of vector-borne or zoonotic, reservoir-borne diseases.

The findings from this study suggest that relatively coarse-resolution, digitized satellite data (in the form of NDVI values), do not predict bank vole population fluctuations. However given the limited number of data points, this conclusion must be considered tentative. Additional studies using NDVI values obtained with higher precision and more frequently monitored animal reservoir population fluctuations would be ideal. Improving NDVI precision may involve the use of advanced technology, higher resolution remote sensing instruments with the ability to obtain more frequent habitat assessments in narrow band widths, especially in the red and infrared wave-length regions. Coupling a more precise NDVI with more frequently monitored reservoir population numbers would offer a better test of the ability of NDVI values to predict rodent

reservoir cycles. Figures 7.0.-1. and 7.0.-2. summarize the findings from this study and illustrate by shading how poorly correlated NDVI values are with the number of standardized bank voles trapped by site. Although not drawn to scale, the cells represent the individual, 5x5 km, trapping sites. The darker the shading the higher the values. Note how NDVI values, when ranked from lowest to highest, are oriented generally in a west to east direction, while bank vole concentrations follow a mostly northeast to southwest direction. Quadrant NDVI and bank vole population densities are shown in 7.0.-2.A. and Figure 7.0.-2B respectively. Again, note how a clear pattern does not emerge.

In this study, NDVI values were found to be strongly correlated among ever-increasing geographic areas: individual site NDVI values were strongly correlated with their quadrant NDVI value and quadrant NDVI values were strongly correlated with the NDVI obtained from the entire 100x100 km scene. This finding confirms the usefulness of the AVHRR sensor to obtain information on vegetation dynamics at a regional scale. As long as the geographic area under study is relatively homogeneous and absolute precision is not a strict requirement, information on vegetation collected at a continental scale is possible. Improving the precision of the remote sensing instrument would only serve to improve the potential uses of such data.

Conversely, this study was not able to confirm an association between meteorological variables and monthly NDVI values. Although, initial results, before de-seasonalizing, were significant, once residuals were substituted the initial relationships were lost. Thus, de-seasonalizing is an important requirement when searching for the true associations in variables that ebb and flow normally on a somewhat regular time series.

Other findings included a prevalence of 24.3 percent of Puumala virus antibody positives within the bank vole population trapped in the study area. This result may slightly overestimate the true prevalence of Puumala virus antibody in bank voles. Several very closely related serotypes of Puumala virus, both pathogenic and non-pathogenic strains, are thought to exist; the current ELISA laboratory test may falsely group all strains into the pathogenic group. A monoclonal antibody test is currently being perfected and will have the required sensitivity and

specificity to detect accurately only the pathogenic strains. The monoclonal antibody test will provide an accurate estimate of the true prevalence of the disease-causing Puumala virus strains.

Furthermore, this study was unable to predict the population cycle amplitudes of the antibody positive bank voles given total bank vole population numbers: no relevant statistical relationships emerged either spatially or through time when Puumala antibody prevalence was regressed on total bank vole population numbers. Again, the monoclonal antibody test mentioned above may provide the precision necessary to make such a forecast. It is important to be able to predict the virus positive population cycles, because focusing on the virus-carrying reservoir-population will make human disease prevention efforts more efficient.

The number of bank voles trapped in the Fall always exceeded Spring captures. Further, Spring bank voles tended to weigh more than those captured in the Fall. Finally, Puumala antibody-positive bank voles tended to weigh more than the negative ones. Except in pregnant or lactating female voles, weight can be used to estimate age. Therefore, those voles that survived the winter, to be trapped in the Spring, were slightly older than Fall captures, and older voles were at slightly greater risk for exposure to Puumala virus. Knowing that population numbers are low at the beginning of each breeding season and that older voles are more likely to sero-convert, may improve the timing of any bank vole population-control efforts; preventing the vole population surge that occurs over the summer months, would probably also decrease the potential for Puumala virus transmission to humans.

Based on limited data, this study was unable to find an association between bank vole population cycles and NDVI values and, thus, it was not possible to develop an infectious disease model using satellite data to predict human Puumala virus outbreaks in Sweden. Nevertheless, this area of Sweden with its cyclic reservoir populations is an ideal natural laboratory and deserves further study. In addition to improving the satellite measure, the bank vole population frequency measure, and the diagnostic laboratory test, the actual biological mechanisms that serve to trigger bank vole cycles should be better identified. Also, differences among bank vole populations that are Puumala virus-free and virus-infected requires further study. Of the sero-positive bank voles,

more details into how Puumala virus-shedding affects the vole and the environment are crucial to understanding the human risk of disease. Armed with the information from the above studies, a model able to forecast the potential for Puumala virus outbreaks would be much closer to becoming a reality. In a more broad context, given a vector- or reservoir-borne zoonotic disease that has a readily identifiable environmental marker, the potential for using satellite remote sensing techniques as an epidemiologic tool shows great promise and should remain a research priority.

Fig.7.0.-1.A. Vegetation Index or NDVI by Individual Site, 1982-87

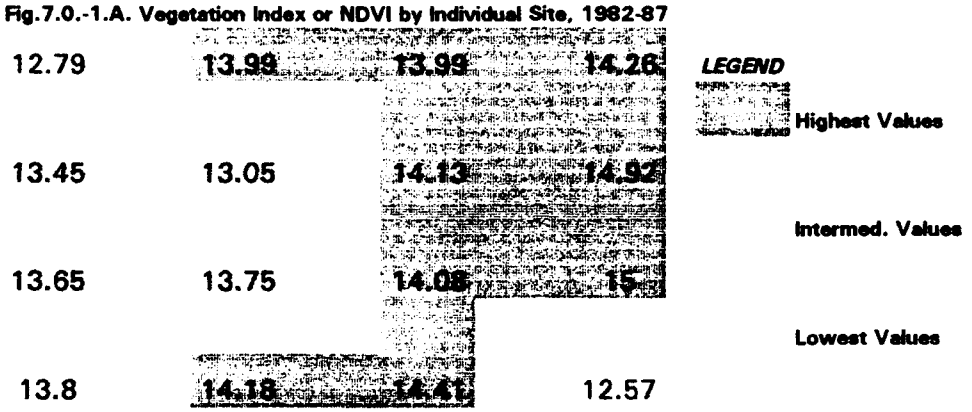

Fig.7.0.-1.B. Standardized Bank Vole Population by Site, 1982-87

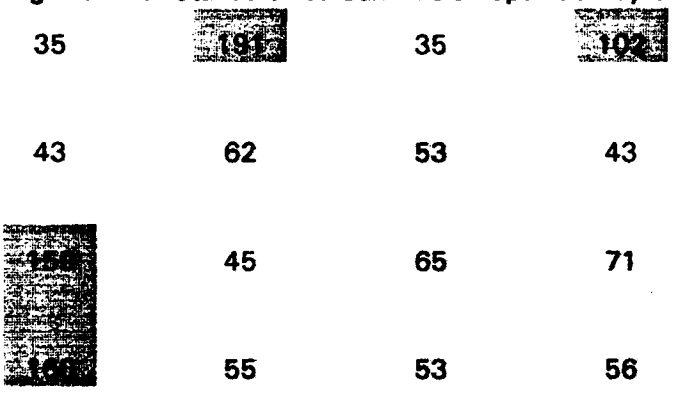

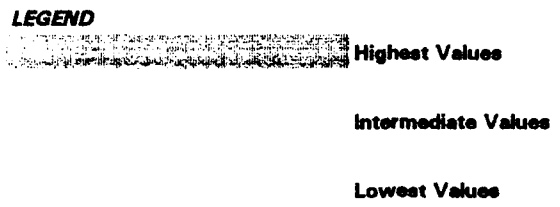

Fig.7.0.-2.A. NDVI Values by Quadrant, 1982-87

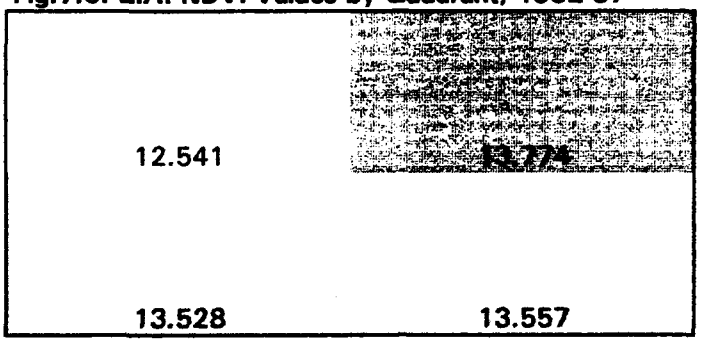

Fig.7.0.-2.B.Standardized Bank Vole Population by Quad 1982-87

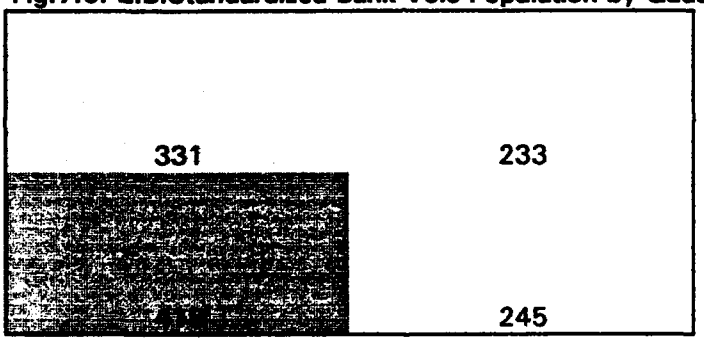

APPENDIXES

Appendix 1 Unadjusted Satellite Data

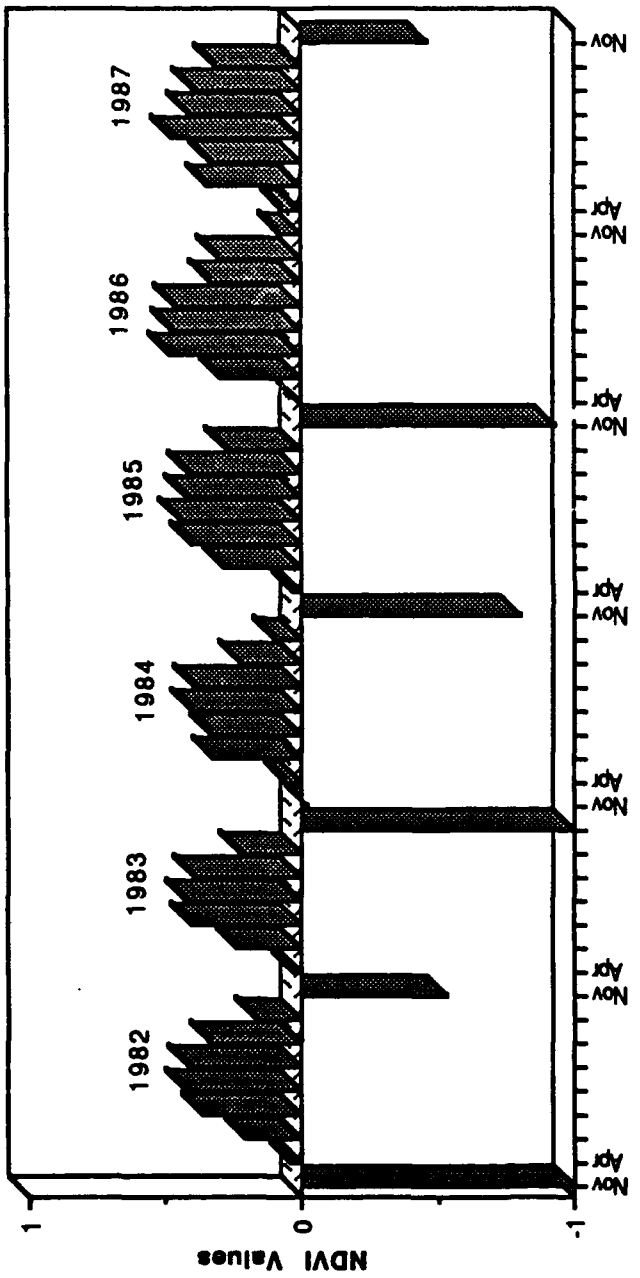

Fig. 5.1.-2. Satellite Data - Kalvtrask Quadrant 50x50 km (96 pixels)

Fig. 5.1.-3. Satellite Dat.. - Ajaur Site

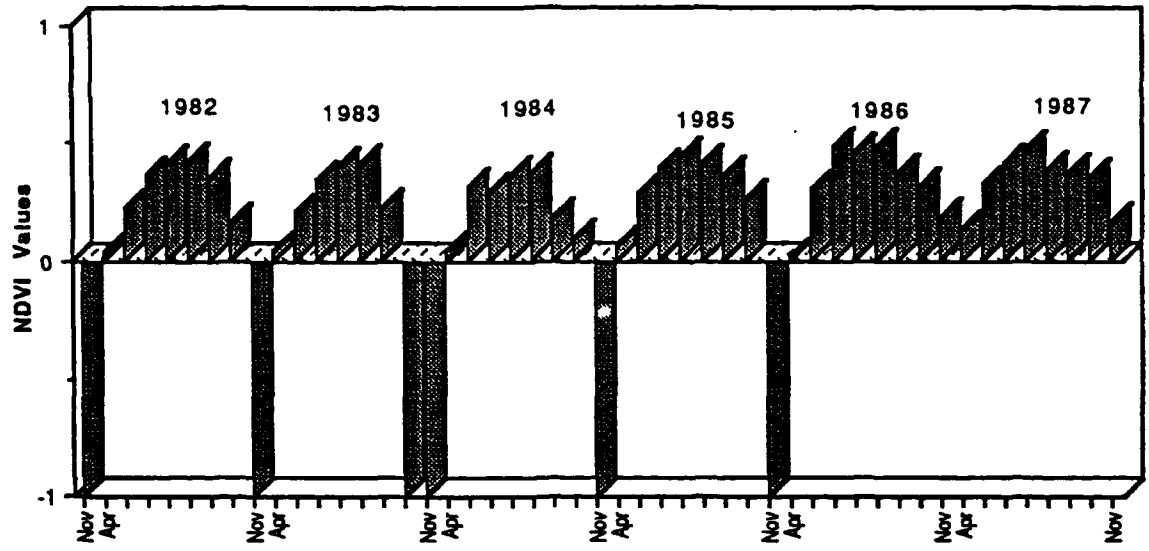

Fig. 5.1.-4. Satellite Data - Vildbacken Site

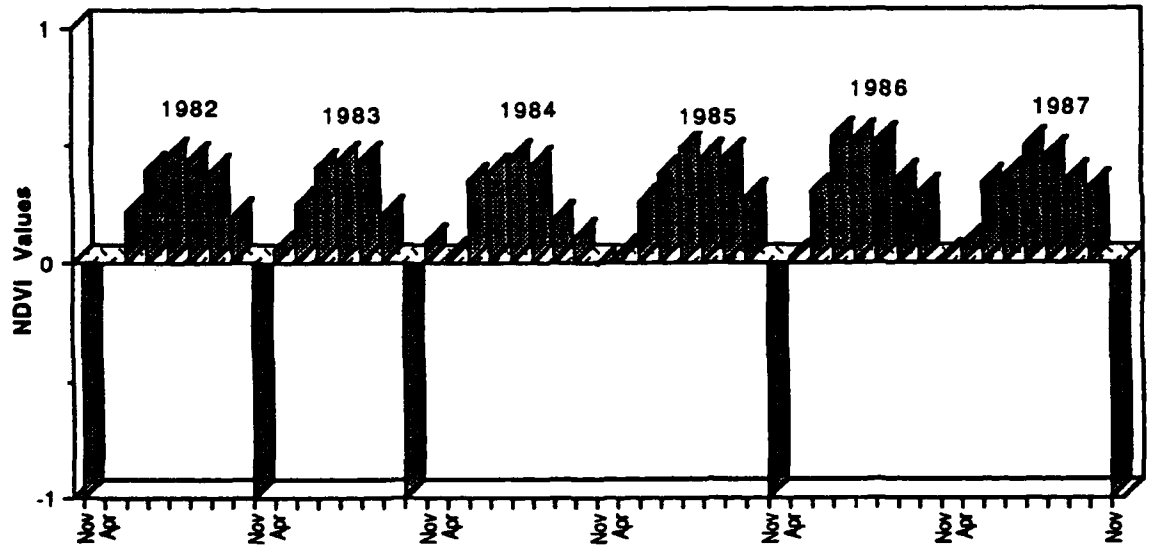

Fig. 5.1.-5. Satellite Data - Bjurselefors Site

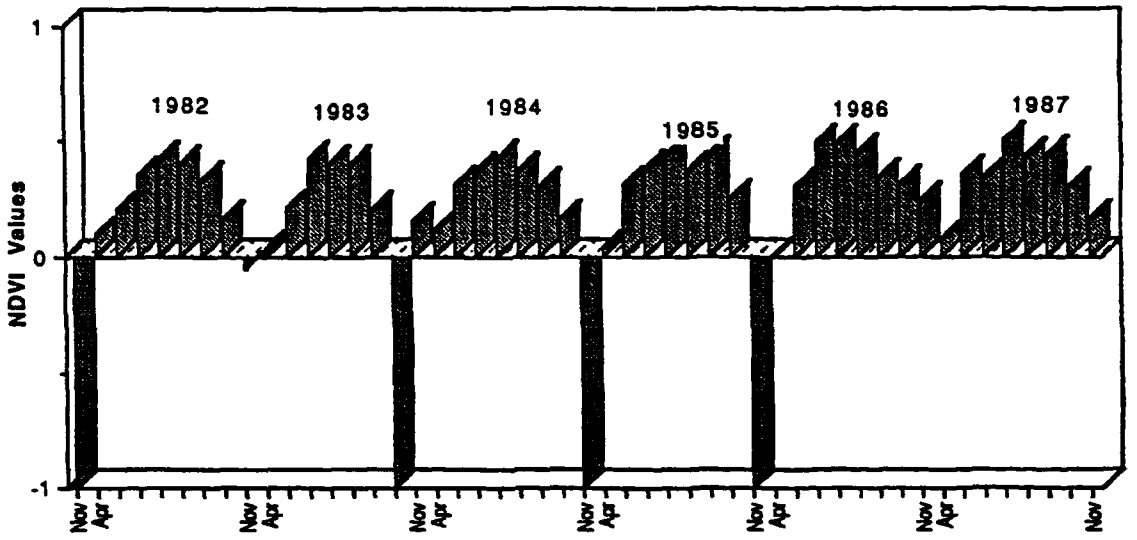

Fig. 5.1.-6. Satellite Data - Ektrask Site

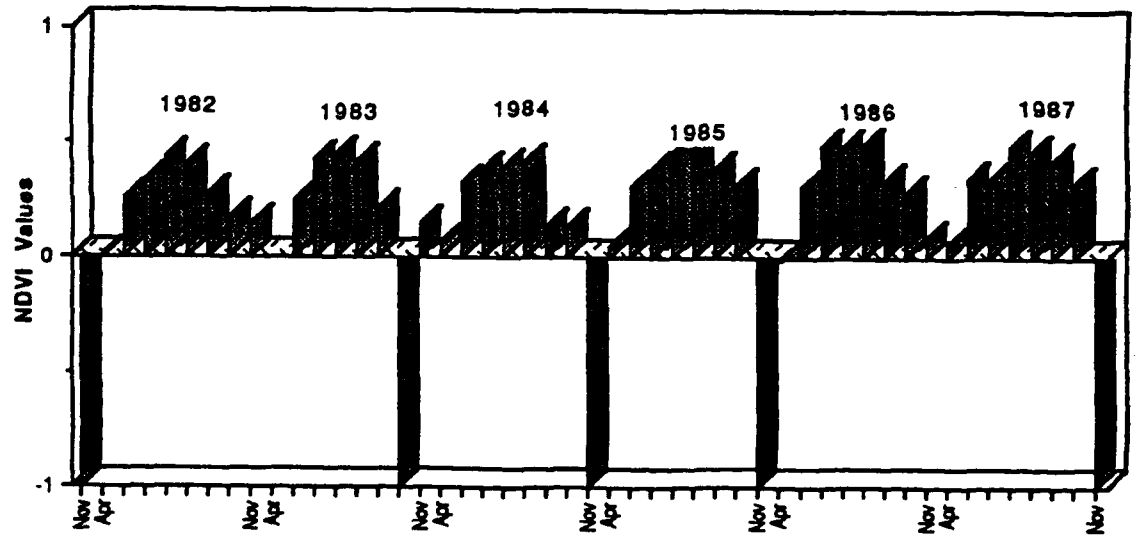

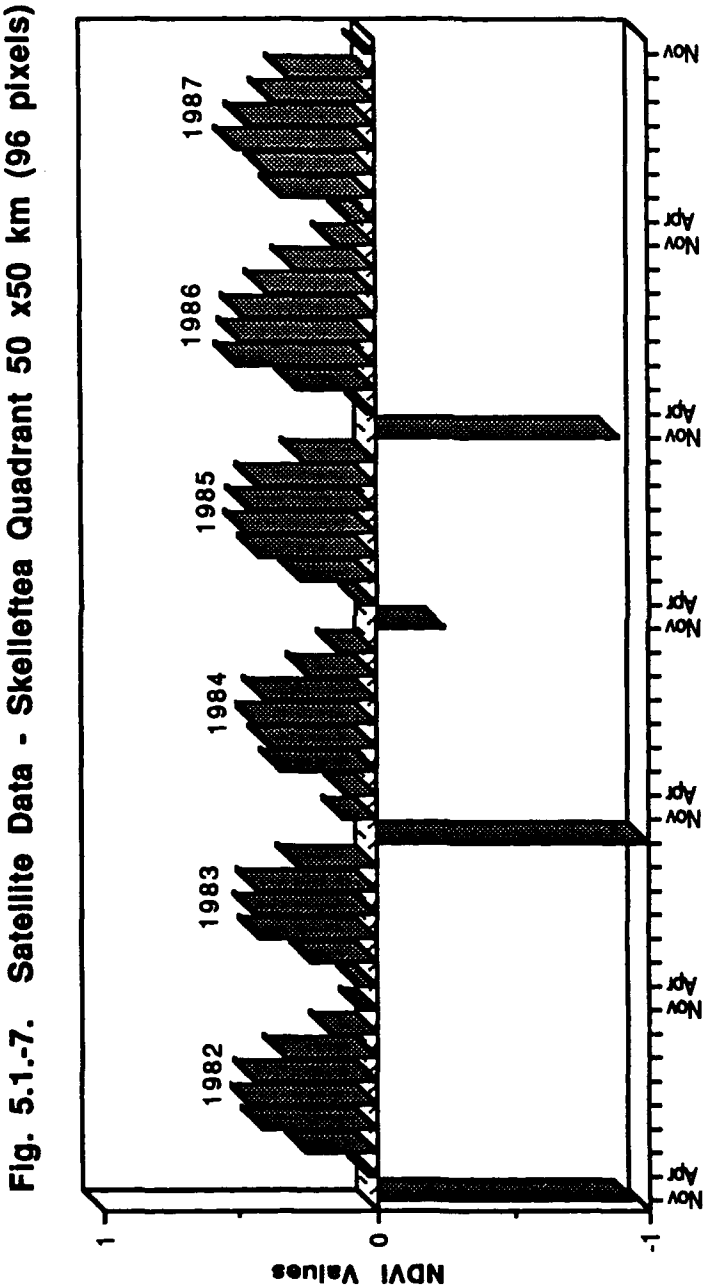

Fig. 5.1.-7. Satellite Data - Skelleftea Quadrant 50 x50 km (96 pixels)

Fig. 5.1.-8. Satellite Data - Örrtrask Site

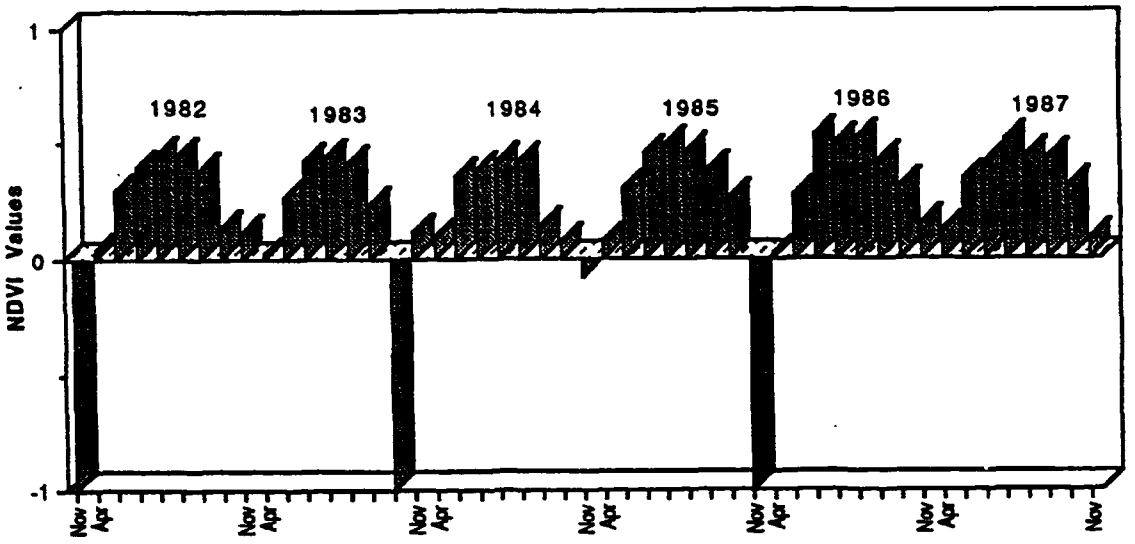

Fig. 5.1. -9. Satellite Data - Mullbacka Site

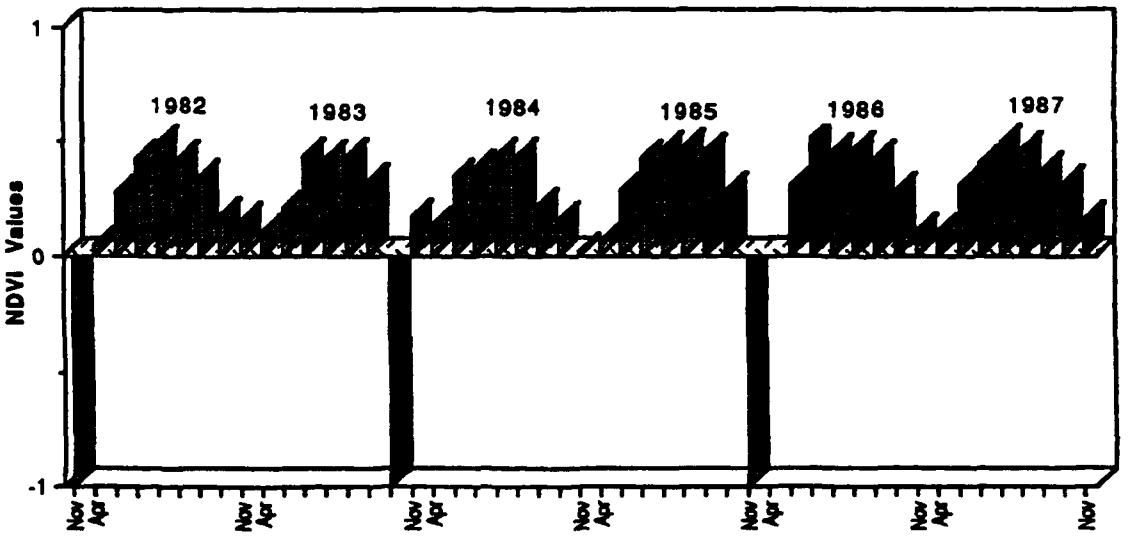

Fig. 5.1.-10. Satellite Data - Talitrask Site

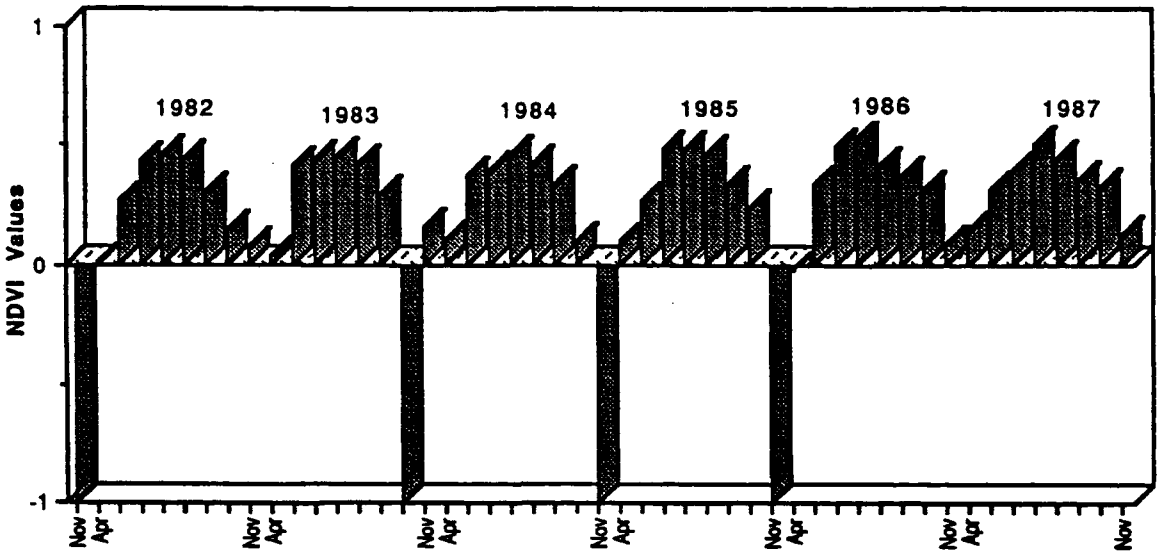

Fig. 5.1.-11. Satellite Data - Bodbyn Site

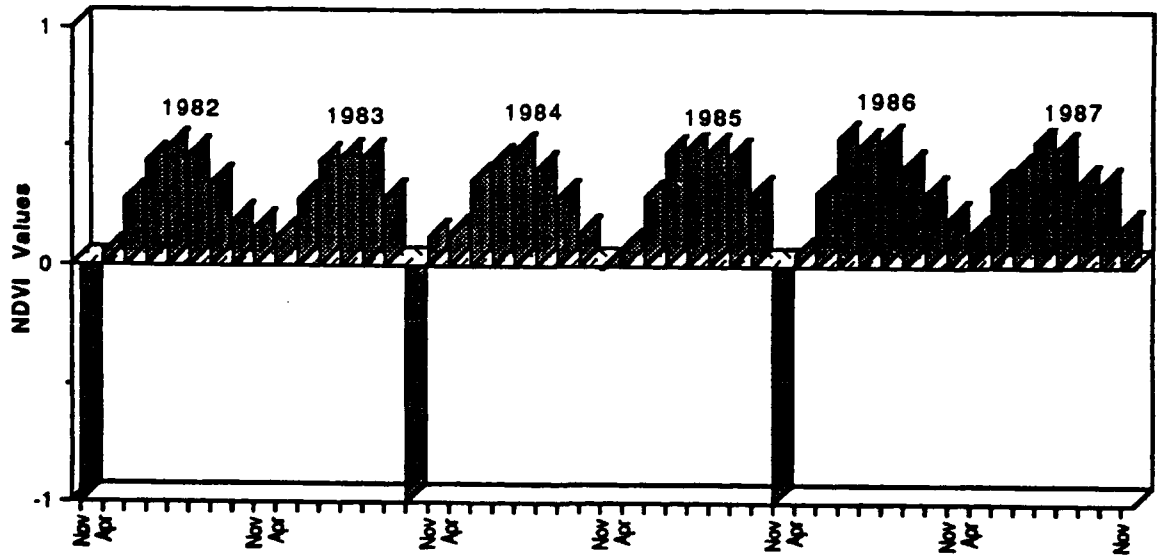

Fig. 5.1.-12. Satellite Data - Vindeln Quadrant 50x50 km (96 pixels)

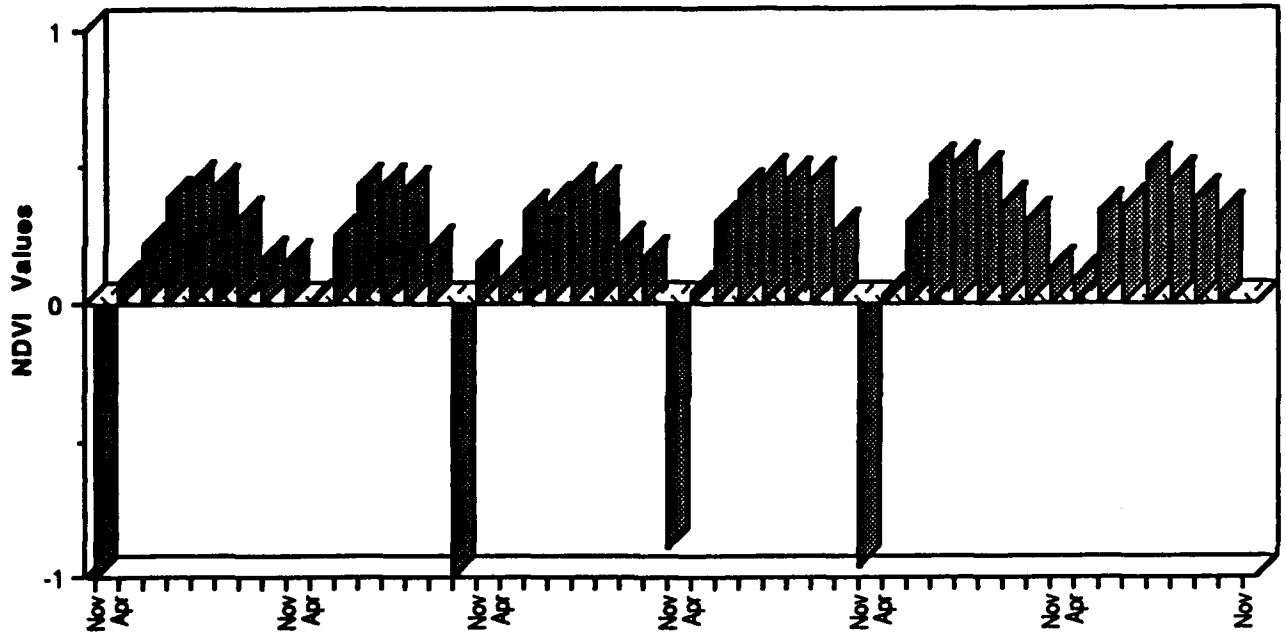

Fig. 5.1.-13. Satellite Data - Vidalund Site

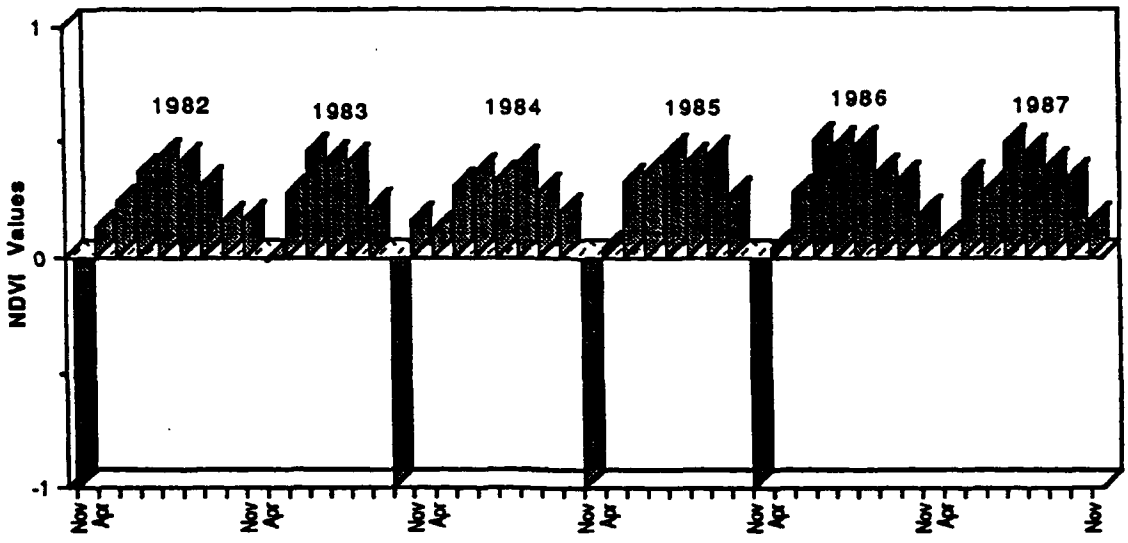

Fig. 5.1.-14. Satellite Data - Yftersjon Site

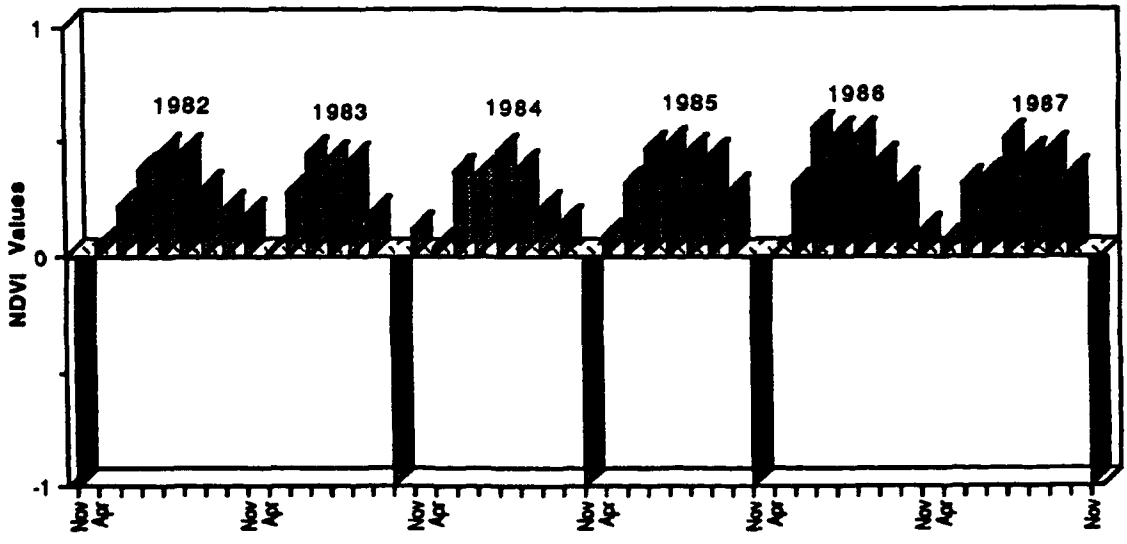

Fig. 5.1.-15. Satellite Data - Lillgodberg Site

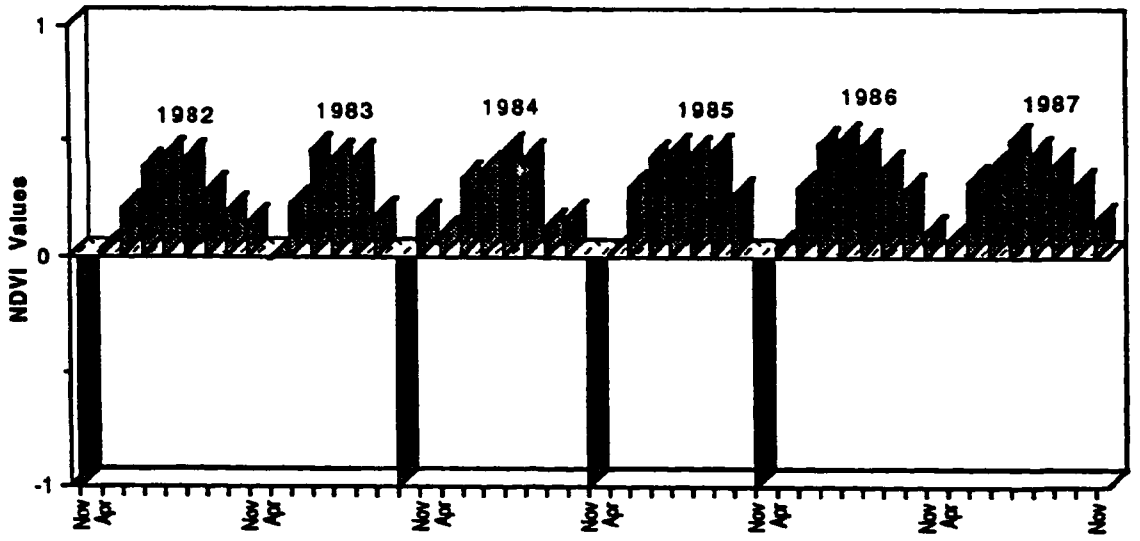

Fig. 5.1.-16. Satellite Data - Hogas Site

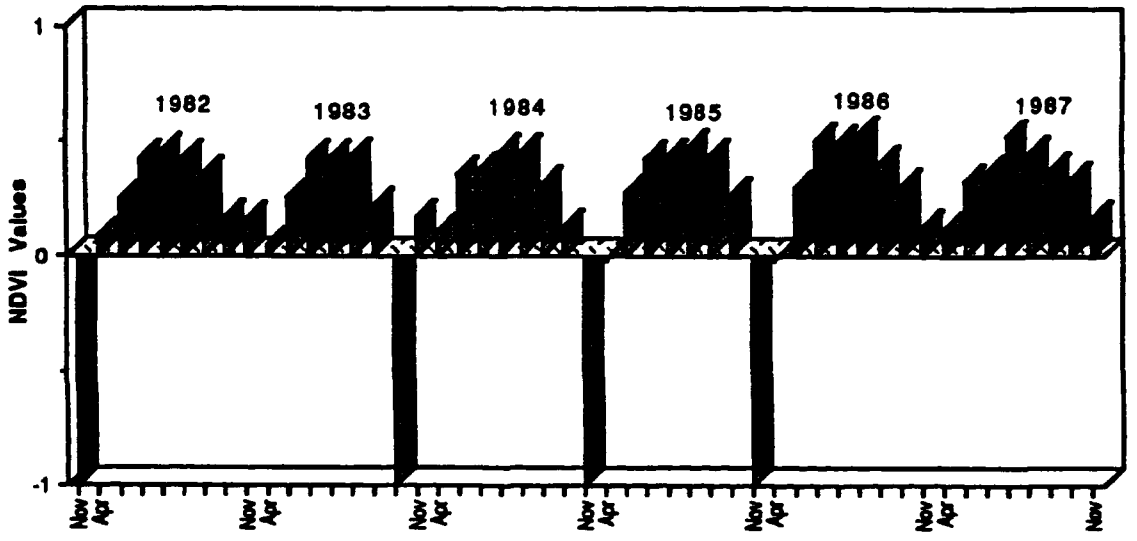

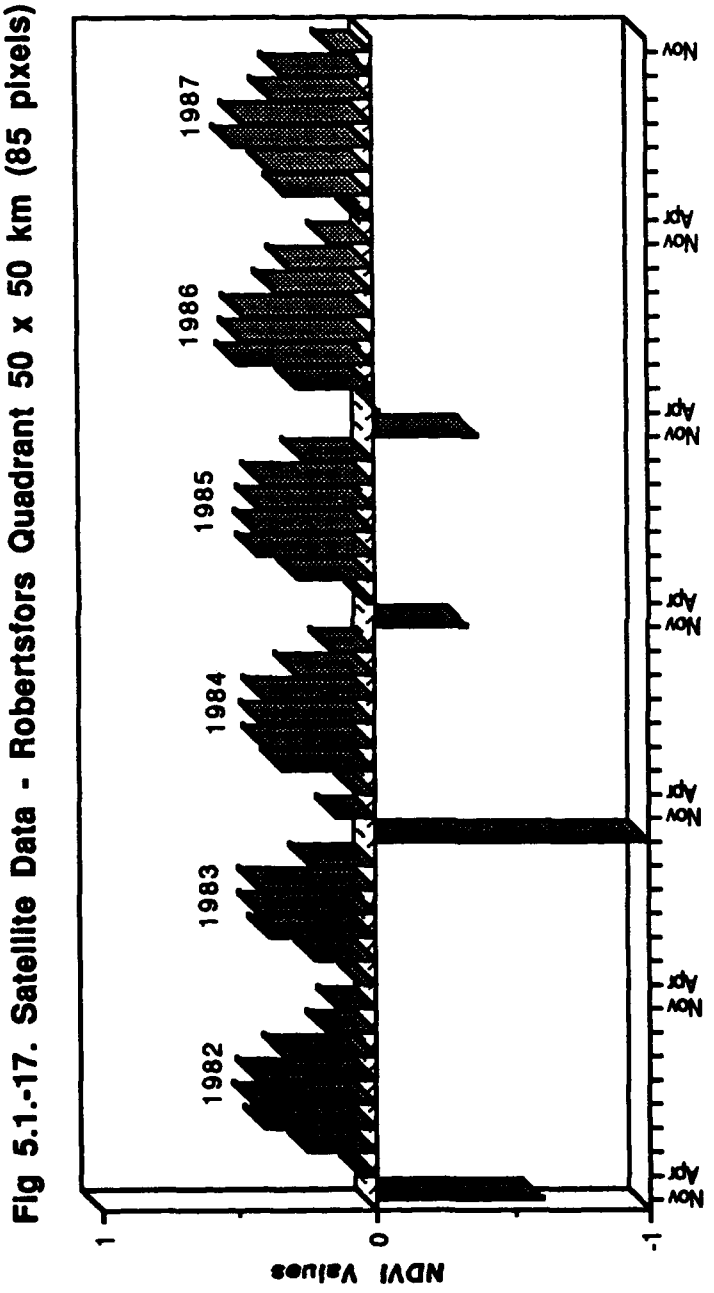

Fig 5.1.-17. Satellite Data - Robertsfors Quadrant 50 x 50 km (85 pixels)

Fig. 5.1.-18. Satellite Data - Vastermark Site

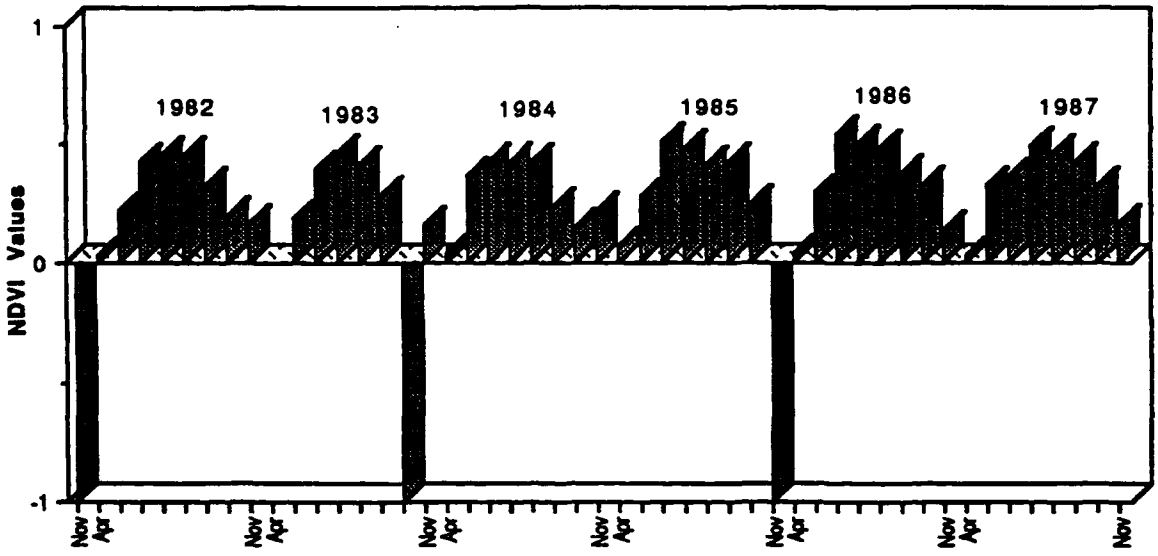

Fig. 5.1.-19. Satellite Data - Ostbyn Site

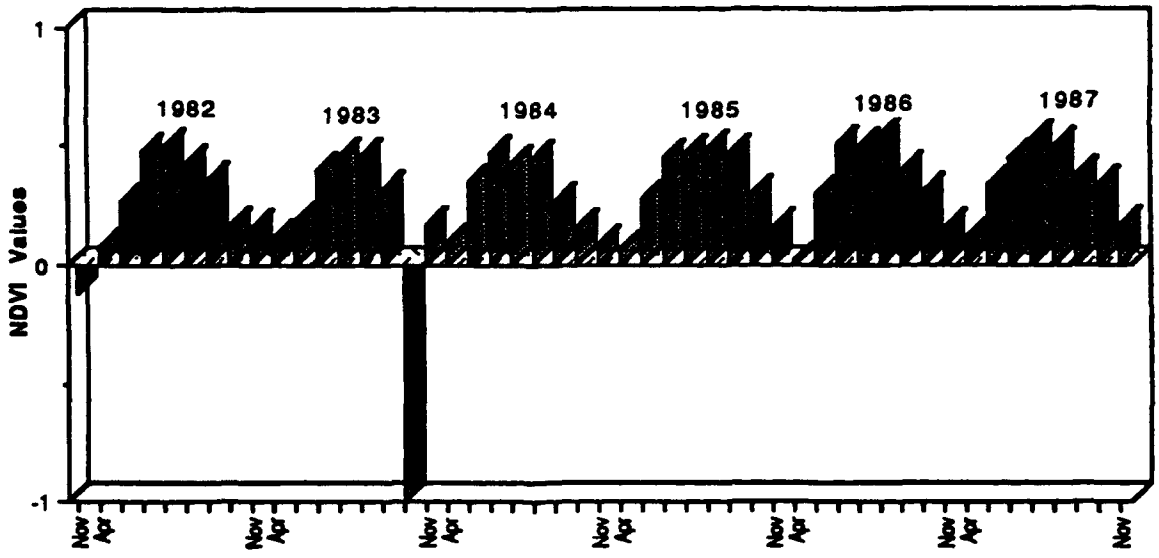

Fig. 5.1.-18. Satellite Data - Vastermark Site

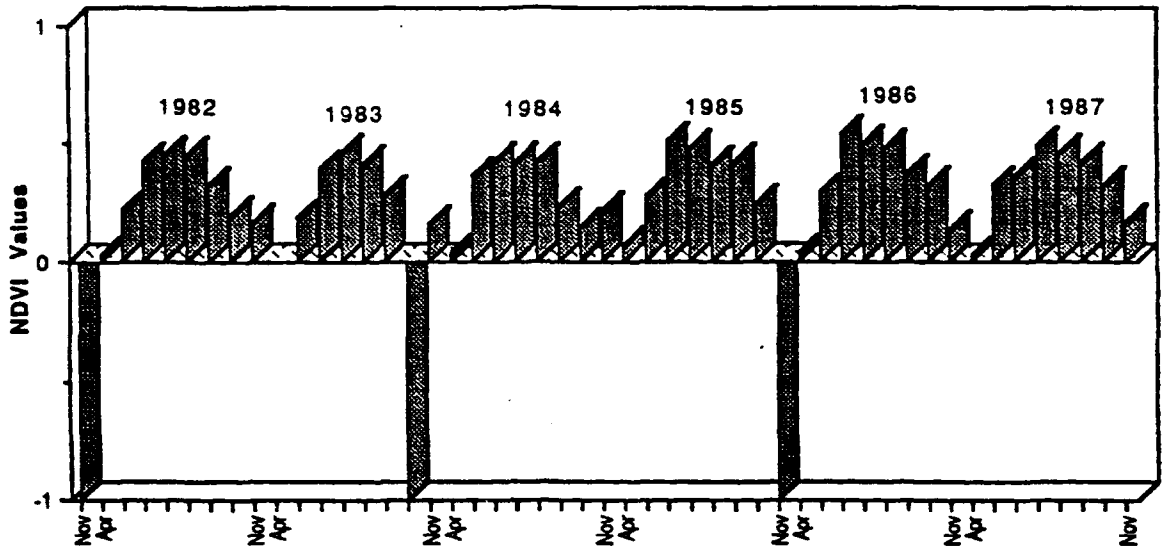

Fig. 5.1.-19. Satellite Data - Ostbyn Site

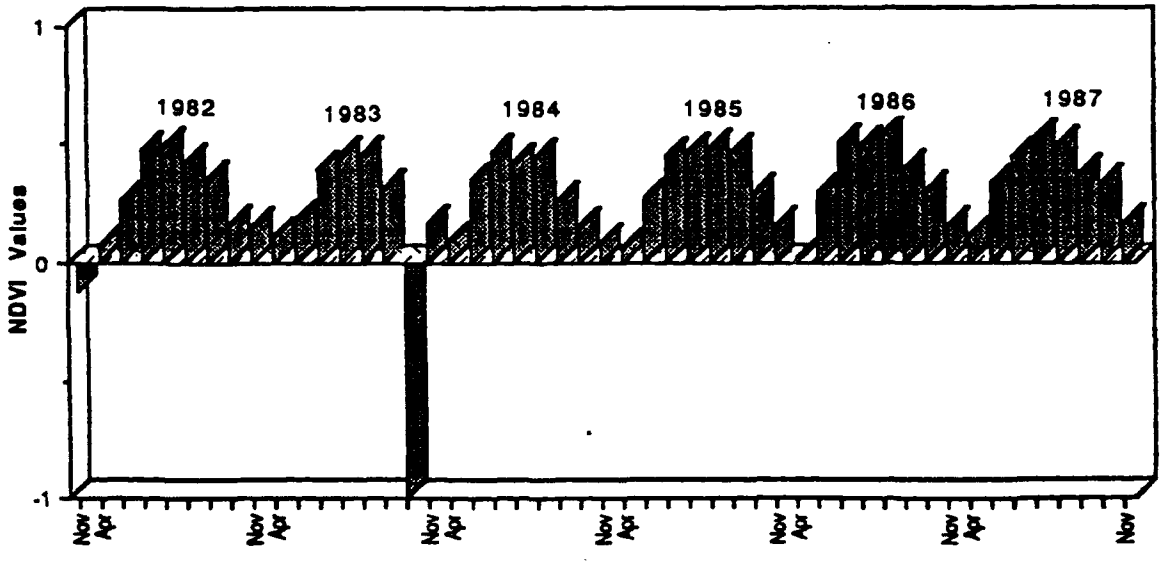

Fig. 5.1.-20. Satellite Data - Adala Site

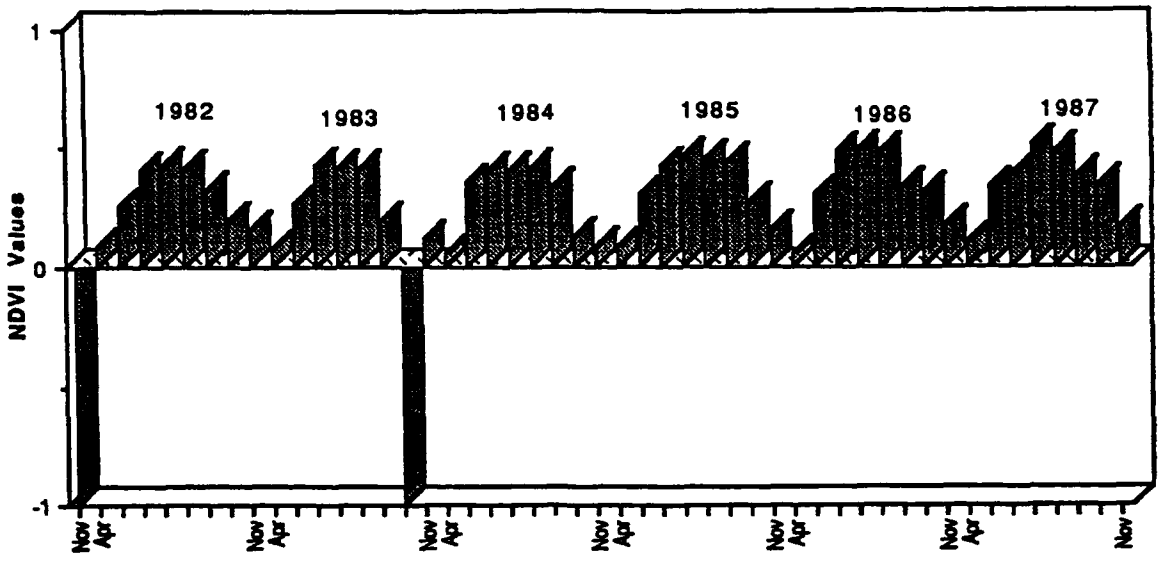

Fig. 5.1.-21. Satellite Data - Ratubacken Site